



High-resolution 3D geological modelling of heterogeneity in poorly exposed glacial deposits using sedimentary and glaciotectonic architectural element analysis: a case example from Sellafield in west Cumbria, UK

Nicholas T. Smith^{1,2*}, Jonathan W. Merritt³ and Emrys R. Phillips³

¹ National Nuclear Laboratory, 5th Floor, Chadwick House, Birchwood Park, Risley, Warrington WA3 6AE, UK

² Department of Earth, Ocean and Ecological Sciences, University of Liverpool, Jane Herdman Building, 4 Brownlow Street, Liverpool L69 3GP, UK

³ British Geological Survey, Lyell Centre, Research Avenue South, Edinburgh EH14 4AP, UK

NTS, 0000-0002-4146-857X

* Correspondence: nick.t.smith@uknnl.com

Abstract: Three-dimensional modelling of superficial geology is challenging, particularly for complex industrial sites such as the Sellafield nuclear site, Cumbria, UK. A lithostratigraphic approach is sufficient to show distribution of key units where only a general understanding of hydrogeology is required. For many sites, however, a much higher-resolution understanding is needed to better characterize heterogeneity and identify potential pathways for contaminant transport within safety case development and remediation planning. Models that focus on often thin, laterally discontinuous, heterogeneous sedimentary units are beset with issues including (1) a lack of exposure coupled with a dearth of data gathered by low-intrusive and intrusive means, (2) structural, stratigraphic and sedimentological complexities making correlation between data points difficult and (3) uncertainties associated with data quality. However, these problems may be overcome by combining land-system-based sedimentary and glaciotectonic architectural analysis of local field analogues with the creation of a portfolio of generic unit-bounding surface geometries. We test this through the development of a high-resolution 3D geological model of Sellafield nuclear site, where exposures are sparse, but shallow site-investigation boreholes are many. The results demonstrate that land-system-based sedimentary and glaciotectonic architectural element analysis can be applied to capture substantial subsurface heterogeneity resulting from dynamic glacial processes.

Received 16 March 2022; revised 17 July 2022; accepted 26 July 2022

Research into the subsurface behaviour of radioactivity at complex industrial sites such as the Sellafield nuclear site in the UK has shown that coarse-grained unconsolidated deposits have the potential to form preferential pathways for the transport (within groundwater) of contaminants such as radionuclides, whereas finer grained deposits act as aquitards that baffle, hinder or redirect flow (Kuras *et al.* 2016; Smith *et al.* 2020). Understanding the location, extent and 3D geometry of these deposits therefore provides an important step towards improving the conceptual understanding of contaminant transport. It underpins contaminant ‘fate and transport’ modelling and subsequent predictions of risk to human health during safety case development in response to regulatory requirements.

High-resolution ‘real’ (as accurate or representative as possible) computer-developed 3D models, as opposed to more simplified ‘conceptual’ models (e.g. Fookes 1997) can better facilitate understanding of the distribution and geometry of these sediment (soil) pathways. However, geological investigation at industrial sites is challenging owing to a general lack of exposure. Suitable subsurface data for 3D modelling are typically confined to pre-construction geotechnical borehole logs, trial pits and sparse geophysical survey data. Although such data may allow the overall extent of a body of sediment to be defined, they represent only a very small percentage of that body. The building of a high-resolution 3D model that is geologically robust, and can communicate the main sources of heterogeneity, whilst understanding the degree of uncertainty (i.e. risk) therefore presents challenges, including: (1) achieving better computational

representations of geological information whilst highlighting the differences between digital representation and the real phenomena; (2) responding to uneven spatial distribution of data, whilst allowing for variations in data quality; (3) creating simulated, digital versions of geological phenomena that are indistinguishable from their real counterparts (Wycisk *et al.* 2009).

Three-dimensional geological models where borehole logs are the primary data source can be created in several different ways, but most rely on connecting units that possess similar features. For example, the modelling of mineral ore bodies has for many years involved interpolation via a ‘kriging’ algorithm to create a ‘volume’ bounded by a 3D envelope that defines the geometry of the ore body (Krige 1951). More recent refinements have involved the use of geometric reconstruction and finite-difference modelling (Feltrin *et al.* 2009), and incorporation of geostatistical variogram analysis and fractal modelling (Wang *et al.* 2013). Inevitably, correlation involves some type of representation of ‘bulk lithology’, but the key to this is how it is interpreted and generalized. In many pseudo-lithostratigraphic models, it is often this generalization that removes the understanding of heterogeneity.

Models created using borehole data are invariably based on the correlation between boreholes of the tops and bottoms of lithologically or stratigraphically similar units, typically resulting in a grid of cross-sections (Kessler *et al.* 2009; Lelliott *et al.* 2009; Wycisk *et al.* 2009) and the creation of a ‘modelling stratigraphy’. Depending on the level of detail, this hierarchical sequence of units, which is used to construct the 3D model, may reciprocate known regional ‘lithostratigraphic’ sequences (e.g. Lee 2018). However,

pure ‘layer-cake’ lithostratigraphy (Salvador 1994) is limited as a stratigraphic technique for glacial successions because units are commonly heterogeneous, disparate and fragmented (Rose and Menzies 1996; Lee 2018), resulting from a variety of tectonic, sedimentary, gravitational and other processes (e.g. Phillips *et al.* 2007; Lee *et al.* 2017; Lee 2018). In effect, lithostratigraphy relies upon lateral continuity of lithologies and simple rules relating to way-up, facies replication (or lack of it) and superposition, but Quaternary environments (and especially glacial and constrained fluvial settings) lack this owing to the restricted accommodation space within the landscape and presence of geological processes that were active at multiple levels within that space.

Units may also be spatially limited for purely depositional reasons: for example, channels within a braided river system change course, resulting in repeated, stacked, amalgamated fluvial sequences (Medici *et al.* 2015). Furthermore, in formerly glaciated regions such as west Cumbria, many units within glacial sequences have been affected by subglacial and glaciotectonic processes at various scales, resulting in localized thickening or removal, structural repetition, deformation, post-depositional subglacial injection of sediment by hydrofracturing, shrink-and-swell architectures and the development of widespread, gently undulating, sharp bounding surfaces (Nirex 1997*a, b, c, d, e*; Busby and Merritt 1999; Merritt and Auton 2000; Williams *et al.* 2001; Smith and Merritt 2008; Cross *et al.* 2018; Smith *et al.* 2020).

A different approach to pure lithostratigraphy is therefore required to satisfactorily model a higher level of heterogeneity, particularly regarding granular aquicludes. We describe a case study here in which these issues are addressed by utilizing and developing ‘architectural element analysis’ (Miall 1985; NACSN 2005; Slomka and Eyles 2013) and ‘glaciotectonic architectural analysis’ (*sensu* Pedersen 2014), together with the assessment of structural style related to deposition environments (*sensu* McCarroll and Rijdsdijk 2003).

Our procedure first involves the definition of a sedimentary and glaciotectonic architectural element framework based on prior knowledge of the Quaternary sequence and placed within a land-system classification (see Cross *et al.* 2018; Evans and Benn 2021). A new portfolio of generic geometries for erosional bounding surfaces of architectural elements or lithofacies is then developed, which is used to aid confident correlation between boreholes. Our workflow comprises seven phases:

- (1) literature review of site and regional geology (geological background);
- (2) analysis of sedimentary and glaciotectonic architectural elements, facies associations, palaeo-environmental reconstruction and definition of generic 3D geometries of erosional-bounding surfaces;
- (3) assessment of appropriate level of heterogeneity for high-resolution 3D modelling;
- (4) manipulation (rationalization and homogenization) of borehole logs;
- (5) cross-section construction using geological correlation of specific units within a modelling stratigraphy;
- (6) refinement of modelling stratigraphy and redraft of sections according to new modelling stratigraphy;
- (7) conversion to a 3D surface model and visualization and interrogation of the model itself.

The key to this approach is a thorough understanding of the geological and geomorphological processes that created the geometries and bounding surfaces of the units to be correlated. This study focuses on available field exposures of Pleistocene sediments within 5 km of Sellafield (Fig. 1), the log of borehole BH7 from the site investigation described by Kuras *et al.* (2016) and Smith *et al.* (2020), together with representative logs from the same

study, and thin sections obtained from samples from boreholes (e.g. Drigg offsite borehole C) and field exposures examined during the Nirex investigations in the 1990s.

Geological background

The study area forms part of the west Cumbrian coastal plain, between the Irish Sea and foothills of the Lake District National Park (Fig. 1). As shown in Figures 1 and 2 (a representative correlation panel using sections of exposures and borehole logs throughout the study area as shown in Fig. 1), superficial, recent sediments such as blown sand are underlain by glacial sediments that lie mainly on sandstones of the Permo-Triassic Sherwood Sandstone Group and partially on older Paleozoic rocks including limestones (Barnes *et al.* 1994; Jones and Ambrose 1994; Akhurst *et al.* 1997; Stone *et al.* 2010; Kuras *et al.* 2016; Smith *et al.* 2020). Nearby to the east, the foothills are formed of volcanoclastic rocks of the Borrowdale Volcanic Group and fine-grained, weakly metamorphosed, sedimentary rocks of the Skiddaw Group (Akhurst *et al.* 1997).

Early in the 20th century a ‘tripartite’ Pleistocene stratigraphy was recognized in western Cumbria (Eastwood *et al.* 1931; Trotter and Hollingworth 1932; Trotter *et al.* 1937). This comprised a ‘Lower Boulder Clay’, ‘Middle Sands and Gravels’ and an ‘Upper Boulder Clay’, although additional units were known to occur locally and the two tills (for a definition of till see p. 83 of Griffiths and Martin 2017) could not be distinguished where the intervening sand and gravel was absent. The lower till was linked to the last major glaciation of the region (Late Devensian), whereas tills higher in the sequence were linked to readvances of Scottish ice into the Irish Sea basin, either the Gosforth Oscillation, or the succeeding Scottish Readvance (Evans *et al.* 2005). Subsequent work along the coast by Huddart (1971), Huddart and Tooley (1972) and Huddart *et al.* (1977) broadly reconfirmed the tripartite stratigraphical model, but dismissed evidence for the earlier Gosforth Oscillation.

Following extensive investigations in western Cumbria undertaken in the 1990s on behalf of UK Nirex Ltd (Nirex 1995, 1996, 1997*a, b, c, d, e, f, g, h, i, j, k, l, m*; Michie and Bowden 1994; Bowden *et al.* 1998), a more comprehensive lithostratigraphical framework was established (Nirex 1997; Merritt and Auton 2000). This scheme (Fig. 3), which has been further developed by Smith and Merritt (2008) and McMillan *et al.* (2011), includes three subgroups, 13 formations and 46 members. The Central Cumbria Glacial Subgroup includes erratics derived predominantly from the Lake District and Shap Fell, whereas the Irish Sea Coast Glacial Subgroup (ISCD) includes material from southern Scotland, the Solway Lowlands, the west Cumbrian Coalfield and the northern Cumbrian mountains. The deposits of the latter subgroup were laid down by ice flowing through the Solway Lowlands, swinging around the northwestern side of the Lake District, and feeding into the Irish Sea Ice Stream (Livingstone *et al.* 2012). Formations and members within the two subgroups interdigitate locally, notably beneath Lower Wasdale, where they reveal former interactions between locally sourced and far-travelled ice. An increase in the proportions of Scottish erratics in tills occurs towards both the coast and the top of several multi-till sequences in the district, indicating that Scottish ice flowing into the Irish Sea basin gradually became dominant over ice emanating from the mountains to the west (Eastwood *et al.* 1931; Trotter *et al.* 1937; Nirex 1997*g*).

Merritt and Auton (2000) concluded that the products of at least one major pre-Devensian glaciation are represented in cored boreholes around Drigg and Lower Wasdale. Ice possibly flowed out of Wasdale during Marine Isotope Stage (MIS) 4 to lay down the Maudsyke Till. Varved glaciolacustrine deposits (Carleton Silt) were subsequently deposited in proglacial lakes when the glacier retreated, possibly on two occasions. The Carleton Silt passes

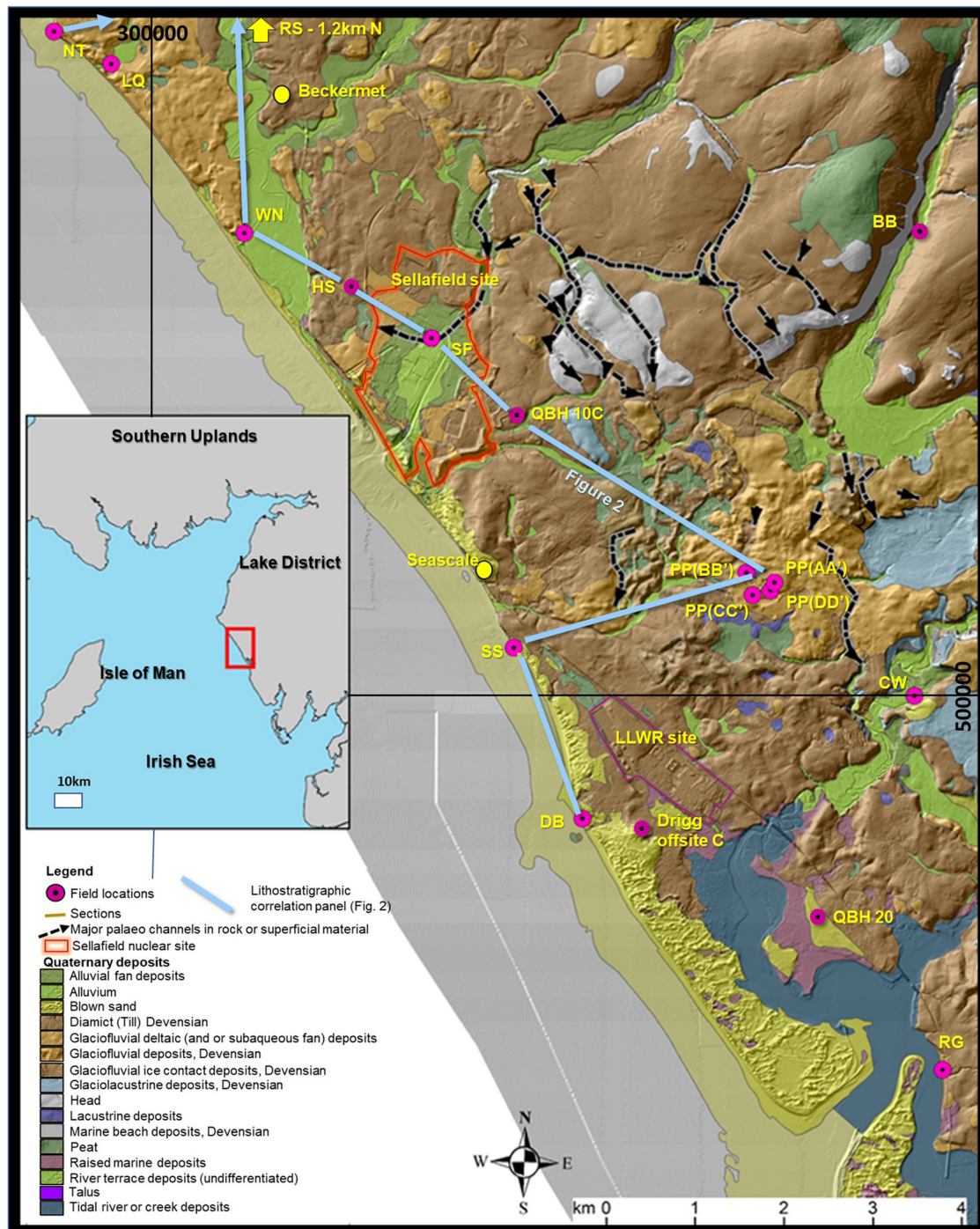


Fig. 1. Map of study area showing superficial geology (superficial geology (BGS 1999) superimposed on hillshade digital terrain model, the Sellafield nuclear site, field locations and boreholes. NT, Nethertown; RS, Rothery Scar; LQ, Lowside Quarter; WN, Warborough Nook; HS, High Sellafield; SF, Sellafield; SS, Seascale; PP, Peel Place Quarry (AA', BB', CC', DD' are cross-section locations; see Fig. 8 for detailed location map); CW, Cookson Wood; DB, Drigg Beach; RG, Ravenglass; BB, Blengdale Bridge. Environment Agency Digital Terrain Model LiDAR data; EDINA Digimap <https://digimap.edina.ac.uk/>, created 15 July 2022; Geological Map Data BGS © UKRI 2022.

upwards into cold-water marine deposits (Glannoventia Formation) recording a marine transgression and contemporary sea-level of *c.* 20 m below Ordnance Datum (OD), probably during MIS 3. Glaciers emerged once again from the western valleys of the Lake District, particularly Wasdale, to lay down the very stony Holmrook Till. This occurred during the build-up of ice towards the Last Glacial Maximum (LGM), which probably reached its maximum extent between 27 and 24 ka (Clark *et al.* 2012; Livingstone *et al.* 2012; Chiverrell *et al.* 2013, 2018; Scourse *et al.* 2021), when the whole region was ice-covered. Scottish ice eventually deflected Lake District ice southwards along the coast,

flowing across the valleys of the Ehen, Calder and Lower Wasdale, laying down the Low Wath and Ravenglass tills (Table 1).

The Irish Sea ice stream became dominant during several readvances recorded by thinly interbedded tills, sands and gravels within the Gosforth Glacigenic Formation. The first major readvance (Gosforth Oscillation) followed significant deglaciation. During this first readvance the Irish Sea ice stream thickened and encroached inland, and thick sequences of fine-grained, laminated glaciolacustrine sediment accumulated within Lower Wasdale (Whinneyhill Coppice Clay) and other major valleys of the district (e.g. Ehen Valley Silt). In addition, ice over-rode most of the coastal

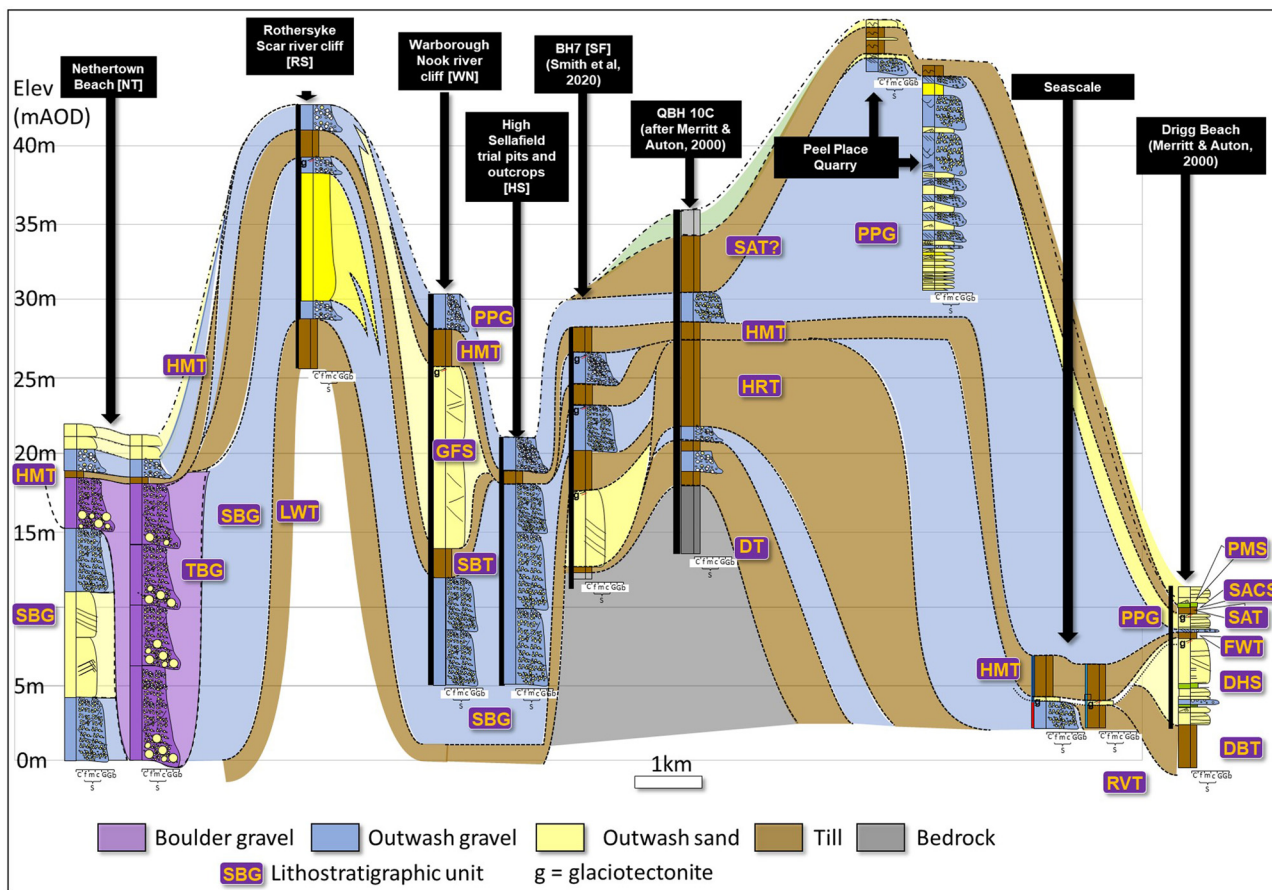


Fig. 2. Study-area-wide lithostratigraphic correlation, utilizing representative sedimentary and lithostratigraphic logs from study locations shown in Figure 1 (see Table 1 for explanation of lithostratigraphic unit abbreviations).

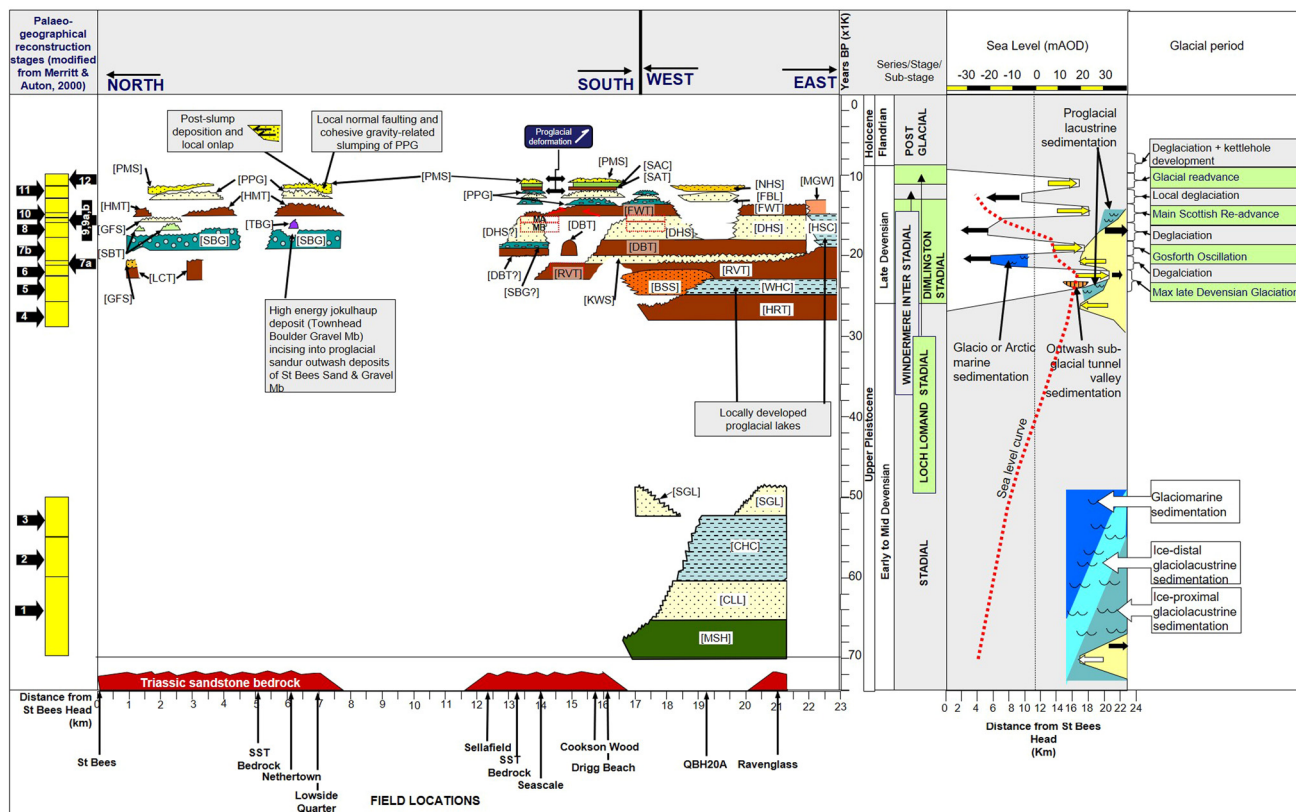


Fig. 3. Chronostratigraphic chart illustrating key sequences in the west Cumbrian area with respect to field locations in this paper, Quaternary stages, sea-level changes, glacial periods and palaeogeographic reconstruction stages (modified from Smith and Merritt 2008).

Table 1. Lithostratigraphy of the Irish Sea Coast Glacigenic Subgroup (ISCD) in west Cumbria

MIS	Lithostratigraphy	Regional event
	Irish Sea Coast Glacigenic Subgroup (ISCD)	
2	Gosforth Glacigenic Fm (GOS) <i>Sellafield to Ravenglass</i>	
	New glaciolacustrine/silt unit: Sandy Acre Clay and Silt Mbr (SACS)	SR
	New till unit: Sandy Acre Till Mbr (SAT)	SR
	Peel Place Sand & Gravel Mbr (PPG)	SR
	Fishgarth Wood Till Mbr (FWT)	SR
	Drigg Holme Sand Mbr (DHS)	GO
	Drigg Beach Till Mbr (DBT)	GO
	Kirkland Wood Sand & Gravel Mbr (KWS)	GO
	<i>St Bees to Sellafield</i>	
	Meadow House Clay Mbr (MHC)	SR
	Peckmill Sand Mbr (PMS)	SR
	Low Mill Gravel Mbr (LMG)	SR
	How Man Till Mbr (HMT)	SR
	Gutterfoot Sand Mbr (GFS)	GO
	Rothersyke Till Mbr (RST)	GO
	St Bees Till Mbr (SBT)	GO
	Aikbank Farm Glacigenic Fm (AIK) <i>Lower Wasdale only</i>	
	Mainsgate Wood Sand & Gravel Mbr (MGW)	GO
	Holmeside Clay Mbr (HSC)	GO
	Green Croft Till Mbr (GCT)	GO
	Whinneyhill Coppice Clay Mbr (WCC)	MLD
2/3	Seascale Glacigenic Fm (SEA) <i>Seascale to Ravenglass</i>	MLD
	Ravenglass Till Mbr (RVT)	
	Barn Scar Sand & Silt Mbr (BSS)	
	<i>Ehen valley</i>	
	Ehen Valley Sand & Gravel Mbr (EVS)	
	Ehen Valley Silt Mbr (EVL)	
	Catgill Wood Sand & Gravel Mbr (CWG)	
	Low Wath Till Mbr (LWT)	
	Meadow View Sand & Gravel Mbr (MVG)	
	<i>St Bees to Sellafield</i>	
	Townhead Boulder Gravel Mbr (TBG)	
	St Bees Sand & Gravel Mbr (SBG)	
	St Bees Silt Mbr (SBL)	
	Lowca Till Mbr (LCT)	
3?	Glannoventia Fm (GLV)	
	Kokoarrah Shelly Sand Mbr (KKS)	
	Stubble Green Silt Mbr (SGL)	
	Carleton Hall Clay Mbr (CHC)	
4–6	Carleton Silt Fm (CLL)	
	Drigg Till Fm (DGT)	

Mbr, Member; SR, Scottish Readvance; GO, Gosforth Oscillation; MLD, Main Late Devensian glaciation; MIS, Marine Isotope Stage (modified after Nirex 1997 and McMillan *et al.* 2011).

plain, much as proposed by Trotter *et al.* (1937). Local ice possibly expanded across Lower Wasdale to lay down the Green Croft Till. During the subsequent retreat of the Irish Sea Ice Stream, an ice marginal lake re-formed in Lower Wasdale, within which the glaciolacustrine Holmeside Clay and deltaic Mainsgate Wood Sand and Gravel were deposited. The margin of the ice stream oscillated several times, laying down the clay-dominated Drigg Beach, Fishgarth Wood and other thin tills along the coast. These minor oscillations were possibly contemporaneous with the creation of the push moraine at St Bees, widely attributed to the Scottish Readvance (Huddart and Glasser 2002, and references therein; Williams *et al.* 2001).

Subsequent research in the region has generally developed and established this account of events (Thomas *et al.* 2004; Evans *et al.* 2005; Roberts *et al.* 2007; Thomas and Chiverrell 2007; Ballantyne *et al.* 2009; Stone *et al.* 2010; Clark *et al.* 2012; Livingstone *et al.* 2012; Chiverrell *et al.* 2013; Cross *et al.* 2018; Smith *et al.* 2020). A radically different interpretation has been offered by Eyles and McCabe (1989), who attempted to reconcile much of the evidence described here into their controversial model of glaciomarine ice sheet retreat caused by a rapid marine ingress into a glacio-isostatically depressed Irish Sea basin. For example, they reinterpreted the widespread ‘upper till’ as a glaciomarine mud ‘drape’, inferring former relative sea-levels of up to 152 m OD. However, their local evidence has been dismissed by Huddart (1991, 1994), Huddart and Clark (1994), Nirex (1995, 1996, 1997*a, b, c, d, e, f, g, h, i, j, k, l, m*), and Merritt and Auton (2000). A key difference between submarine and subglacial depositional systems is the types of deformation associated with each. Large- and small-scale soft-sediment deformation features within stratified glaciomarine and associated valley infill complexes are the result of syndepositional gravity loading in response to high deposition rates and/or post-depositional slumping, whereas the compressional and extensional features in subglacial material result from glaciotectionism (McCarroll 2001). Several researchers (e.g. Harris *et al.* 1997; Williams *et al.* 2001; Phillips *et al.* 2007; Thomas and Chiverrell 2007) have demonstrated the unequivocal and common presence of the latter at sites around the Irish Sea Basin such as Abermawr, Dinas Dinlle, St Bees, Aberdaron, Porth Neigwl, Gretna and Killiney Bay. Glaciomarine sediments such as mud drapes have a high water content (Powell 1984) and are simply not coherent enough to have been deformed by such brittle deformation features. Eyles and McCabe (1989) did not identify evidence of glaciotectionic deformation at these sites, meaning that their sedimentary interpretation was severely compromised. In fact, their glaciomarine paradigm pertaining to the Irish Sea basin has since been categorically rejected (McCarroll 2001).

The idea of mud drapes, however, has been resurrected recently by Coleman *et al.* (2020), who concluded that the massive, clay-dominated ‘upper tills’ exposed in the cliff at Drigg Beach and elsewhere in the district are glaciolacustrine clay, rather than till. Together with the intervening glaciofluvial units, they identified three lake fill–lake drainage cycles, rather than the generally accepted glacial advance and retreat scenario. They adopted this alternative idea to develop a new simplified regional lithostratigraphic framework and 3D geological model for the area around the Low-Level Waste Repository (LLWR) at Drigg. This reinterpretation has implications for future 3D modelling and site investigations in the region and is addressed further in the Discussion below.

Method for architectural element and facies analyses

Architectural element analysis allows the characterization of sedimentary geometry and facies relative to a hierarchy of erosion bounding surfaces that define the architecture of the sediments (Miall 1985, 1988, 1996, 2006*a, b*; Fielding 2006; Hughes 2010; Slomka and Eyles 2013, 2015). It has been shown to be very effective in the characterization of clastic fluvial sequences (Mountney and Thompson 2002; Cain and Mountney 2009; Ghazi and Mountney 2009; Banham and Mountney 2014), and has been applied to a range of glacigenic settings (Eyles *et al.* 1998; Boyce and Eyles 2000; Duller *et al.* 2008; Slomka and Eyles 2013, 2015), improving attempts to extrapolate the understanding of sedimentary geometries and properties in the subsurface, particularly in connection to hydrogeological modelling (Slomka and Eyles 2013; Medici *et al.* 2018). It is therefore appropriate for the high-resolution 3D geological modelling described here, as well as

for modelling lower-resolution, lithostratigraphic bounding surfaces, although the effects of glaciotectonic deformation cannot be ignored (see below), for these can generate new elements (e.g. tills) or may alter pre-existing sediments in such a way as to affect hydraulic transmissibility (e.g. pervasive glaciotectonites).

Sedimentary architectural element analysis is essentially a hybrid of lithofacies analysis and allostratigraphy. The former is the interpretation of the genetic origin of sediments utilizing observations of lithology and sedimentary structures (Cain and Mountney 2009; Slomka and Eyles 2013; Medici *et al.* 2018), whereas allostratigraphy is the hierarchical arrangement of discontinuities or bounding surfaces that compartmentalize packages of rock or sediment (Chang 1975; NACSN 1983; Lee 2018). Allostratigraphy focuses on the geometrical arrangement of units rather than simply their lithological properties (Salvador 1994; Rawson *et al.* 2002) and provides a suitable stratigraphic framework to investigate detailed architectural relationships that a purely lithostratigraphic approach cannot (Lee 2018). Although it shares principles of sequence stratigraphy (Emery and Myers 1996, 2009; Miall 1997), it is not controlled by cyclical changes in sea-level or sedimentation (Slomka and Eyles 2013, 2015). The lithostratigraphy adopted here, as outlined by Nirex (1997) and Merritt and Auton (2000) and incorporated into a larger scheme proposed by McMillan *et al.* (2011), is fundamentally a hybrid of litho- and allostratigraphy (McMillan and Merritt 2012).

Glaciotectonic architectural analysis is based on the identification of packages of glaciotectonically generated or deformed sediment bounded by structural features such as décollement surfaces (Pedersen and Gravesen 2009; Pedersen 2014; Pedersen and Boldreel 2015; Lee *et al.* 2017; Gehrmann *et al.* 2019). It recognizes that certain deformation styles comprising combinations of structural types are associated with specific depositional environments (McCarroll and Rijdsdijk 2003), providing additional constraints on the correlation between subsurface data points in 3D geological modelling. Local and regional field analogues of glaciotectonic deformation can be used to better predict the nature and geometry of likely deformation features within glacial and non-glacial sediments underlying poorly exposed industrial sites.

The first stage of architectural element analysis is typically an assessment of all the lithofacies present within a study area (Medici *et al.* 2015). Considering the complex glacial sequence in west Cumbria, particularly with respect to till units that locally include other interbedded deposits, Cross *et al.* (2018) proposed a land-system-based, process–form model for the Sellafield area that relates glaciation style and dynamics. This approach provides a broad template for interpreting glacial landform–sediment or ‘facies’ associations (Evans 2017). Although, from observations made in the field, we have separated architectural elements possessing ‘ice contact’ from ‘ice marginal’ architectures (*sensu* Slomka and Eyles 2013; although we use the term ‘proglacial’ rather than ‘ice marginal’, as the latter must logically include ice contact architectures). The base of the ice sheet was probably underlain by a deformable bed of water-saturated sediment during the glacial readvances that affected the district (Cross *et al.* 2018), which would have aided rapid ice flow and the deposition of subglacial traction till and glaciotectonite (*sensu* Benn and Evans 1996; Evans *et al.* 2006; Evans 2018).

The next stage involves defining contact relationships. Miall (1985, 1988, 2006a, b) defined several orders of unit-bounding erosional discontinuities for clastic sedimentary sequences, but here we adopt a modified version of the hierarchies suggested by Boyce and Eyles (2000) and Slomka and Eyles (2013, 2015), as shown in Figure 4. For instance, we define facies associations by laterally continuous fifth-order erosional bounding surfaces that can be traced within a defined lithostratigraphic unit, thus aiding unit

correlation during 3D geological modelling. Typically, as also noted by Slomka and Eyles (2013), facies associations record changes in allocyclic-controlled conditions within a depositional environment, whilst also systematically organizing complex, heterogeneous and otherwise unmappable units. Our scheme also embraces variations in surface geometry caused by the effects of glaciotectonic processes. At sites such as Sellafield, where there is little or no exposure, any closely available natural and anthropogenic exposures provide important information regarding the geometry and architecture of units to aid correlation between boreholes. Such information, as presented below, allows a more informed 3D model to be created than relying on computer algorithms alone. This has been a focus in recent years of geological modelling packages such as GSI3D (Kessler *et al.* 2009; Smith 2010) and Groundhog, both developed by the British Geological Survey, wherein it is up to the geologist to draft correlation lines (themselves representing surfaces) with geometries that are appropriate to the units they bound.

Architectural element analysis: description and interpretation of lithofacies and architectural elements

In the following section we present the results of architectural element analysis, providing a description and interpretation of each element, with associated field examples. Where possible, on each graphic log of a field exposure we note lithofacies, architectural element, relevant bounding surfaces according to the approach described above and palaeoflow indicator rose diagrams (data comprise azimuth and dip of clinoforms, and we use GeoRose software; Yong Technology Inc. 2014). We also identify relevant lithostratigraphic units that have been formally established for the region by McMillan *et al.* (2011), the abbreviations of which are shown in Table 1. Particular attention is paid to structural evidence observed at exposures, as it is crucial to fully understanding the 3D relationships of units, for accurate correlation and aiding critical examination of borehole core.

Following the results of comprehensive investigations in west Cumbria reported by Huddart (1991, 1994), Huddart and Clark (1994), Nirex (1995, 1996, 1997a, b, c, d, e, f, g, h, i, j, k), Merritt and Auton (2000), Smith and Merritt (2008) and Smith *et al.* (2020), most clay-rich diamicton units are judged here to have been formed subglacially; gravel, sand and silt deposits record glaciofluvial deposition, whereas laminated clay deposits formed mostly in a glaciolacustrine setting. The term ‘diamicton’ has been used following the definition of Martin *et al.* (2017), which states that ‘a diamicton is a granular deposit with limited fine-grained material that engineering geologists would describe as either gap-graded or part of a soil sequence containing lenses/layers of different grain-size materials’.

In total, 19 lithofacies are recognized in the study area as shown in Figure 5 and Table 2 (see also figs 5 and 7 of Smith *et al.* 2020). These occur in five facies associations that accommodate 11 sedimentary architectural elements (AE) and two mélange elements (Fig. 6). Deposition of sheet-like massive diamicton (facies association FA1, Fig. 6) is recorded by the occurrence of massive diamicton (matrix- and clast-supported) and laminated diamicton on bedrock sedimentary architectural elements (MD, MDc and DLbr), and pervasive and non-pervasively deformed mélange architectural elements (Mp and Mnp). Gravelly confined flow to unconfined flow deposition (FA2, Fig. 6) is recorded by presence of channel bar confined flow sedimentary architectural element (F1), unconfined flow gravel sheet element (F2), confined flow gravel clinoform element (F3), solitary sand/silt concave fill element (F4) and stacked, amalgamated sand/silt unconfined flow element (F5). Deposition of the transition from confined flow to lacustrine deposition (FA3, Fig. 6) is characterized by stacked amalgamated

Till / Glacioteconite			Stratified deposits		
Glacioteconic and till bounding surface	Appearance on exposure cross section annotations	Description of glacioteconic bounding surface	Order of sedimentary erosion bounding surface	Appearance on exposure cross section annotations	Description of sedimentary erosion bounding surface
No equivalent			7th		Surface representing the base of a major depositional system/complex – e.g. the bedrock surface at Sellafeld delineates the overlying ice-contact-related land system.
G.5th		Glacioteconic décollement and erosion surface representing the base and top (respectively) of a subglacially generated traction till	6th		Surface representing major boundary between groups of genetically-related facies associations. It delineates the base or top of a mappable stratigraphic unit – e.g. the boundary between a glaciofluvial outwash unit and an underlying till sheet.
No equivalent			5th		Surface that bounds specific facies associations
G.4th		Surface representing the transition between massive matrix-supported massive diamict element (subglacial traction till), and fissile, clast-supported, massive diamict (representing interfingering A and B horizons). Can be represented by a transition with no definable surface or a distinct surface typically representing a shear plane.	4th		Surface that represents facies contact that delineates packages of genetically-related lithofacies (delineates individual architectural elements with a characteristic geometry and lithofacies composition (e.g. channel bars))
G.3rd		Surface representing transition, often abrupt and represented by a shear plane, between glacioteconic element Mp (Type A (penetrative) glacioteconite) and element Mnp (Type B (non-penetrative) glacioteconite)	3rd		Surface representing facies contact which cross-cuts 0 to 2nd order surfaces – it may separate similar or dissimilar facies (e.g. contact between subaqueous bedforms recording a change in palaeoflow direction)
G.2nd		Surface, often indistinct, representing transition between element Mnp (Type B (non-penetrative) glacioteconite) and underlying, un-deformed sedimentary architectural element	2nd		Conformable facies contact separating dissimilar lithofacies (e.g. conformable contact between ripple crest and overlying draped clay)
G.1st		Surface representing a fault (thrust or normal fault) at the base of detached sediment package	1st		Surface representing facies contact separating similar lithologies
No equivalent			0th		Intra-unit sedimentary structure such as lamination

Fig. 4. Hierarchy of sedimentary unit bounding surfaces (after Boyce and Eyles 2000; Slomka and Eyles 2013, 2015; Pedersen 2014).

gravel, sand/silt element (F6) and rhythmite element (Rh). Sand-dominated, unconfined flow deposition (FA4, Fig. 6) is recorded by the occurrence of channel bar unconfined flow element (F1), unconfined flow gravel sheet element (F2) and stacked, amalgamated gravel, sand sheet element (F6), whereas high-energy channelized flow (FA5, Fig. 6) is characterized by the presence of large-scale high-discharge channel element (HDC). As shown in Figure 6, groups of facies associations record deposition in two distinct ice sheet related land systems: those displaying ice-contact architectures (FA1, FA2 and FA3), and those displaying proglacial architectures (FA1 (Mnp mélange element only), FA2, FA4 and FA5).

Channel bar concave element (F1)

Element F1 is a fine- to coarse-grained gravel with some cobbles and boulders. Clasts are subrounded to rounded and up to 70 mm in diameter. Imbrication together with planar and trough cross-bedding (Gp and Gt; Table 2 and Fig. 5) is displayed within the Peel Place Sand and Gravel Member (PPG) at Peel Place Quarry (section A–A', Fig. 7; section B–B', Fig. 8; section D–D', Fig. 9), whereas a much smaller development comprising massive, unstructured gravel (Gm) was observed within the Drigg Holme Sand Member (DHS) at Drigg Beach (location g, Fig. 10f). Element F1 typically rests on, or is interbedded with, fluvial sheet sands of element F5 as observed in BH7 (Smith *et al.* 2020), and in the exposures at Peel Place and Drigg Beach. Hence the upper boundary between F1 and overlying sediments is sometimes gradational (e.g. where it underlies element F5), but usually forms an abrupt second-order bounding surface. The lower bounding surface of the element

is typically concave-upward and erosional, and is commonly lined by a coarse-grained basal lag as shown in Figure 9 (section D–D') and Figure 10g (location g). The surface itself typically inherits the upper boundary of the unit below, which is commonly a fourth-order surface. Units of F1 are not typically laterally extensive and may be interbedded with or isolated within other elements such as F2 and F5.

Interpretation. The stacked sets of massive and planar or trough cross-bedded pebble gravel of element F1 are interpreted to form the infill of a variety of channel types within a fluvial environment generated by repeated meltwater flood cycles (see Miall 1985). The finer part of the element records cyclic sequences of reactivation of ephemeral channels during high stage flow conditions, depositing coarse-grained bedload during waning flow and finer grained material during abandonment (Williams and Rust 1969; Slomka and Eyles 2013). Coarser material may record the formation of scours owing to channel avulsion or confluence during higher energy flow events, with deposition of coarse-grained facies and boulders within the scours (Maren 2005; Kostic and Aigner 2007; Slomka and Eyles 2013), as shown in Figures 7–9. F1 elements probably represent incision of stable channels owing to base-level change and/or avulsion and deposition of subaqueous bedforms within the channel (Miall 1985; Olariu and Bhattacharya 2006; Slomka and Eyles 2013).

Unconfined flow gravel sheet element (F2)

Element F2 comprises a medium- to very coarse-grained sand and gravel. It is locally massive (Gm) or horizontally laminated (Gh), but trough and planar cross-bedding (Gt and Gp) are most typical,

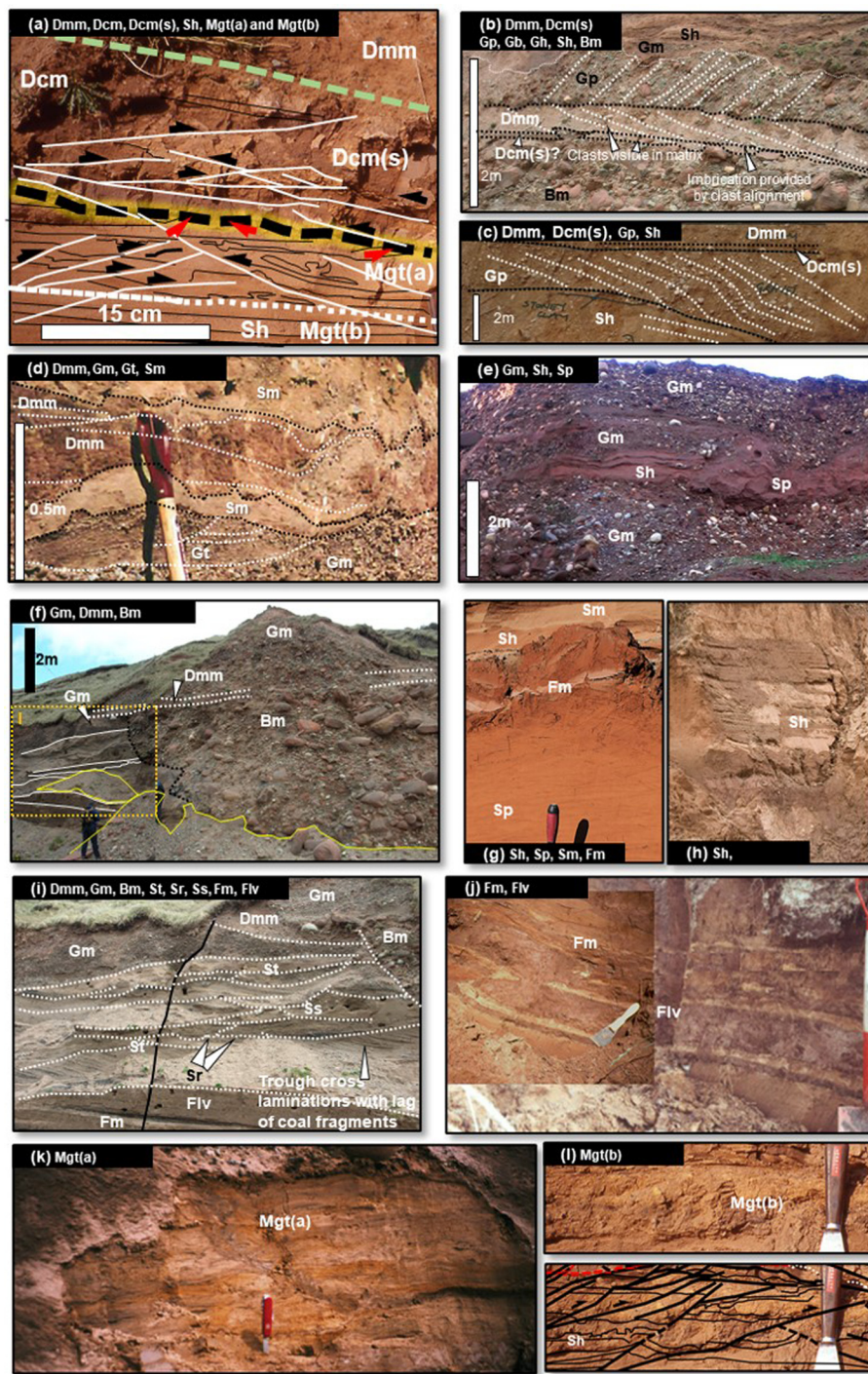


Fig. 5. Representative lithofacies. (a) Subglacial till at Drigg Beach: Dmm overlying sheared sandy Dcm(s) with Sh at base. (b) Subglacial till at Nethertown: Dmm and Dcm(s) sandwiched between Gp and bouldery Bm. (c) Subglacial till in temporary site investigation at Sellafield: Dmm and sheared Dcm(s) overlying Gp. (d) Subglacial till at Peel Place Quarry: Dmm overlying structureless sand (Sm), trough cross-bedded Gt and Gm. (e) Proximal outwash at Peel Place Quarry: structureless gravel (Gm) interbedded with Sh and Sp. (f) Catastrophic flow at Nethertown: chaotic boulder gravel (Bm) capped by subglacial till (Dmm). (g) Distal outwash facies at Drigg Beach: planar cross-laminated sand (Sp) passing up into Sm and Sh. (h) Distal outwash at Drigg Beach: horizontally laminated sand (Sh) (height of face = 1 m). (i) Complex of facies at Nethertown (see inset shown in (f)), including Dmm, laminated silt (Fl), sigmoidally laminated sand (Ss), trough cross-laminated sand (St), Gm and Gp (height of face = 1 m). (j) Subaqueous facies at Drigg Beach: laminated clay and silt (Fm), locally with silt graded couplets (Flv); mélange lithofacies at Drigg Beach. (k) Type A glacioteconite (Mgt(a)). (l) Type B glacioteconite.

with the geometry of foresets recording a southeastward palaeo-flow direction. The element consists of thick, laterally extensive, fine- to coarse-grained gravel sheets with a tabular geometry within the PPG in Peel Place Quarry (section A–A', Fig. 7) consisting of clast-supported pebbly gravel with some sand. The element is generally massive and structureless (lithofacies Gm as in Table 2 and Fig. 5) as displayed in the PPG at Peel Place Quarry where F2 forms several laterally extensive and laterally continuous units overlying a thick sequence of silts and sands of element F5 (section A–A', Fig. 7; section C–C', Fig. 9), and at Drigg Beach where element F2 is represented by the lower gravelly unit of the PPG (Fig. 10f–h), together with smaller developments at the base of the DHS, and stratigraphically higher in the sequence (Fig. 10b and c). Element F2 also can be seen in the cliffs at Seascale beach, where it

forms a laterally continuous sheet (Fig. 11), and at Ravenglass (Fig. 12). It locally displays planar cross-bedding (lithofacies Gp) as within the PPG at Drigg Beach, where clinoforms indicate a southeastward palaeoflow direction.

Both upper and lower surfaces typically display a horizontal to subhorizontal topography and are covered unconformably by till sheets or other fluvial sheet-like elements, as at Sellafield (Fig. 13) and Drigg Beach (Fig. 10), although both surfaces may also display hummocky or non-horizontal relief.

Interpretation. Element F2 is interpreted as fluvial sheet gravel or channel floor sediment (*sensu* Thomas and Chiverrell 2007). Observed clinoforms are interpreted to be foresets, recording downstream aggradation and migration of gravel bars in a braided fluvial environment (see Miall 1985; Reesink and Bridge 2009).

Table 2. Lithofacies with descriptions and interpretations (see also Fig. 5)

Facies	Description	Relevant figure	Interpretation	Equivalent 3D modelling unit
1 Dmm	Clayey, gravelly diamict (till ‘boulder clay’). Dark brown or red, stiff, matrix-supported, massive clay-rich, gravelly, diamict with subangular to rounded clasts up to 90 mm. Slight imbrication seen at outcrop; evidence of deformation seen in XCT images. Typically, uppermost till unit	Figure 5a–d, f and i; figures 5 and 6 of Smith <i>et al.</i> (2020)	Till deposited subglacially. Presence of shattered clasts and imbrication, but lack of shears and fractures, indicates that this forms the upper part of a tripartite division of till, possibly equivalent to the A horizon of Benn and Evans (2010) and Evans <i>et al.</i> (2006)	Clay
2 Dcm	Sandy, clayey diamict (till). Orange brown, very stiff, slightly sandy, matrix- to clast-supported clayey diamict. Medium to coarse clasts up to 50 mm. X-ray of borehole core (BH7) shows increased sand content, as does outcrop. No evidence of deformation	Figure 5a; figure 5 of Smith <i>et al.</i> (2020)	Till deposited subglacially. Increased sand and gravel content suggests original deposition by mass flowage prior to subglacial deformation. Lack of clast imbrication and fractures together with shears and fractures within the matrix suggest that this facies represents a midpoint between basal ice and underlying substrate, like the A/B horizon of Benn and Evans (2010) and Evans <i>et al.</i> (2006)	CSAG (silty, sandy gravelly clay)
3 Dcm(s)	Sheared sandy, clayey, gravelly diamict (till). Pale brown, very stiff, gravelly (in places) clay. Fine- to coarse-grained, subangular to rounded clasts up to 90 mm, clast-supported. Sandy towards base, but less sand than Dcm. Highly compressed and deformed. Base: unconformable over sheared outwash deposits (Type A and B glaciectonites)	Figure 5a–c; figure 5 of Smith <i>et al.</i> (2020)	The lowest part of the tripartite till division suggested above, deposited subglacially by overriding ice, causing compression of unit and severe deformation leading to shear zones, fractures and other deformation features indicating proximity of substrate. Equivalent of B horizon of subglacial traction till (Benn and Evans 2010; Evans <i>et al.</i> 2006)	CSAG (silty, sandy gravelly clay)
4 Dml	Massive or slightly laminated stiff clay (till). Dark brown, very stiff clay. Highly compressed and deformed. Infills depressions in bedrock. Mostly structureless, but some laminations apparent	Not shown in figure	Lodgement till, deposited subglacially. Mostly eroded but forms infill in depressions in bedrock surface (Benn and Evans 1996, 2010; Evans <i>et al.</i> 2006; Smith <i>et al.</i> 2020)	Gravel
5 Bm	Coarse-grained, cobble and boulder gravel. Mainly clast-supported. Massive and structureless. Boulders up to 2 m in length	Figure 5b and f	Deposition by very high-energy debris flow, migration and deposition under jökulhlaup flow regime, similar to Type II, Bm lithofacies jökulhlaup deposits of Maizels (1997)	Gravel
6 Gm	Massive, medium- to coarse-grained (occasional cobbles) gravel. Mostly massive and structureless, occasional crude bedding observed	Figure 5d, e, f and i	Deposition by relatively high-energy debris flow and gravelly barforms under upper fan or braided river flow regime (Slomka and Eyles 2013)	Gravel
7 Gt	Trough cross-bedded, coarse-grained gravel (up to pebble size). Trough cross-bedded gravel units, often occurring with trough and planar cross-bedded sand (St)	Figure 5d	Migration and deposition of high-relief pebbly barforms, channels and bedload sheets in upper fan flow regime (Thomas and Chiverrell 2007)	Gravel
8 Gp	Planar cross-bedded, coarse-grained gravel (up to pebble size), planar cross-bedded gravel units	Figure 5b and c	Migration and deposition of pebbly barforms in upper fan flow regime following incision in sandur surface. Prograding, medium- to high-angle foresets up to 5 m tall may have formed on a prograding Gilbert-type delta (Smith 1990; Smith and Edwards 1991; Maizels 1997; Kostic <i>et al.</i> 2005; Longhitano 2008; Backert <i>et al.</i> 2010)	Gravel
9 Sm	Sand: structureless (massive), mottled orange or brown, coarsening upwards (medium- to coarse-grained)	Figure 5d and g	Migration and deposition of sheet sands infilling channel floors (Thomas and Chiverrell 2007)	Sand
10 Sh	Horizontally laminated, fine- to coarse-grained sand ranging in thickness from a few centimetres to 5 m. Bed-parallel laminations	Figure 5a, c, e, g and h	Migration and deposition of sandy barforms during unconfined flow events (i.e. not within channels) under upper flow regime conditions (Medici <i>et al.</i> 2015)	Sand
11 Sp	Planar cross-laminated medium- to coarse-grained sand. Planar cross-lamination. Units range in thickness from a few centimetres to 5 m	Figure 5e and g; figure 7 of Smith <i>et al.</i> (2020)	Migration of linguoid and transverse bars within a braided-river or mid-lower alluvial fan or delta front setting (Miall 1977; Hjellbakk 1997; Opluštil <i>et al.</i> 2005; Thomas and Chiverrell 2007; Slomka and Eyles 2013)	Sand
12 St	Trough cross-laminated medium- to coarse-grained sand units ranging in thickness from a few centimetres to 0.55 m. Trough cross-lamination	Figure 5i; figure 7 of Smith <i>et al.</i> (2020)	Migration of sinuous crested 3D dunes and scour fills within a mid-lower alluvial fan or braided river or delta-front depositional setting (Miall 1977; Hjellbakk 1997; Opluštil <i>et al.</i> 2005; Thomas and Chiverrell 2007; Slomka and Eyles 2013)	Sand
13 Ss	Sigmoidally cross-laminated, medium- to coarse-grained sand ranging in thickness from a few centimetres to 0.5 m. Sigmoidal cross-lamination	Figure 5i	Interpreted to record the migration of sinuous crested 3D dunes and scour fills (Hjellbakk 1997; Opluštil <i>et al.</i> 2005; Thomas and Chiverrell 2007; Slomka and Eyles 2013)	Sand

(continued)

Table 2. *Continued*

Facies	Description	Relevant figure	Interpretation	Equivalent 3D modelling unit
14 Sr	Fine- to medium-grained, ripple-laminated sand. Often associated with fine-grained material such as silt and lacustrine clay. Sometimes located at the top of Sp facies	Figure 5i	Interpreted to record the migration of sinuous crested 3D dunes, scour fills and ripple trains (Miall 1977; Hjellbakk 1997; Opluštil <i>et al.</i> 2005; Thomas and Chiverrell 2007; Slomka and Eyles 2013). Thick developments of Sr facies associated with finer grained deposits such as silts may record rapid deposition of suspended sediment in a delta environment (Eyles and Clark 1985). Sr facies close to the upper surface of Sp facies record the ripple train migrating over the surface during waning flow (Reesink and Bridge 2009)	Sand
15 Fm	Silt with intercalations of fine to very fine brown to red sand, and coal, mostly massive and structureless, but with occasional horizontal and planar cross-laminations	Figure 5i and j	Deposition during unconfined flow events (i.e. not in channels). Records deposition during low flow velocities by fallout from suspension and traction currents in a low-energy environment, such as abandoned streams or glacial lakes (Slomka and Eyles 2013)	Silt
16 Flv	Clay and silt: grey and brown laminated clay and rhythmites (varves) of alternating clay and silt	Figure 5i and j	Records deposition in lacustrine, very low or zero flow environment by fallout from suspension, with occasional (seasonal?) input of slightly coarser silty sediment (Bennett <i>et al.</i> 2002)	Clay
17 Pe	Peat	Figure 10a	Vegetation records emergence of land surface	Peat
18 Mgt(a)	Deformed (ductile and brittle) clay, silt and sand horizons. Thin (millimetre to centimetre) apparently repeating horizons of brown and orange clay, silt and sand, with rootless and sheath folds forming a fabric or sometimes creating a homogeneous zone of deformation. Water release structures visible throughout. Sedimentary structure appears to be obliterated. Lithofacies often deformed by compressional brittle structures such as thrusts	Figure 5a and k	Type A glacioteconite: zone of intense ductile and brittle deformation that often occurs in the sediment immediately beneath a deforming bed (subglacial traction till). The original sedimentary structure is obliterated and replaced with a structural fabric formed by stretched sheath folds created during shearing (Benn and Evans 2010; Evans <i>et al.</i> 2006)	
19 Mgt(b)	Deformed (brittle only) horizons typically underlying Mgt(a) or Dcm(s). Typically comprising outwash lithofacies deformed by brittle deformation structures such as thrusts, but with the sedimentary structure still visible	Figure 5a, l	Type B glacioteconite: zone of less intense brittle deformation that often occurs in the sediment immediately beneath a deforming bed (subglacial traction till). The original sedimentary structure is obliterated and replaced with a structural fabric formed by stretched sheath folds created during shearing (Benn and Evans 2010; Evans <i>et al.</i> 2006)	

Confined flow gravel cliniform element (F3)

Element F3 comprises stacked sets of large planar cross-bedded, fine- to coarse-grained gravel (Gp). As the exposures shown in Figures 8 and 13 illustrate, the unit is several metres thick and mostly conformable with under- and overlying units. Multi-sensor core logging (MSCL) data from borehole BH7 at Sellafeld suggest that the element contains clay (Smith *et al.* 2020), although it is not clear whether this is within the matrix or as clay lenses. The element is sometimes continuous with F2, but with a visible lateral transition from Gp to massive, structureless Gm lithofacies typical of F2 (e.g. below location h, Fig. 10f). F3 possesses an upper surface that is typically flat and mostly horizontal, and mainly represented by an abrupt transition from coarse-grained gravel to overlying finer-grained sediment (compare the boundary between F3 and overlying F5 within the PPG at Drigg Beach; Fig. 10f–h), or an unconformable surface where it is overlain by subglacial traction till sheets. The lower bounding surface is also typically flat or horizontal, although units of F3 display onlap onto existing topography (e.g. location d, Fig. 10f), with cliniforms downlapping onto the surface of the underlying unit.

Units of F3 thus possess a similar sheet-like geometry to F2, with which they are often laterally continuous, ranging in thickness from <0.5 m to tens of metres, but with a much smaller lateral extent than

F2. Both upper and lower surfaces display a topography that ranges from relatively flat and subhorizontal, when deposited on a similar topography and covered unconformably by (for example) till sheets, to hummocky. Contrary to element F2, however, there is a prevalence for the lower surface to possess a concave appearance, whereas the upper surface sometimes displays a hummocky relief, as demonstrated at Sellafeld (Fig. 13) and Drigg Beach (Fig. 10).

Interpretation. The element is interpreted to represent migration of large-scale bedforms during periods of very high-energy flows (see Miall 1985, 1988; Marren 2005; Ghazi and Mountney 2009; Slomka and Eyles 2013). The presence of clay may be the result of reworking of the underlying clay unit, as at Sellafeld (Smith *et al.* 2020). Alternatively, if it is a component of the matrix, it may indicate sudden drops in energy regime with widespread dumping of sediment. The presence of clay lenses, however, implies more quiescent phases of sedimentation within relatively still water conditions. Like element F2, sheet-like geometries of lower surfaces reflect deposition on existing low-relief topography formed by sheet-style erosion during lower energy flooding events, or during emplacement of subglacial traction till. Concave lower surfaces reflect incision during high-energy flow, whereas hummocky relief upper surfaces typically represent erosion during deposition of overlying sediments or the results of proglacial deformation. As with element F2, cliniforms are interpreted to record downstream

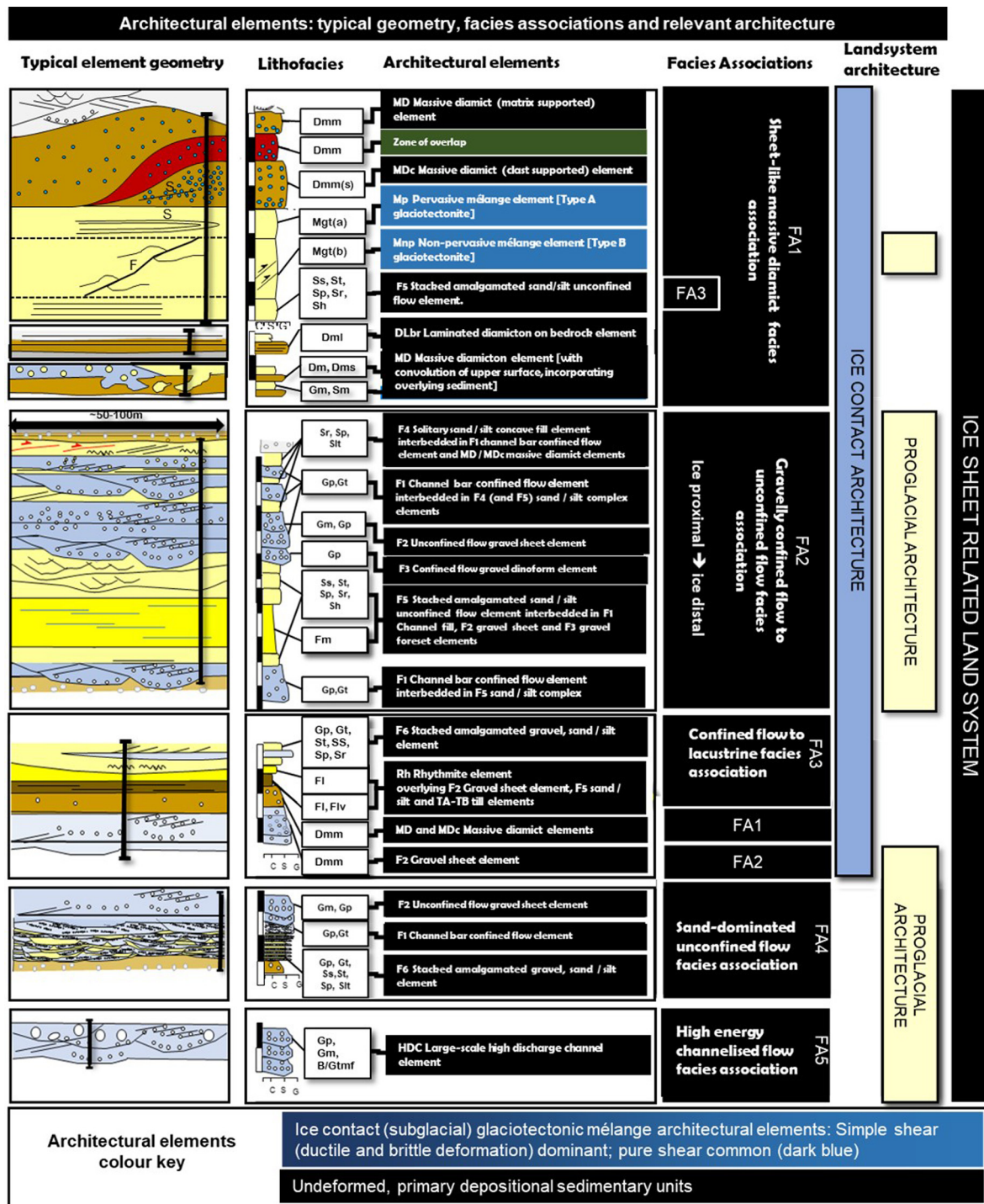


Fig. 6. Representative architectural elements depicting generalized geometries and facies associations characteristic of the study area.

aggradation and migration of gravel bars in a braided fluvial environment (see Miall 1985; Reesink and Bridge 2009).

Solitary sand/silt concave fill element (F4)

This element comprises mostly medium- to fine-grained sands exhibiting horizontal lamination (Sh). At Peel Place Quarry it is 1–3 m thick, several tens of metres in lateral extent, overlies elements F1, F5 and F6, and is overlain by element MD (Figs 7 and 9). Geometrically, F4 forms laterally thinning, onlapping units that infill depressions in the surface of underlying sediment. The upper surface is typically a subhorizontal erosion surface forming the base of overlying coarser material.

Interpretation. This element records a train of superimposed bedforms that represents a decrease in energy of the depositional system in response to declining discharge, leading to short-lived sand-dominated deposition in a braided river or mid-fan environment (see Miall 1977, 1985; Thomas and Chiverrell 2007; Reesink and Bridge 2009; Slomka and Eyles 2013).

Stacked, amalgamated sand/silt unconfined flow element (F5)

This element is similar in style to F4, but rather than a solitary development, it comprises laterally extensive sheets up to 20 m thick, comprising stacked horizons of sand and silt. Horizontal laminations

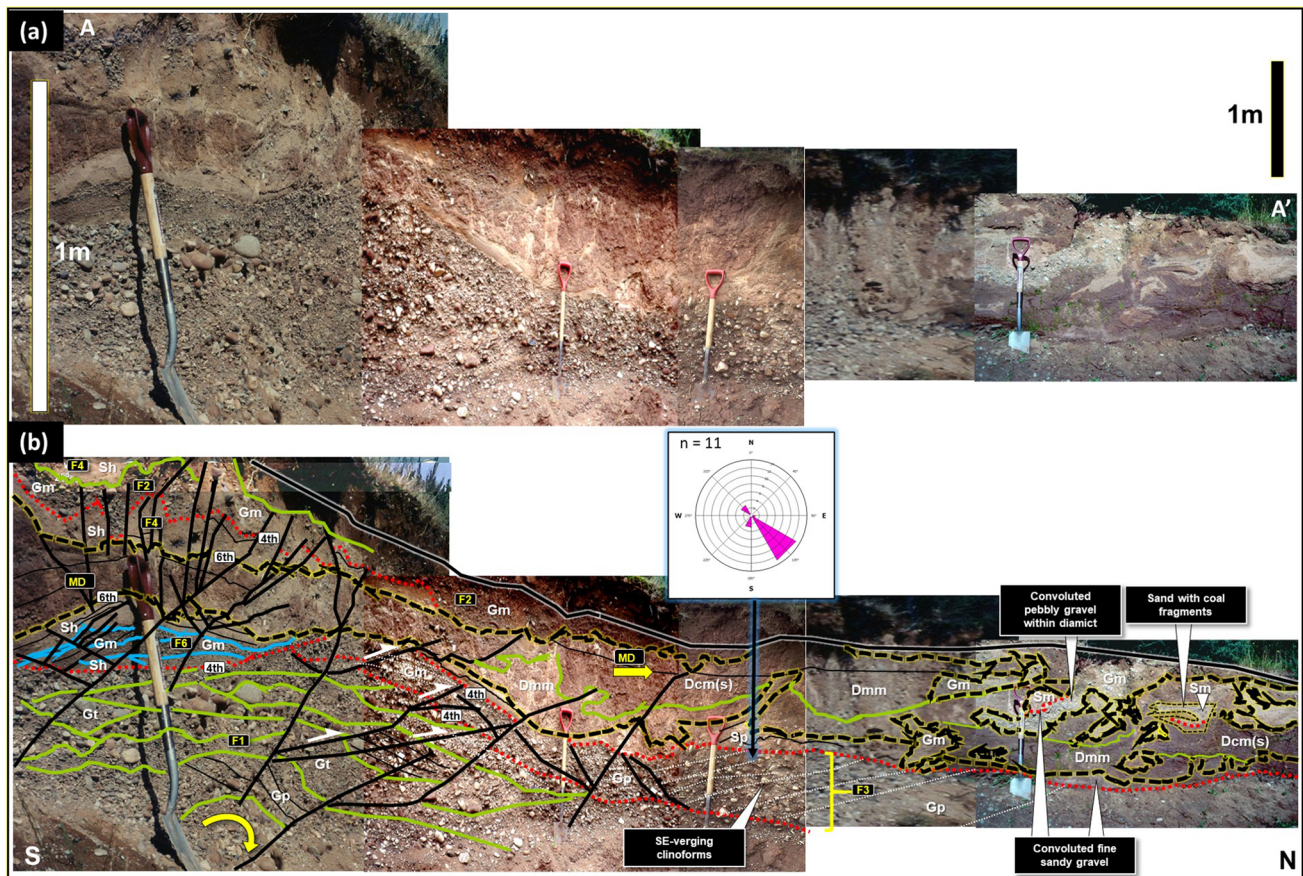


Fig. 7. Quarried section A–A' at Peel Place Quarry (location shown in Fig. 8), illustrating gravel sheet element F2 unconformably overlying solitary sand/silt complex F4, which itself overlies a contorted diamict unit (MD), with a contorted or convoluted top and brittle deformation features at its northern end. Under this is a unit of stacked, amalgamated gravel sand and silt element F6, which overlies confined flow gravel clinoform element F3 (note clinoforms displaying a mean SE palaeoflow direction [as per palaeoflow rose diagram]) and gravel channel bar concave fill element F1 (mean palaeoflow direction indicator rose diagrams compiled from clinoform data), photograph date 1990s).

(Sh) are common, as are planar cross-laminations (Sp). Exposures of F5 have been observed at several locations, including within the Sellafeld site (Fig. 13), where it forms horizontally laminated sand units up to 5 m thick. At Peel Place Quarry it forms the lower 3–7 m of a thick (<14 m) coarsening-upward sequence of interbedded silts, sands and gravels (PPG), as shown section B–B', Figure 8, and section D–D', Figure 9. Thinner (<1 m) exposures of element F5 have been observed in the cliffs at Drigg beach within the DHS, where a thick sequence of silts and fine to medium sands are interbedded with clays of element Rh, sheet gravels (F2) and lag gravels (F1). Glaciofluvial palaeoflow indicators such as clast orientations and cross-bedding indicate SSE-directed palaeoflow (Merritt and Auton 2000). Element F5 is clearly visible in exposures observed at Seascale (Fig. 11a and b) and Ravenglass (Fig. 12a and b), where it forms thin sheets of sand overlying and interbedded with elements F1, F2 and F3, with which it forms fining-upward cycles. F5 typically underlies till sheet elements MD and MDc, and at several locations has been glaciotectonically modified to form new mélangé elements Mp and Mnp (described below).

The observed thickness of <1 m to over 10 m is comparable with that observed in MSCL data from Sellafeld (Smith *et al.* 2020). This element has a conformable, commonly gradational fourth-order bounding upper surface, which is commonly difficult to define as it has typically been created by erosion during deposition of the overlying unit. In such circumstances it is represented by either a fourth- or a sixth-order surface. The lower bounding surface of the element is typically conformable on underlying elements.

Interpretation. Element F5 is interpreted to represent fields of superimposed fluvial bedforms, deposited in an unconfined, sand-dominated braided river or mid- to lower-fan depositional environment,

also as sheet flood deposits during periods of less energetic flow (see Miall 1977, 1985; Reesink and Bridge 2009; Slomka and Eyles 2013).

Stacked, amalgamated gravel, sand and silt confined flow element (F6)

This element comprises planar and sigmoidal cross-bedded (Sp, Ss) and horizontally laminated (Sh) sand, together with units of trough and planar cross-stratified pebble gravel (Gt and Gp) as shown in the exposures in Peel Place Quarry (Figs 7 and 9) and at Drigg Beach (Fig. 10c). Clay is sometimes present in the matrix and as clay stringers, leading to a variable density profile on MSCL data (see Smith *et al.* 2020, fig. 7). The element is a few metres thick at Sellafeld, but >6 m at Peel Place Quarry, where couplets of gravel and sand are clear. It is highly likely to occur throughout the succession at Sellafeld. The upper boundary is undulating, reflecting either ridge development or erosion during deposition of the overlying unit. The lower bounding surface is not definable.

Interpretation. The cross-stratification visible at outcrop and on X-ray computed tomography (XCT) radiographs suggests that element F6 was deposited in laterally migrating, incised channels. Typically located at the base of gravel–sand assemblages, where it overlies sand, the element probably represents fresh incision into older depositional surfaces after a shift in distributary location.

Rhythmite element (Rh)

Element Rh comprises thinly interlaminated clay and silt (Flv), typically forming graded couplets (Flv). Similar deposits form two thick (<30 m) sequences beneath Lower Wasdale (Merritt and

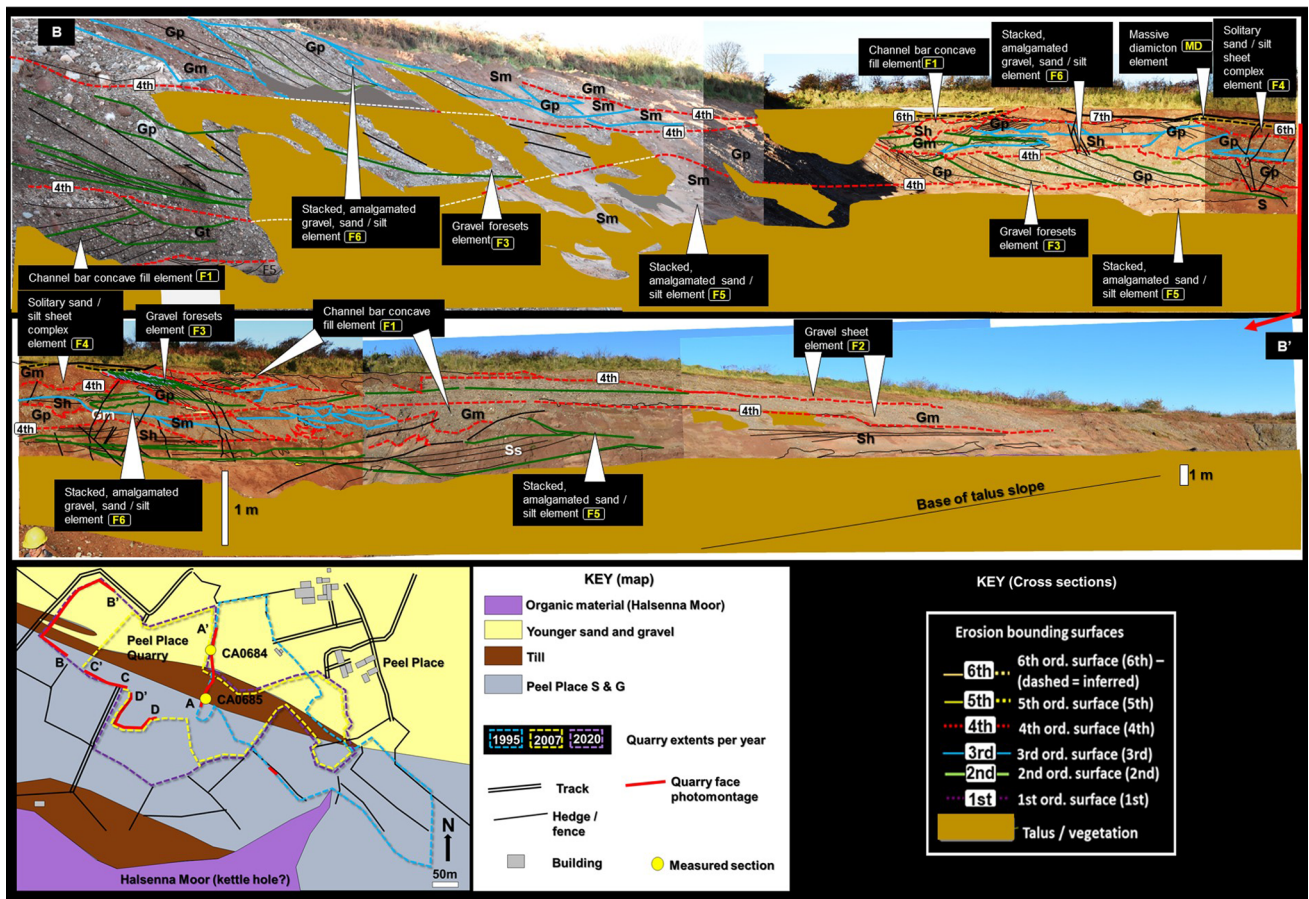


Fig. 8. Quarried section B–B' at Peel Place Quarry (location shown in Fig. 8), illustrating channel bar concave fill element F1, gravel sheet element F2, gravel foresets element F3, solitary sand/silt sheet complex element F4, stacked, amalgamated sand/silt element F5 and stacked, amalgamated gravel, sand/silt element F6, and subglacial traction till element MD (photograph date 2020).

Auton 2000). Laminated clays are recorded on numerous borehole logs in the region, but three thin (<1 m) units exposed in the cliffs at Drigg Beach are much more restricted in their lateral extent, infilling and onlapping onto pre-existing topography of underlying units (Fig. 10c, f and h). We recorded no evidence of limestones within the exposed units.

Interpretation. This element represents subaqueous deposition in a low-energy, glaciolacustrine environment. A thin section of a sample of the lower sequence (Carleton Silt Formation, Fig. 3) taken from borehole QBH 20 near Hall Carleton, in Lower Wasdale (Fig. 1), revealed rhythmic, upward-fining silt–clay couplets, well-developed fine internal lamination and dropstones, confirming that the graded laminae are true, annually deposited varves (Nirex 1997k). The upper sequence (Whinneyhill Clay Member, Fig. 3) includes similar graded couplets (Merritt and Auton 2000), but other occurrences may simply represent episodic input of slightly coarser material during fluvial or slump activity into otherwise still water. Deposition mostly occurred within ice-dammed lakes that formed at several localities and times (Trotter *et al.* 1937; Huddart 1991; Merritt and Auton 2000; Coleman *et al.* 2020).

Large-scale high-discharge channel element (HDC)

Element HDC has been observed at Nethertown (Fig. 14), where it comprises a thick, chaotic body of cobbles and boulders of up to 2 m in diameter (the Townhead Boulder Gravel Member of Merritt and Auton 2000). The lower boundary of the unit is highly erosive, channelized and locally undercuts the underlying F5 element. The whole body exposed at Nethertown is over 25 m wide and a little over 6 m in height.

Interpretation. Element HDC records very high flow energies, transporting huge boulders that infilled channels created by the flow itself. Recent jökulhlaup events in Iceland recorded flows of around $4500 \text{ m}^3 \text{ s}^{-1}$ in similar ice-proximal areas (Maizels 1997; Russell *et al.* 2000, 2010; Duller *et al.* 2008; Slomka and Eyles 2015).

Laminated diamicton on bedrock element (DLbr)

The most striking exposure of element DLbr can be seen at St Bees where it is represented by the Lowca Till Member, which can be observed directly overlying fractured bedrock of the Triassic-aged Chester Formation (St Bees Member). In the Sellafeld–LLWR area the element also rests on bedrock and is represented in Blengdale and beneath Lower Wasdale (for example) by the Holmrook Till Member (HRT) of the Blengdale Glacigenic Formation, which is exposed downstream of Bleng Bridge, near Gosforth (Fig. 1). At Ravenglass (Fig. 12) and Seascale (Fig. 11c) this element is represented by the Ravenglass Till Member (RVT), which comprises a very stiff, matrix-supported, massive, stony, silty clayey diamicton (Dmm or Dml containing moderately well-dispersed, angular to well-rounded clasts up to boulder size of granophyre, granite, Borrowdale Volcanic Group lithologies and siltstones; some red sandstone, ironstone concretions and shell fragments are also present (Merritt and Auton 2000). At Ravenglass this element possesses bed-parallel and near vertical joints that strike $074\text{--}096^\circ$ (Fig. 15a–c). DLbr possesses a well-developed clast microfabric, which gives it a laminated appearance.

The element is <5 m thick at Ravenglass, where it is deformed into roughly east–west-trending folds with a wavelength of 20 m and an amplitude of 3 m. It has a sixth-order upper bounding surface

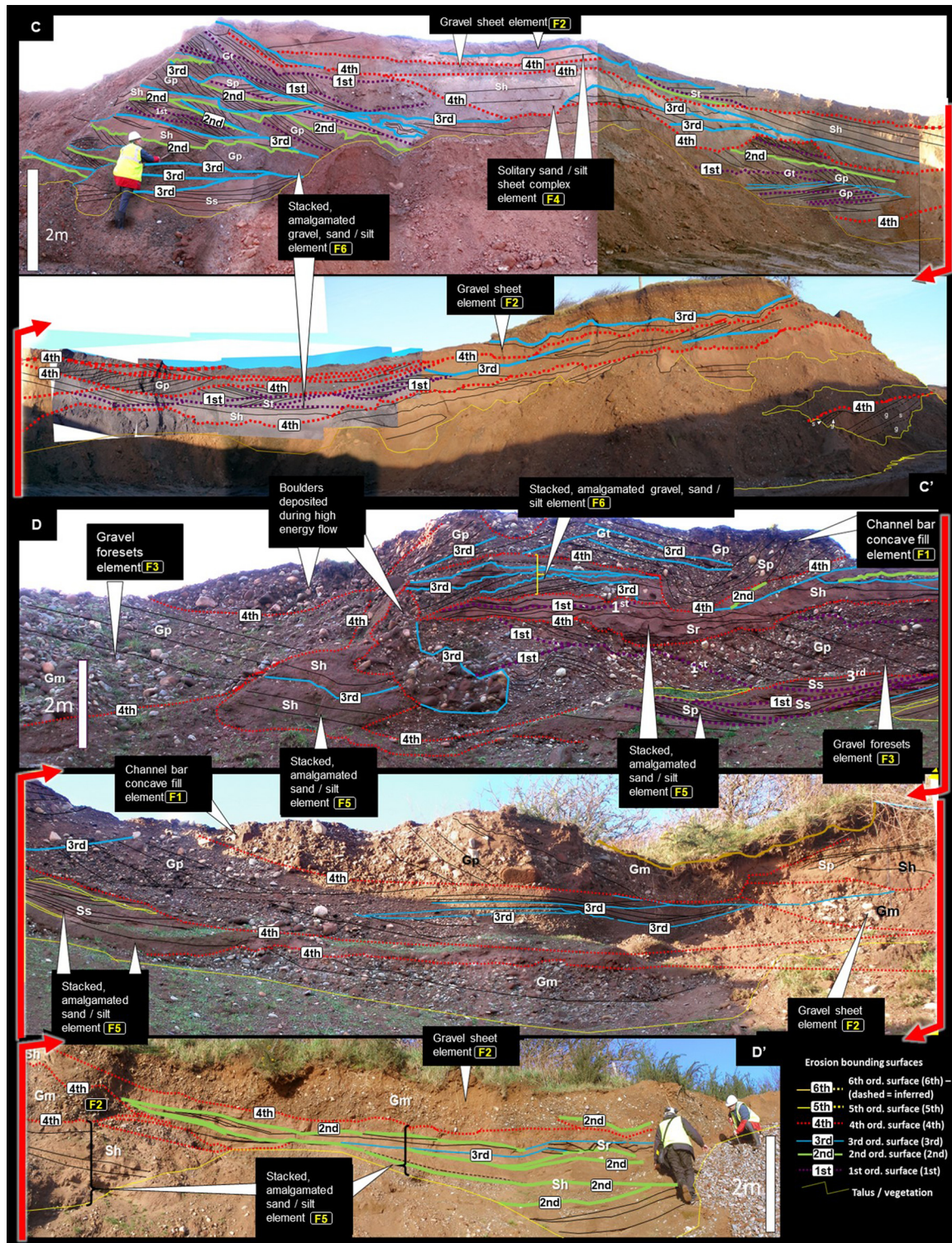


Fig. 9. Quarried sections C–C' and D–D' at Peel Place Quarry (location shown in Fig. 8), illustrating channel bar confined flow element F1, gravel foresets element F3, stacked, amalgamated sand/silt unconfined flow element F5, and stacked, amalgamated gravel, sand/silt element F6 (photograph date 2009).

that has a gently undulating or hummocky relief, also observed at Seascale. Folds are bisected by shallow-angle to steep thrusts that are sometimes lined by wispy laminae of sand. At Ravenglass the lower surface is represented by a seventh-order lithostratigraphic boundary and unconformity where the element rests on bedrock. In other locations, such as in the vicinity of the LLWR site, it rests unconformably on an older sequence of tills and outwash sediments and is therefore underlain by a sixth-order surface. At both Ravenglass and Seascale the element is overlain by a conspicuous thin (5–8 cm) seam of yellow–brown, thinly laminated silt or very

fine-grained sand that locally merges with wispy veins within the diamicton below (Fig. 12b and c) (Merritt and Auton 2000). At St Bees clear deformation of underlying bedrock can be observed under the Lowca Till Member, in the form of fractured and displaced blocks of sandstone. Clay can be observed infilling the fractures.

A thin section of a sample obtained from the Holmrook Till Member at Bleng Bridge is of a coarse- to very coarse-grained, very poorly sorted, immature, lithic-rich, open-packed, matrix-supported, massive diamicton, illustrating microfeatures of element

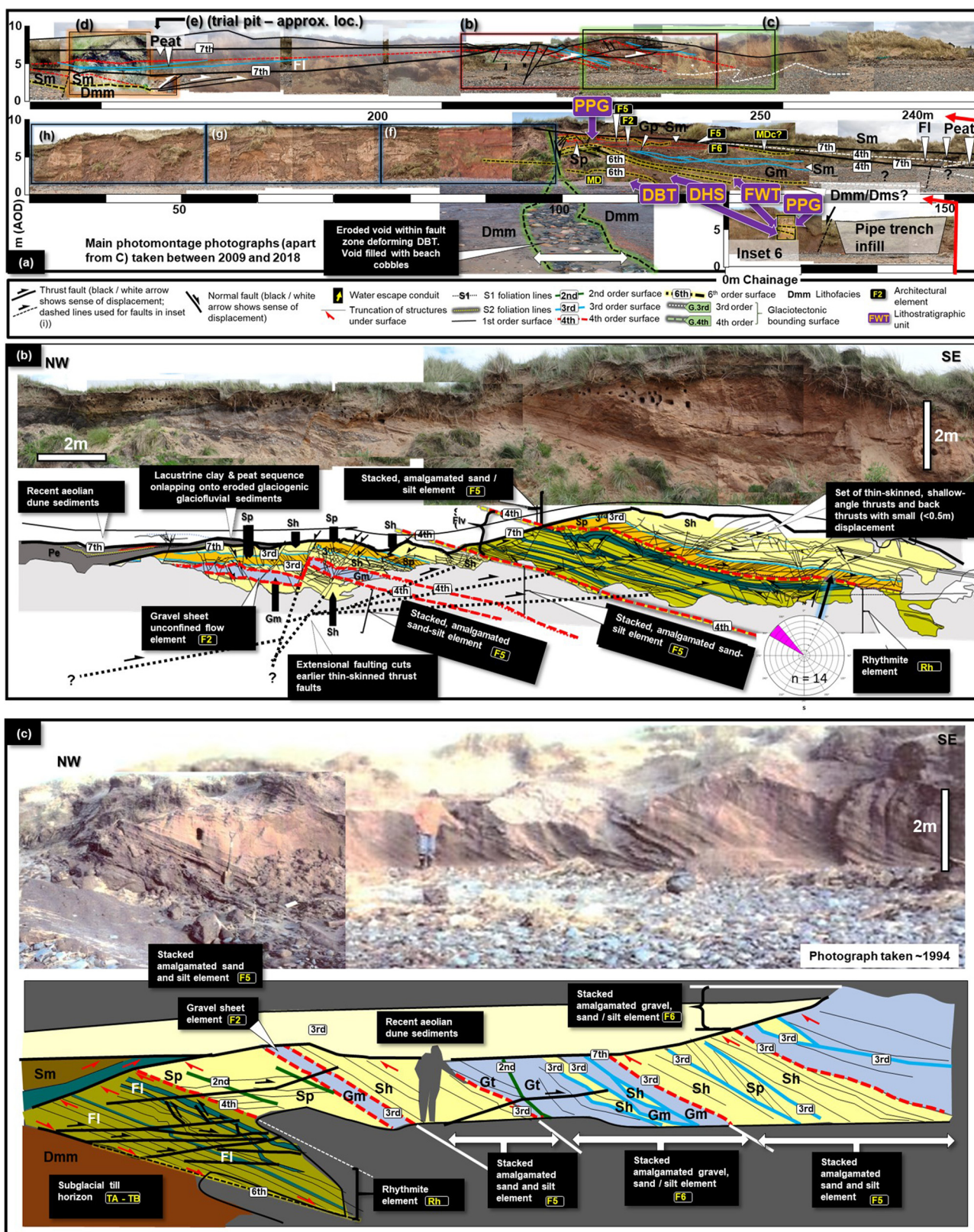


Fig. 10. Photomontage and interpretation of the cliff exposure and foreshore at Drigg Beach. (a) Overall montage showing eroded glacial sequence unconformably overlain by a sequence of post-glacial lacustrine clay-peat (bounded at the top and base by seventh-order surfaces), themselves overlain by recent aeolian dune deposits. (b) Southerly dipping, rhythmite element Rh interbedded with elements F2, F5 and F6, deformed by set of southerly verging high-angle thrusts and back-thrusts and accompanying compressional folds, themselves overprinted by conjugate extensional faults. (c) Deformed exposure (overlaps with (b)) showing element Rh overlapping onto elements MD-MDc, and overlain by interbedded elements F5, F2 and F6. Palaeoflow direction indicator rose diagrams compiled from clinof orm data.

DLbr (Fig. 16a), but containing no obvious sedimentary structures (Nirex 1997k). Clasts are angular to subangular in shape with low to moderate sphericity, and comprise andesite, dacite, felsite,

microcrystalline granodiorite and granite. Also present are several diffuse, poorly defined or preserved pebbles of diamicton (possibly till). Clasts are locally enclosed within a rim or coating of slightly

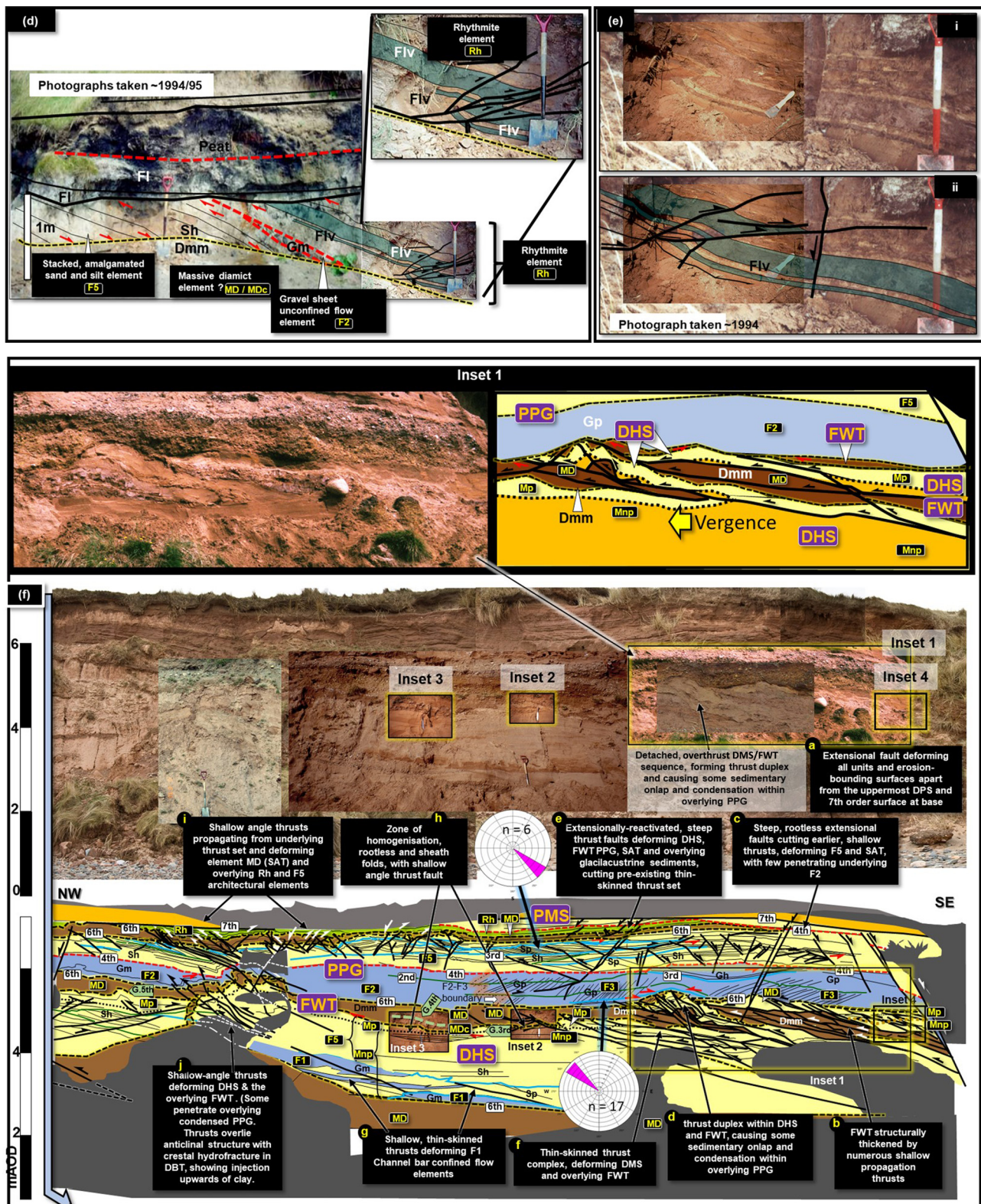


Fig. 10. Continued. (d) Elements F2 and F5 onlapping onto element MD–MDc and overlain by compressively deformed element Rh. (e) Photograph (date 1994) of exposure in trial pit dug some metres behind cliff, showing southerly verging, shallow-angle thrusts deforming element Rh. (f) Photomontage and interpretation of cliff to north of extensional fault at 100 m, illustrating three instances of elements MD–MDc, interbedded with elements F1, F2, F5 and F6, some of which have been modified to become Type A and B glacioteconites (mélange elements Mp and Mnp respectively). Inset 1: higher resolution photograph and interpretation of northerly verging thrust-duplex. (Insets 2–5 are shown in detail in Fig. 17 (inset 5 is shown in (h)). Palaeoflow direction indicator rose diagrams compiled from clinofold data.

darker clay or silt, and a well-developed concentric to weakly radial, circular arrangement of finer grained clasts can be observed locally adjacent to larger lithic clasts. This arrangement is commonly accompanied by a skelsepic plasmic fabric within the clay matrix or coating. Also noted is the localized development of a weak circular

arrangement of medium to coarse sand-grade clasts without any ‘core stones’ (Fig. 16a). The red–brown to orange–brown matrix is composed of fine silt and clay. At higher magnification a weakly developed lattisepic plasmic fabric, defined by short highly birefringent clay domains, has been observed. Towards the

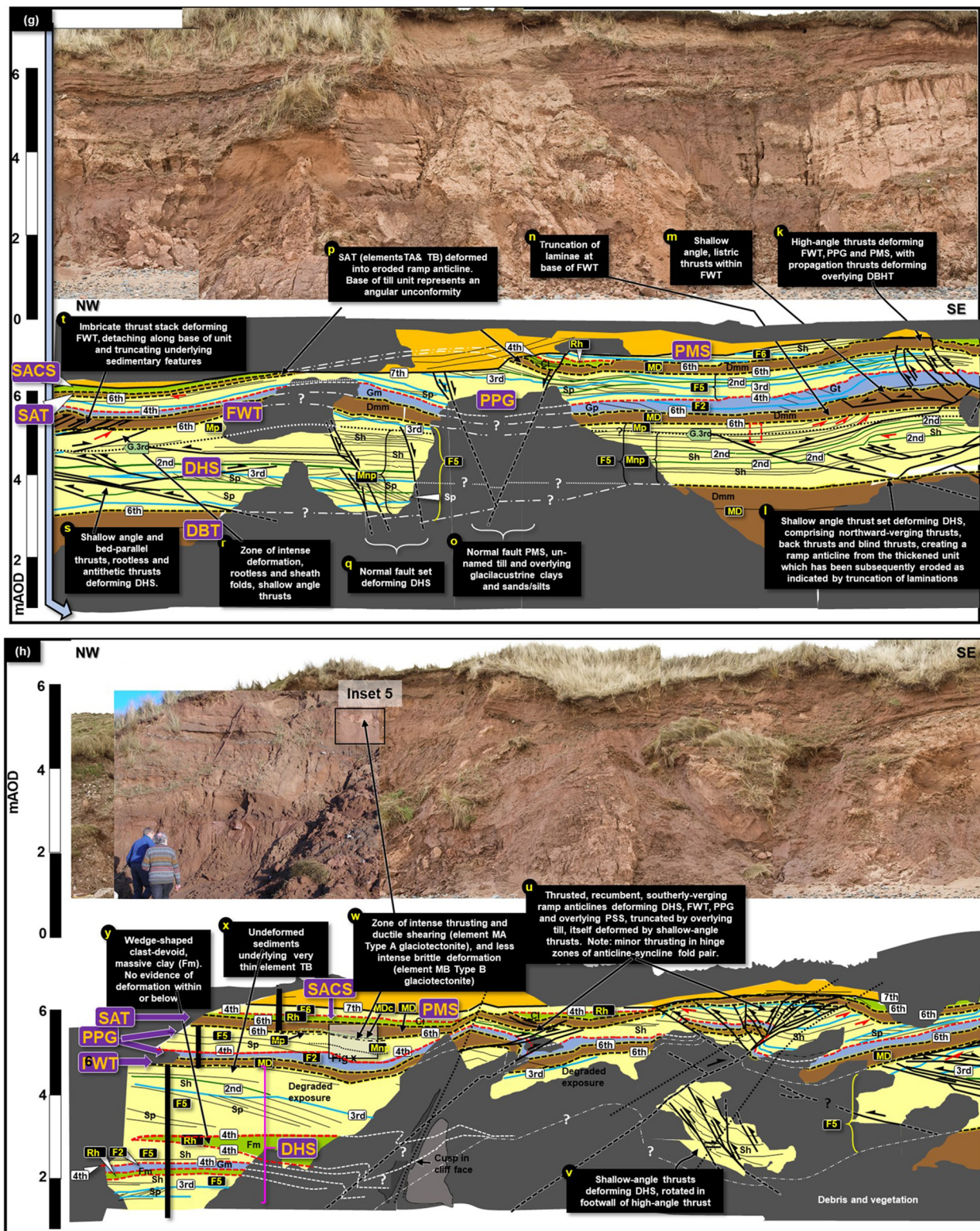


Fig. 10. Continued. (g) Continuation from (f). (h) Continuation from (g).

bottom of the thin section is a set of irregular fractures and voids filled with very fine-grained sand and silt. Some are filled by a microbreccia formed of small, randomly oriented fragments of the fracture walls.

Interpretation. Element DLbr possesses many of the attributes of a subglacial traction till (*sensu* Evans 2018). This interpretation is reinforced by the brittle deformation of underlying bedrock observed at St Bees. At Ravenglass and Seascale, initially, intra-unit deformation and intermixing would have occurred through

subglacial entrainment and soft-sediment deformation as the unit was originally accreted, but the truncated, intensely sheared top of the element observed at Ravenglass and Seascale was possibly formed during a subsequent glacial advance (Merritt and Auton 2000).

The observations made of the thin section described above are fully consistent with a subglacially formed diamicton containing abundant Borrowdale Volcanic Group and Ennerdale Intrusion pebbles derived from the Lake District. The microstructures and

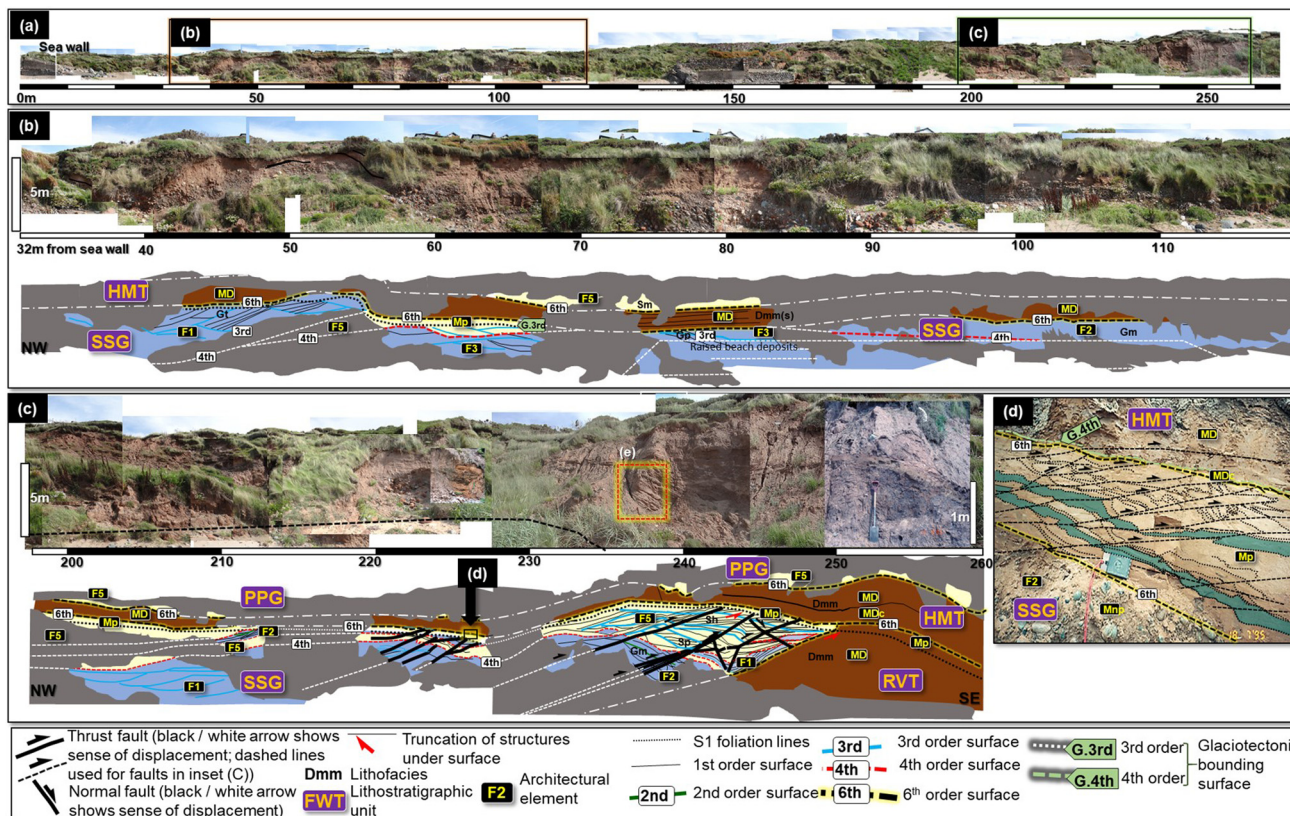


Fig. 11. Photomontage and interpretation of cliff exposures at Seascale Beach. (a) Whole section. (b) Element MD overlying F1, F2, F3 and F5, illustrating the local development of glaciotectionic element Mp and apparent absence of Mnp. (c) Element MD-MDC overlying fining-upward sequences comprising F1, F2 and F5, and locally directly on a lower unit of MD. (d) Inset showing where glaciotectionic element Mp is particularly clear and where the underlying brittle deformation represents element Mnp. (e) Inset shown in Figure 17e.

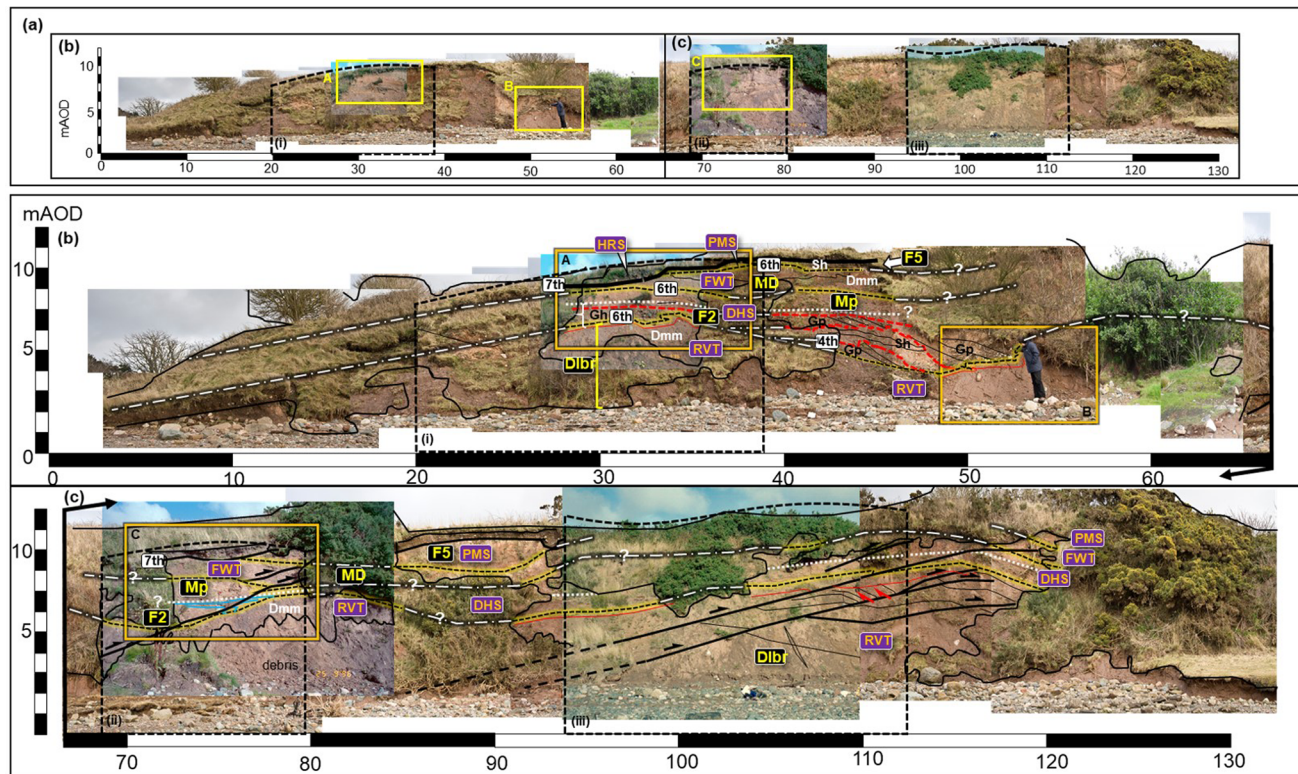


Fig. 12. Photomontage and interpretation of cliff exposures at Ravenglass. (a) Full montage. (b, c) Two units of element MD separated locally from units of F2 that become pervasively modified upwards into glacial mélangé element Mp. Insets A, B and C are shown in Figure 15; Insets (i), (ii) and (iii) represent those shown by Merritt and Auton (2000).

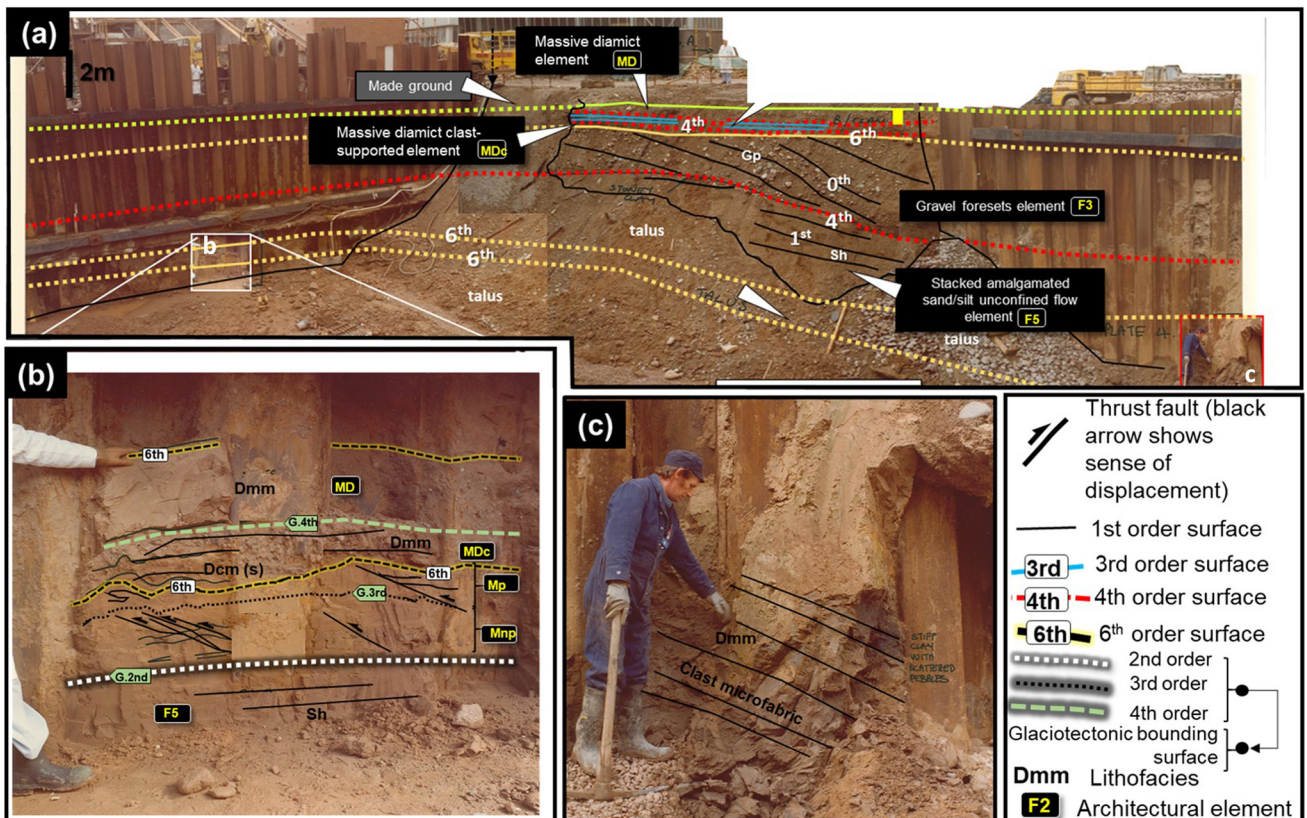


Fig. 13. (a–c) Deep excavation created during the 1970s at Sellfield. Three elements of subglacial till (MD, MDc) overlying gravel foresets (F3), with large planar cross-beds recorded in imbrication of cobble and boulder clasts. This unit overlies stacked, amalgamated sand/silt unconfined flow element (F5), which in turn overlies another development of MD–MDc. (Modified from Smith *et al.* 2020.)

larger structures both indicate a subglacial traction till. The microbreccia-filled fractures appear to have formed after the till was partially lithified and probably resulted from subglacial hydrofracturing (see Phillips *et al.* 2013a, b).

Massive diamict element (MD)

Element MD is generally a massive, poorly sorted, clay-rich, sometimes silty, fine- to medium-grained diamicton (Dmm) (Fig. 5 and Table 2), with blocky jointing and well-dispersed, angular to

subrounded granules and pebbles. Units range in thickness from *c.* 50 cm to >5 m, as observed at Drigg Beach (Fig. 10h), Ravenglass (Fig. 12), Seascale (Fig. 11) and Nethertown (Fig. 14). Two units of MD have also been recorded in a historical (1970s) excavation at Sellfield (Fig. 13) (Smith *et al.* 2020), and a probable correlative of the element is exposed at Cookson Wood, Holmrook (Fig. 1), where it includes striated blocks of sandstone (Nirex 1997g, k). It has also been penetrated by numerous boreholes, including Drigg offsite borehole C (Fig. 1), as described here.

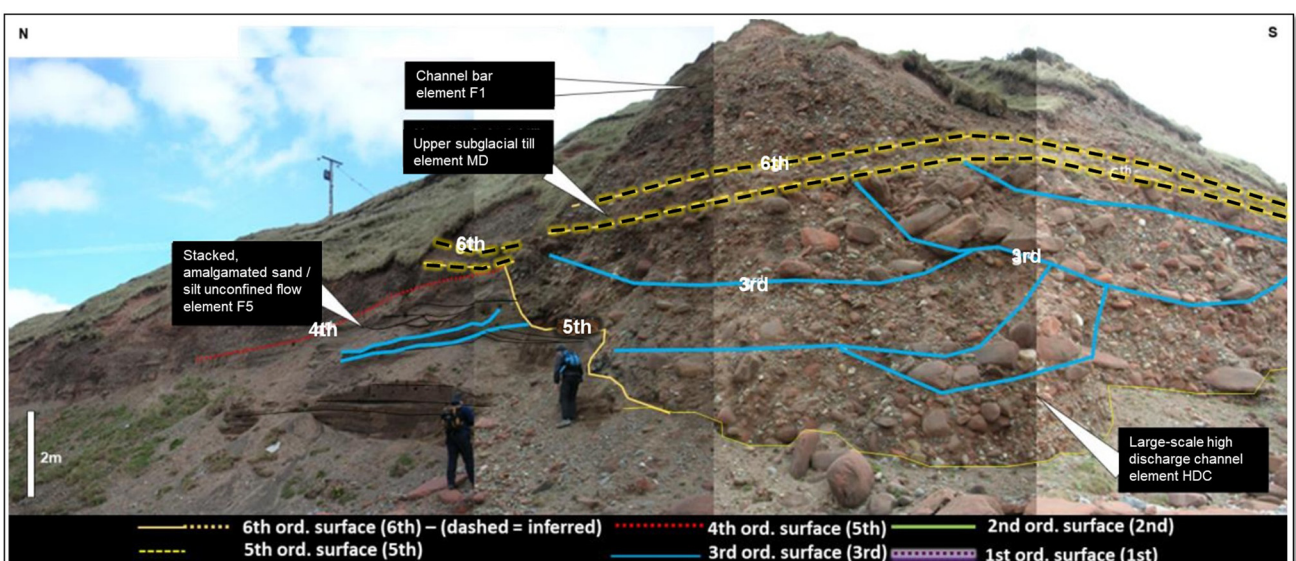


Fig. 14. Cliff exposure at Nethertown Beach, showing high-energy, large-scale discharge channel element HDC overlying stacked, amalgamated sand/silt unconfined flow element F5.

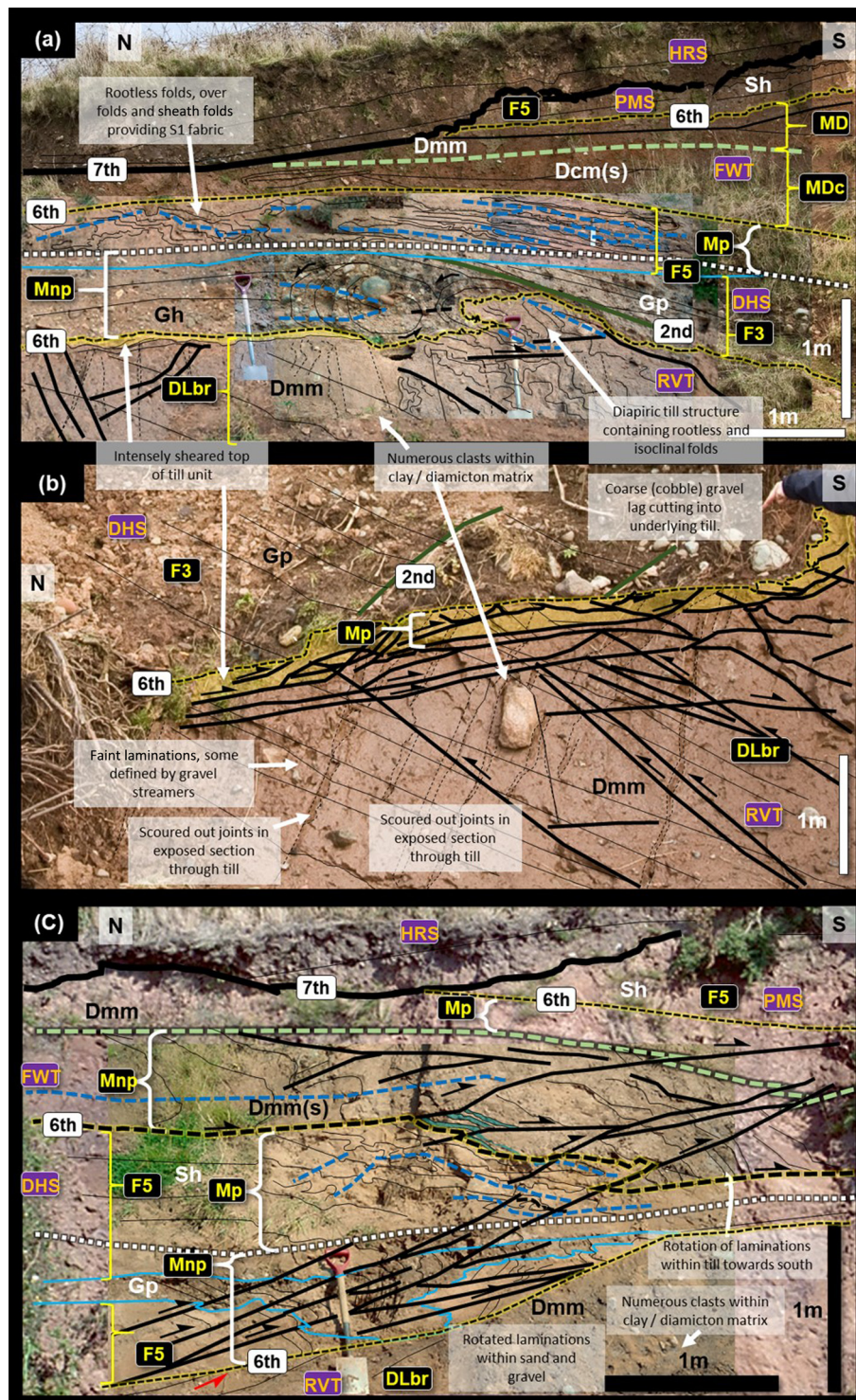


Fig. 15. Detailed insets of cliff exposures at Ravenglass (location shown in Fig. 12). (a) Northern end of exposure, inset A. (b) Middle of exposure, inset B. (c) Southern end of exposure, inset C. Showing element F5 overlying F3, sandwiched between RVT at the base of the exposure and the overlying FWT (both elements MD and MDc). F5 (modified to Mp) displays intense shearing, with sheath and rootless folds forming an S_1 foliation, all of which have been subsequently deformed by further thrusting and rotation.

The lowest exposed unit of MD (the Drigg Beach Till Member; DBT) at Drigg incorporates intraclasts of gravel, sand, silt and clay derived from underlying units (Merritt and Auton 2000). Few examples of macro- or meso-scale deformation were observed at any of the coastal exposures of the DBT, apart from large-wavelength folds and both compressional and extensional faults. These structures also deform the overlying sequence (Fig. 10a and b) and are thus post-depositional in nature. However, three thin sections obtained from the DBT and RVT in the 1990s provide useful microstructural information.

Thin section PY432 (Fig. 16b) was obtained from a sample of moderately brown, sandy clay diamicton (DBT) some 17 m down Drigg offsite borehole C (Nirex 1997k) (Fig. 1). The thin section is

of a poorly sorted, matrix-supported, fine- to medium-grained massive diamicton containing several well-dispersed, pebble-sized (>7 mm) lithic clasts. It reveals a broadly similar clast assemblage to that observed in the Holmrook Till thin section described above, including lithic clasts with a Borrowdale Volcanic Group and an Ennerdale Granite provenance. The clay to locally fine silt-grade matrix has no obvious planar fabric(s) or discrete shears, although a weak, sporadic skelsepic plasmic fabric and clay coatings are locally developed upon or adjacent to larger lithic clasts. The sample is cut by several irregular veinlets, which are infilled with opaque material and brown coloured clay. This poorly sorted, sandy diamicton is massive with no obvious sedimentary lamination or fissility, and no obvious deformation fabrics or

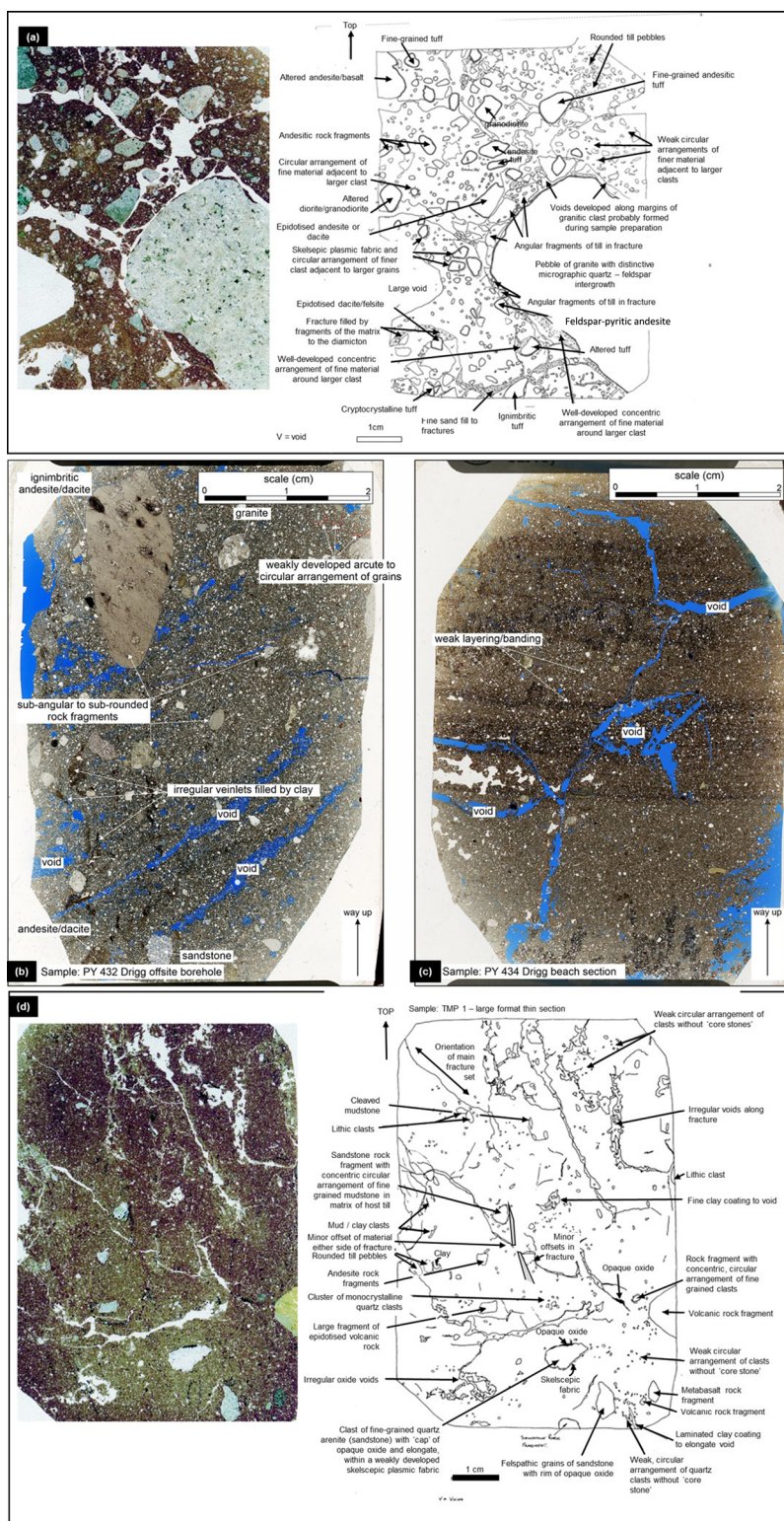


Fig. 16. Annotated thin sections of (a) element DLbr, and (b - d) element MD: (a) Sample TMF 3 of stony diamict (HRT) collected near Blanddale Bridge. (b) Sample PY432 of RVT/DBT obtained from Drigg offsite borehole C. (c) Sample PY 434 of DBT from Drigg Beach. (d) Sample TMP 1 of clay-rich diamict (FWT) exposed at Cookson Wood, Holmrook. BGS registered samples and images, modified from Nirex (1997g, k) [©UKRI 2022; ©Nuclear Decommissioning Authority 2022].

textures. Apart from minor brittle fractures the sample is relatively undeformed.

Thin section PY434 (Fig. 16c) was obtained from exposures of the DBT at Drigg Beach and comprises a thinly interlaminated, very compact, fine- to medium-grained sand and pebbly silty clay diamict containing very well-dispersed fine pebbles (Nirex 1997k). The thin section shows a fine-grained, matrix-rich and weakly laminated diamict, where the lamination is defined by a slight colour variation within the clay matrix. No obvious grading has been recognized. The sample possesses a similar clast assemblage to PY432. The matrix is very fine-grained (clay- to

silt-grade) and is locally stained dark by a secondary opaque or organic phase. A variably developed lattiseptic to omnisepic plasmic fabric, defined by aligned, high-birefringent (in cross-polarized light) clays, is locally developed within the matrix, although the later staining overprints these fabrics. Also visible are circular arrangements of quartz clasts, and alignment of fine silt-grade clasts adjacent to the relatively large clasts. There are hints of a weakly developed skelsepic plasmic fabric next to the latter.

X-ray computed tomography data of core from a borehole drilled within the Sellafield site exhibits additional evidence of two anastomosing microfabric crenulation fabric domains in the form of

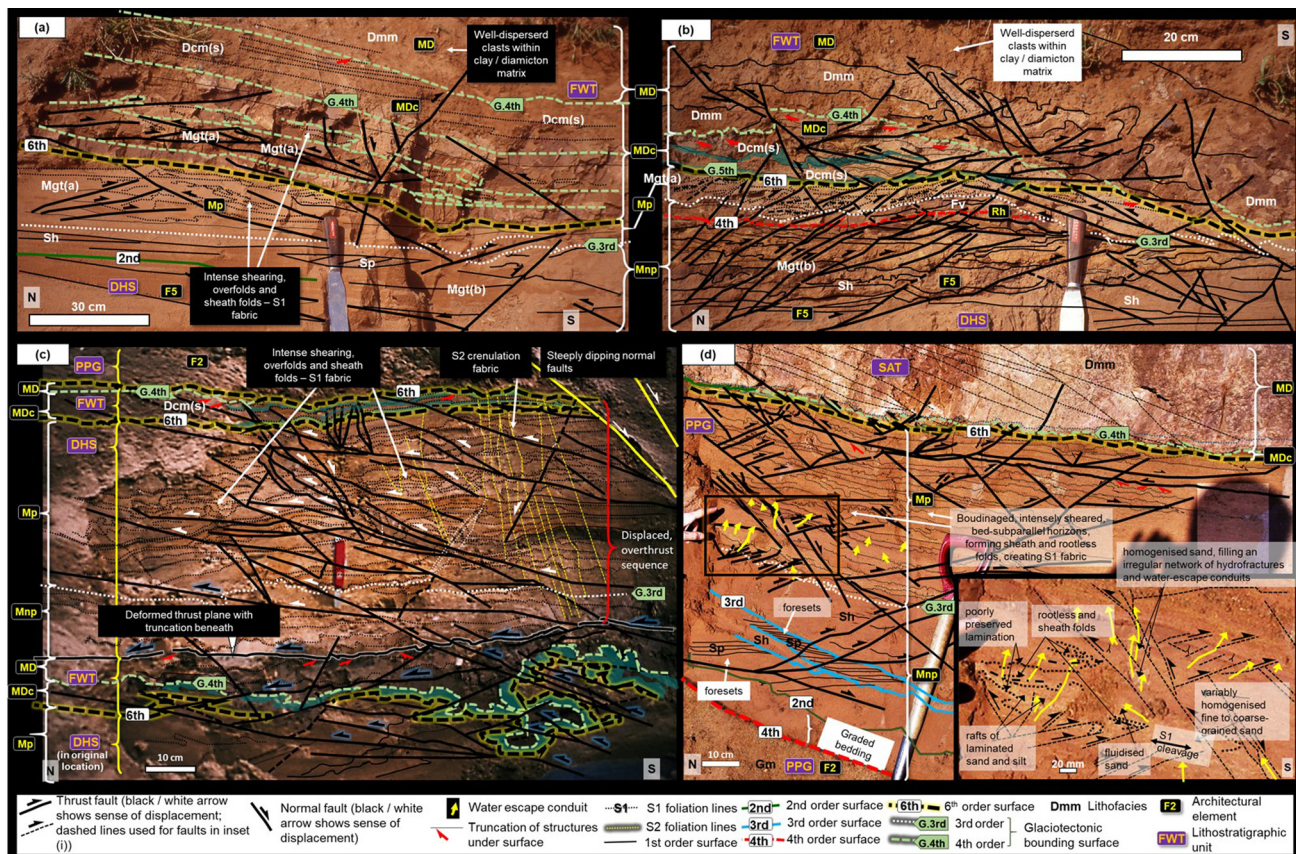


Fig. 17. Detailed insets 2–5 of the Drigg Beach section (location shown in Fig. 10). (a) Inset 2. (b) Inset 3: deformed units at the interface between the DHS and overlying FWT, comprising architectural elements F5/Rh, and MD/MDC, respectively. The DHS has been modified from F5 to an upper zone of penetrative (Type A) glaciectonite with an S_1 foliation, representing glaciectonite *mélange* element Mp, and an underlying zone of brittle, non-penetrative (Type B) glaciectonite representing glaciectonite *mélange* element Mnp. (c) Inset 4: overthrust component of elements MD, MDC, Mp and Mnp, illustrating development of a nearly vertical S_2 fabric. (d) Inset 5: zones of penetrative and non-penetrative deformation in the upper sand component of the PPG, underlying a hitherto unreported additional subglacial traction till unit at this site, named here as the Sandy Acre Till Member (SAT). This unit represents element MD with a very thin development of MDC at its base.

clast axis alignment, within the uppermost diamicton of a ‘tripartite’ sequence near ground level (Smith *et al.* 2020). The unit is matrix-supported with well-dispersed clasts of at least two distinct mineralogies. It probably correlates with the Fishgarth Wood Till Member (FWT) at Drigg Beach, which reveals more associated macro- and meso- structures than the lower diamicton (DBT) at that site. There is little apparent macro- or meso-scale intra-unit deformation, with only sporadic shallow-angle fractures (Fig. 17a–d) and imbricate stacks of shallow-angle thrusts resulting in some intra-unit thickening (locations m and t, Fig. 10g).

A thin section (TMF1) of a sample collected from a superficial, probable correlative of the FWT at Cookson Wood (Figs 1 and 16d) shows no preferred shape or length alignment of clasts but does reveal irregular clusters and a locally developed circular arrangement of sand-grade clasts without obvious ‘core stones’ (Nirex 1997g, k). A thin, opaque oxide coats lithic clasts, lines the margins of fractures, fills veinlets and stains the reddish-brown matrix, which is composed of fine silt and clay. Clasts within a higher unit of element MD (FWT) at Drigg Beach are similar in distribution and provenance to those within the lower (DBT) unit of the element. A weak lattisepic plasmic fabric has developed within the matrix of the thin section (Fig. 16d), and a variably developed skelsepic plasmic fabric occurs on, or adjacent to, larger clasts, locally associated with a concentric, circular arrangement of fine-grained sand grains around a central ‘core stone’ formed by the larger clast. Two sets of fractures may be observed: (1) oblique, irregular fractures (with limited minor displacement of material either side) that are locally offset by short, more steeply inclined fractures; (2) complex steeply

inclined fractures (in this plane of section) that, in detail, are composed of an anastomosing network of finer, irregular features. A thin, finely laminated coating of fine silt or clay clearly rims voids. The clay fillings and coatings are characterized by a concentric to planar, highly birefringent fabric that is locally deformed by very fine kinks that are recognized by their sharp changes in extinction, indicating a sequence of till accretion followed by fracture, fracture infill and subsequent shearing.

Throughout all exposures, element MD is penetrated and deformed by variably common, shallow-angle to relatively steep thrusts associated with ramp anticlines and fault propagation folds, together with conjugate sets of normal faults, many of which are truncated at the base of the overlying sedimentary unit (locations b, d and f, Fig. 10f). This is especially apparent at location f in Figure 10f, where the sequence has been deformed into an eroded, NW-verging thrust-duplex *sensu* McClay (1992), preserved in the footwall of the large normal fault zone. Parts of the sequence have been completely detached and thrust over themselves, preserving the sequence of glaciectonite deformation features described above, within detached and overthrust units as shown in Figure 10e (and inset 1) and Figure 17c. The duplex is not extensive, with overall individual fault displacements of 50–200 mm and an overall shortening of *c.* 0.5 m for the whole duplex, which, allowing for the post-depositional erosion of its top, contributes to an overall structural thickening of <0.5 m. The deformation has resulted in local structural repetition of the sequence and a vertical crenulation fabric (S_2) (Fig. 17c), which appears to deform an older S_1 fabric within the detached portion of DHS.

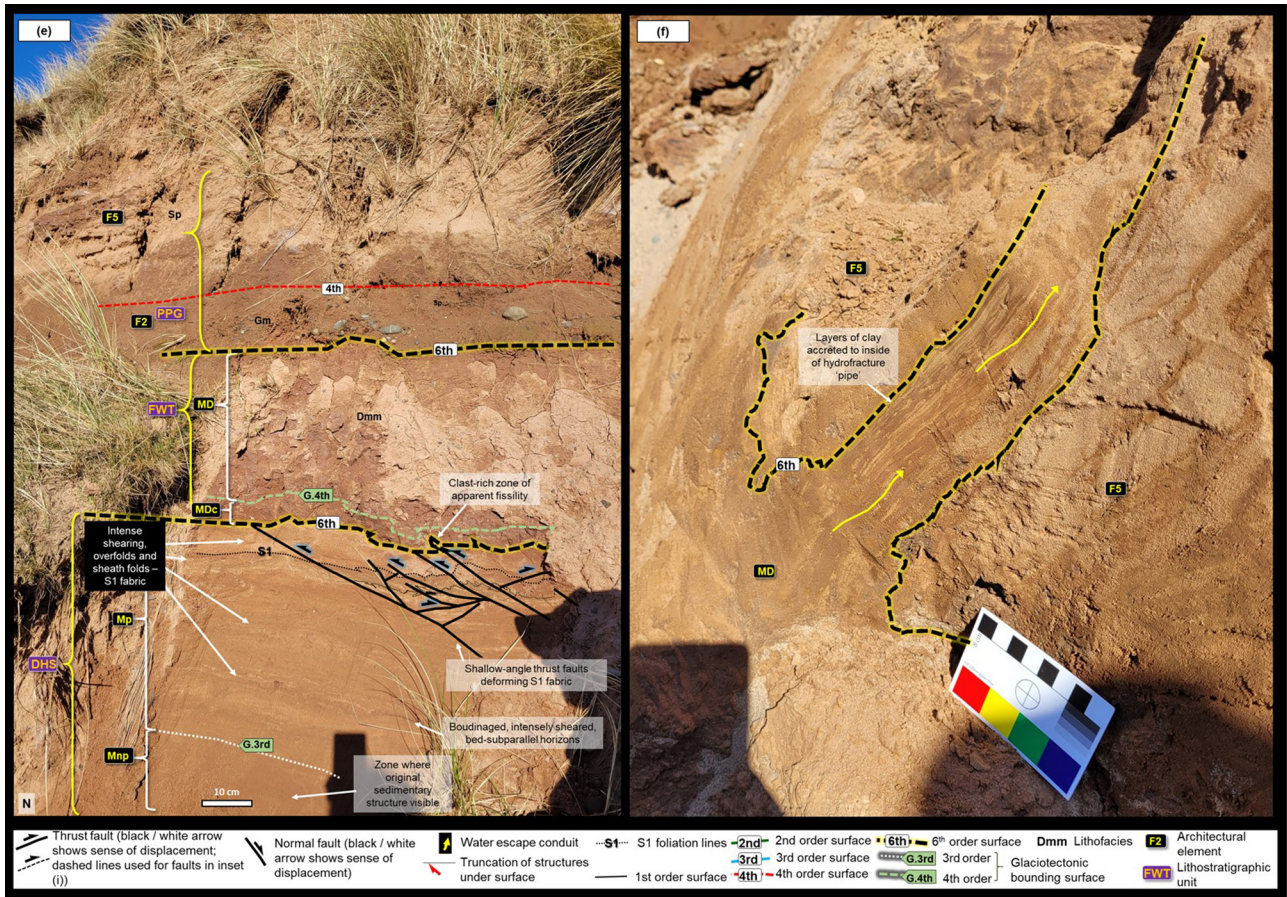


Fig. 17. Continued. (e) Detailed inset 6 of the Drigg Beach section (location shown in Fig. 10): similarly deformed units comprising DHS modified into pervasive (Type A) and non-pervasive (Type B) glaciectonites representing mélangé elements Mp and Mnp, overlain by elements MD and MDc, both forming FWT, which is overlain by undeformed elements F2 and F5. (f) Inset e of the Seascale Beach section (location shown in Fig. 11): a hydrofracture filled with thin accreted layers of clay, apparently injected up through element F5.

Element MD forms thin (<1 to 5 m), sheet-like units that generally become thinner higher up in the succession. They locally have an erosive base (Fig. 11c) truncating underlying strata, and commonly drape underlying topography. Although typically laterally extensive over tens, if not hundreds of metres, units may be absent or thin considerably, especially where the upper sixth-order surface is erosive. These features typically create an undulating, 'shrink-and-swell' architecture, whereas the topography of both upper and lower surfaces may itself have a hummocky appearance. The upper surface of exposures of element MD are locally convoluted, incorporating sediments from the overlying element into the convolutions.

Interpretation. It is important to critically examine the genesis of this element and the underlying one described in the next section, as, together, they are the subject of some debate (Trotter *et al.* 1937; Eyles and McCabe 1989; Merritt and Auton 2000; Smith and Merritt 2008; Cross *et al.* 2018; Coleman *et al.* 2020). The clay-rich, pebbly lithology, with an overall absence of sedimentary structures (for example, grading or lamination), suggests that subaqueous reworking or deposition is unlikely, and that deposition directly from glacier ice is more plausible. For instance, the sparse, well-dispersed clasts within a massive structure, together with an overall lack of macro- or meso-deformation structures, yet a demonstrable presence of ductile and brittle micro-structures, together with an observed sharp or abrupt décollement-like base, are indicative of subglacial deformation (Benn and Evans 1996; Phillips *et al.* 2002; Evans *et al.* 2006). Also diagnostic, are the horizontal to subhorizontal fractures, which form when bed-parallel or bed-subparallel fissility is reactivated during unloading of the till as the glacier retreats (Evans *et al.* 2006).

The element may represent the dilated 'A' horizon of a subglacial traction till (see Evans *et al.* 2006, 2016). However, as such horizons are typically much thinner and rarely preserved (Evans 2018), it is more likely that it represents pre-existing sediment (e.g. glaciolacustrine clay) that has been homogenized subglacially into a subglacial traction till. This is supported by the extensive investigations summarized by Merritt and Auton (2000), which revealed that the lithology of tills in the region, notably those associated with glacial readvances, are strongly influenced by the lithology of underlying sediments. For example, tills thin, become more clay-rich and include far fewer, more dispersed clasts shortly beyond where the ice has crossed over fine-grained glaciolacustrine deposits.

The sedimentological features observed in the two thin sections of DBT, particularly the brittle minor fractures and associated veinlets in Figure 16b and the aligned fabrics illustrated in Figure 16c, are typical of a subglacial traction till that has undergone pervasive deformation. The Cookson Wood thin section (Fig. 16d) also displays sedimentary features and brittle glaciectonic features typical of a subglacial traction till.

The NNW-verging thrust duplex and associated brittle structures that deform both the FWT and underlying DHS at Drigg Beach post-date the deposition of the FWT but predate deposition of the overlying PPG. The duplex records re-deformation of subglacially deposited and deformed sediments along thrusts that appear to have propagated from pre-existing subglacial thrusts but are steeper than the underlying décollement planes they propagate from. This suggests that the sediments have drained and consolidated a little between deformation events. The structural style corresponds to

submarginal, subglacial simple shear (see Hart and Boulton 1991; Hart 1999). The vergence is opposite to the overall ice palaeoflow direction, but this may reflect a northward component of easterly ice movement.

Massive, clast-supported diamicton element (MDc)

Element MDc appears to form laterally extensive sheets (<2 m) of stiff to very stiff, mostly clast-supported diamict with bed-parallel to subparallel shears giving the impression of laminations (Dcm-s). Never more than 0.3 m (and often no more than 0.05 m) in thickness, the element incorporates less compacted, dilated zones of matrix-supported, non-sheared diamicton (Dmm), resulting in a clear platy fissility. This is illustrated in exposures at Ravenglass (Fig. 15a–c) and Drigg Beach (Fig. 17a–e).

The element mostly underlies element MD in the coastal exposures, where the boundary between them typically is a definable fourth-order glacioteconic surface. Variations in this were observed during this study. For instance, high in the sequence penetrated by BH7 (Fig. 13, this study; figs 8 and 11 of Smith *et al.* 2020) this surface seems to be represented by a relatively thick transition zone between the two elements, with a non-definable top or base.

At Lowside Quarter (Fig. 18a), the element is represented by a c. 30 cm thick, sheet-like seam of stiff, thinly interlaminated clay, silt and sandy silt that dips 6°/180 S (Nirex 1997g, k), generally overlain by 3 m of gravel (Gm), probably representing element F2. The seam sharply truncates climbing-ripple cross-laminae in the underlying 2 m of silty, fine-grained sand. It is formed of fissile, alternating plates of stiff, clay-rich diamict (Dcm) and less stiff, silty, matrix-supported diamict (Dmm), separated by laminae of silt. Meso-scale brittle deformation occurs in the form of shallow and steep-angle thrust faults and associated folding, but there is little evidence of deformation in the underlying sediments except for minor soft-sediment deformation and possible water escape or drainage structures.

A thin section (Fig. 18b and c; Nirex 1997g, k), shows that the lamination is highly disturbed by soft-sediment deformation, including micro-scale flame structures, crenulation-style folds and rounded clay-rich till ‘pebbles’ that locally occur within the silt laminae. Thin sand laminae within the seam are highly deformed, displaying lobate, irregular and wispy flame structures that deform upper and lower boundaries and cause local attenuation. Detachment of a prominent sand lobe or ball has caused intense, localized deformation within underlying sand, silt and clay, which itself has been injected upwards to accommodate lobe formation. Open, synformal, convolute fold structures are preserved within the lobe, deforming fine lamination. A slight convex-upward warping of clay and silt laminae is visible in the upper part of the thin section (Fig. 18b and c), whereas the laminae are offset by several small microfaults that have both normal and reverse senses of movement.

In general, the base of element MDc is sharp, forming an abrupt, laterally continuous and extensive sixth-order erosion bounding surface (fifth-order glacioteconic surface) that commonly overlies subglacially deformed sediment (i.e. glacioteconite *sensu* Benn and Evans 1996; Evans *et al.* 2006; Evans 2018), as shown in Figures 10–12. Underlying sediment, however, is not invariably deformed, as at location x in Figure 10h.

Interpretation. The observed fissility displayed by interfingering of layers of Dmm and Dcm lithofacies and their stiff nature together with observed ‘solid-state’ meso- and micro-deformation structures such as shears, suggest that the occurrences of element MDc probably represent a component of subglacial traction till where dilation was ceasing, or had ceased, and a coherent till matrix was forming, or had formed. Such features may be a response to

progressive formation and collapse of the till-matrix framework within a developing ‘B’ horizon (Evans *et al.* 2006, 2016; Evans 2018). With each successive framework collapse the intensity of bed-parallel foliation increases, resulting in each plate forming a localized subzone of ‘B’ horizon. This whole process is typically driven by repeated fluctuations in porewater pressure, resulting in the accretion of layers of variably deformed, strain-hardened, clast-supported ‘B’ horizon till separated by planar detachment, or erosion surfaces underlying individual, thin layers of massive, homogeneous, matrix-supported ‘A’ horizon till (Evans *et al.* 2006), as observed at Drigg, Ravenglass and Lowside Quarter. The observations of intra-stratification and deformation indicate that the seam at Lowside Quarter is a glacioteconite *sensu* Evans (2018) (glacioteconic architectures are described in the next section). However, Phillips *et al.* (2007) recorded the focusing of subglacial deformation within the water-saturated, stratified base of a till unit near Gretna, Scotland. Indeed, the zone of disturbed laminated silt and fine sand in the central part of the thin section appears to have undergone partial liquefaction and remobilization with the fine sands having been injected such that they locally cross-cut the lamination. This suggests that the zone here may have acted as a fluid pathway during deformation with water or sediment escaping from the underlying sequences via the water escape conduits flowing along the actively deforming zone. The seam also shares many characteristics of hydrofractures, some of which may stretch laterally (subhorizontally) and conformably for several metres within a sediment sequence, before turning abruptly up or down discordantly (Phillips and Merritt 2008; Phillips *et al.* 2013a, b).

The convolute or disharmonic nature of the folding is consistent with deformation of water-rich sediment resulting in localized liquefaction, whereas the presence of water escape or drainage conduits within sediment underlying element MDc at Drigg Beach (Figs 10f and 17d, f) and Lowside Quarter (Fig. 18a) probably records also liquefaction and water escape in the structurally lower parts of the sequence resulting from loading caused by the tectonic thickening of the sequence during high water saturation. The latter probably contributed a water-rich surface on which the ice moved, thus significantly reducing the amount of shear translated into underlying sediments, confining deformation to within element MDc. This resulted in little or no ductile or brittle deformation of the underlying sediment (see Evans *et al.* 2006; Phillips *et al.* 2007). Indeed, if there is a higher than critical porewater pressure, the development of a till matrix framework may be limited.

Although several, not necessarily mutually exclusive interpretations of this element have been provided, in the context of this paper, the importance of this deliberation is to demonstrate that great care is required in interpreting thin, horizontally laminated units within glacial sequences. Even if they are formed of stacked graded couplets, they may not be glaciolacustrine in origin.

Pervasive and non-pervasive mélange architectural elements Mp and Mnp

Although sediment underlying massive diamicton elements MD and MDc is locally undeformed (e.g. Figs 10h and 18a), these elements commonly rest on zones of deformed sediment (Fig. 6). For example, pervasive mélange element Mp directly underlies MDc at Sellafeld (Fig. 13), Drigg Beach (Fig. 10f, location h; Fig. 10g, location t; Fig. 10h, location w; Fig. 17), Seascale (Fig. 9) and Ravenglass (Figs 12 and 15). At these locations the mélange element comprises sediment that has been affected by brittle deformation, resulting in both shallow-angle and steep thrusts together with conjugate sets of extensional faults. Ductile deformation has also occurred, resulting in rootless and sheath folds, boudins, overthrust material and commonly an S₁ fabric that has obliterated the original sedimentary structure and locally is itself

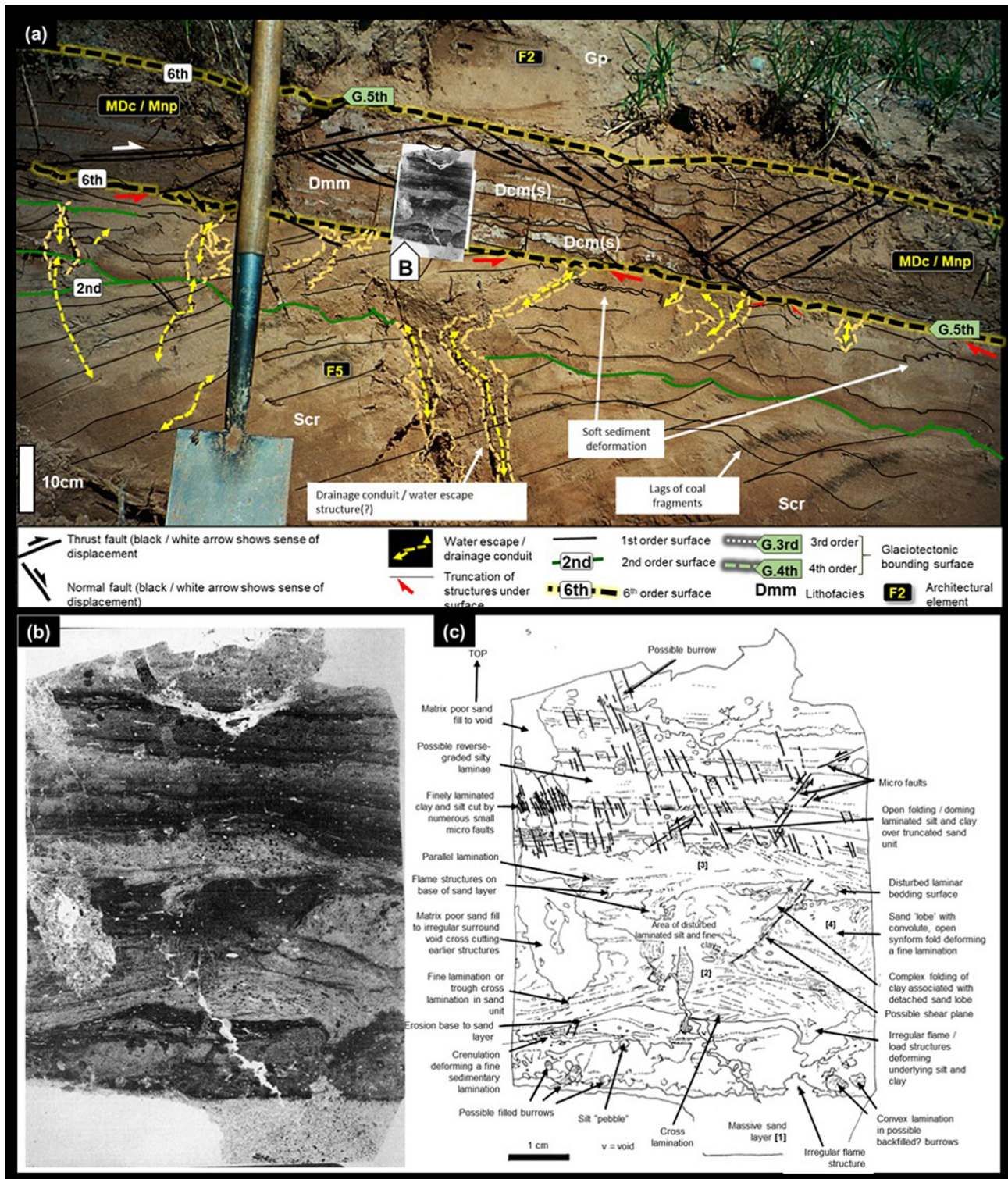


Fig. 18. Former valley side section at Lowside Quarter (location shown in Fig. 1). (a) Annotated image taken in 1994 showing undeformed element F5 overlain by an enigmatic, very stiff seam of element MDC/Mnp. (b, c) Thin section (location shown in (a)), with interpretation. BGS registered sample, thin section and images, modified from Nirex (1997g, k) [©UKRI 2022; ©Nuclear Decommissioning Authority 2022].

homogenized into a *mélange* of material. The fabric is formed of rotated and realigned clasts.

Sediments of element F5 appear to have undergone the most intense deformation. However, the exposures of element Mp in the vicinity of location h at Drigg Beach (Fig. 10f) also incorporate less intensely sheared clay of element Rh, as shown in detail in inset 3 (Fig. 17b). Additionally, as shown in insets 1 (Fig. 10f) and 4 (Fig. 17c), the northerly verging thrust duplex described above also incorporates thrust and displaced units of element Mp. Within that duplex, the S_1

fabric has been itself deformed, resulting in an S_2 crenulation fabric. Some exposures of Mp show distinct water escape fractures and conduits (Fig. 17d). Element Mp was observed to invariably underlie massive diamict elements MD and MDC, and, where present, to overlie non-pervasive *mélange* element Mnp (Fig. 6).

Element Mnp is widespread throughout most exposures, incorporating brittle deformation features that include shallow- and steep-angled thrusts with associated folds and ramp anticlines and conjugate extensional faults (Figs 7, 8, 10–13, 15 and 17).

The original sedimentary structure was observed at all locations where element Mnp was identified (hence the ‘non-penetrative–non-pervasive’ sobriquet). Deformation features could be roughly divided into two sets: those that affect only sediment underlying massive diamicton elements (and are thus truncated on the underside of those units), and those that also affect the diamictons. For instance, shallow-angle thrust faults and associated folds were observed to have deformed sediment of element F5 at Seascale (Fig. 5c and d) and Drigg Beach (Fig. 10h, locations s and u), but are truncated by the sixth-order basal surface of overlying units of MD and MDc. Some structures have propagated up through that surface (e.g. location t, Fig. 10g) and deform the overlying MD and MDc elements, but are truncated at the base of overlying outwash sediments (e.g. locations b–d at the previously described thrust duplex, t and u; Fig. 10f–h), whereas other structures were observed to have deformed the whole sequence up to the seventh-order surface marking the base of post-glacial sediments. For instance, steep-angled, southerly verging thrusts and back thrusts deform the exposed sequence at Drigg Beach up to the base of the uppermost diamicton (Sandy Acre Till Member; SAT) (Fig. 10h, location u), forming a southerly verging, positive half-flower structure with tight ramp anticlines deforming a fining-upward sequence of gravel and sand unit of PPG (representing element F5), and the underlying diamicton (FWT) representing element MD. Some of the steep thrusts appear to have propagated up through the sixth-order surface into the overlying diamicton (SAT), which thus represents a younger occurrence of element MD.

Further south along Drigg Beach, beyond the large normal fault, a large set of low-displacement (<50 cm shortening) thrust faults deform a unit comprising rhythmites of clay and silt (we refer to this as SACS, representing architectural element Rh) and overlying sequence of sands and gravels of elements F5 and F6 (Fig. 10a and b). These themselves have been folded and possess a structural dip towards the SW. Compressional structures and folds were also observed throughout the sequence, where they are bisected by extensional faults, including a large strand with a displacement of *c.* 30 cm and a northerly dip (Fig. 10b), which is probably related to the larger extensional fault. Between the two faults, grey clay and overlying peat infills a depression, onlapping underlying sediment and clearly overstepping linked conjugate, extensional fault strands.

Interpretation. Zones of glacial *mélange* element Mp result from the brittle and ductile pervasive modification of existing sediment (such that original sedimentary structure is obliterated) during the subglacial development of an overlying traction till. The observations above are consistent with a Type A (pervasive–penetrative) glacioteconite (*sensu* Benn and Evans 1996). The S_2 crenulation foliation observed within the thrust duplex described above was probably emplaced during the subglacial formation of the duplex and records the deformation of the S_1 fabric.

The thin and laterally discontinuous occurrence of element Mp, and its local dislocation from the underside of the overlying subglacial traction till, probably results from lateral fluctuations in subglacial water pressures. Translation of shear into sediments underlying till sheets occurred during lower water pressure, and none during higher pressures (see Phillips *et al.* 2007). The much thicker zones of purely brittle, non-pervasive deformation (here termed ‘*mélange* element Mnp’), which commonly underlie element Mp, record the formation of a Type B (non-penetrative) glacioteconite (*sensu* Benn and Evans 1996). The variable presence of brittle deformation also probably results from fluctuations in subglacial water pressure. Observations of structural relationships commonly help in the identification of Type B glacioteconite and thus provide additional supporting evidence for the identification of overlying subglacial traction tills.

Discussion 1: palaeoenvironmental reconstruction, glaciolacustrine v. glacialigenic?

We agree with Coleman *et al.* (2020) that their new ‘glaciolacustrine’ interpretation presented by Coleman *et al.* (2020) has significant implications for future 3D modelling and site investigations, both in the district and in other areas of comparable glacial history. For example, by adopting their glaciolacustrine model, these researchers have projected the enigmatic thin seams of pebbly clay (diamicton) exposed at the coast near horizontally inland. In contrast, previous studies have demonstrated that they gently rise inland towards former glacial limits and take into account the former direction of ice flow (Nirex 1997). For example, in early phases of the last glaciation ice flowed through, and directly out of Lower Wasdale, but during subsequent readvances the Irish Sea Ice Stream became progressively dominant and glided more or less horizontally across deposits buried in the valley (Merritt and Auton 2000).

Distinguishing between glaciolacustrine and glacialigenic sediments presents similar challenges to those encountered in correctly identifying glaciomarine deposits, as opposed to non-marine subglacial or fluvial outwash. For example, McCarroll (2001) concluded that sedimentological evidence alone is not enough to identify glaciomarine sediments, particularly if they were deposited in a glacioteconic setting. The issue is not unique to the Cumbria area and has been discussed in relation to other areas around the UK and Ireland with similar glacial history (e.g. east Yorkshire, north Norfolk, north Wales, Irish Sea coast; Phillips *et al.* 2007; Thomas and Chiverrell 2007; Evans *et al.* 2013; Lee *et al.* 2017; Merritt *et al.* 2018). Rather than seeking unequivocal sedimentological evidence the key to successful discrimination lies in the correct identification of glacioteconic as opposed to gravity-driven deformational features and understanding the role of subglacial processes in sediment deposition, accommodation, accumulation and preservation (Hart and Roberts 1994; Roberts and Hart 2005).

The evidence that Coleman *et al.* (2020) cited against subglacial deposition of pebbly clay units in the Drigg Beach area includes sedimentological, glacioteconic and accumulation style. We examine each facet in turn.

Sedimentology. Coleman *et al.* (2020) interpreted particle size distribution curves of the controversial units to indicate gap-graded clays of glaciolacustrine origin, especially as they assumed that the well-dispersed limestones pebbles are dropstones. Coleman *et al.* (2020) invoke the presence at both macro- and micro-level of finely draped structures and gradational transitions at most of the sand–clay boundaries, like those reported as diagnostic features of glaciomarine sediments by Eyles and Clark (1985) to support their interpretation. In addition, they interpreted pillow and ball structures such as described by Murton and French (1993) to exclusively indicate lacustrine sedimentation. Furthermore, they suggested that the water-escape structures they observed in thin section are the result of glaciolacustrine sedimentation and proposed that thin wispy stringers of silt and sand within the pebbly clay units are similar to those interpreted by Eyles and Eyles (1983) to have resulted from water current re-sedimentation.

In reply, it is generally accepted that tills have the most diverse range of particle size distribution (psd) of any soil (Clarke 2018). The psd curves of Coleman *et al.* (2020) fall partially within the published ranges for many subglacial clayey diamictons, including, for example, the Brewood Till Formation in Staffordshire (Culshaw *et al.* 2017), till and sheared clay from thrust planes collected at Dinas Dinlle, on the Llyn Peninsula (Harris *et al.* 1997), and tills within the Vale of York Formation (Culshaw *et al.* 2017).

Pillow and ball structures such as those described by Murton and French (1993) can be created during lacustrine deposition, but the features described by those researchers are typically meso-scale (i.e.

centimetres to metres) in size, and usually form when sand with a higher bulk density sinks into mud with a lower bulk density, rather than the other way round as Coleman *et al.* (2020) described. Furthermore, such features are more comparable with the complex, lobate, soft-sediment deformation structures described in a broadly similar and correlative readvance till near Gretna (British Geological Survey 2006; Phillips *et al.* 2008) and other locations (e.g. Lee *et al.* 2017).

Mass flows may be introduced locally into a glaciolacustrine environment and others may be generated during periods of exposure (Brodzikowski and Van Loon 1987). However, ultimately the extent and thickness of the mass flow-body depends on the extent of the glaciolacustrine basin and on a range of factors that act to limit the flow-body's preservation. As Merritt and Auton (2000) demonstrated, the units of pebbly clay diamicton in question form units with subplanar boundaries that are tens to hundreds of metres in length yet commonly less than 1 m thick. They can be lithostratigraphically correlated over tens of kilometres via outcrop and borehole data (Fig. 2). Units that are unequivocally lacustrine clay are more geographically confined and commonly much thicker. For instance, the Whinneyhill Coppice and Holmside Clay members located beneath Lower Wasdale are 2–3 km in extent and up to 30 m thick (Merritt and Auton 2000).

Lonestones are indeed very common within the pebbly clay units, but clast-poor subglacially deformed materials often appear this way and in the absence of cited diagnostic evidence of impact and draped lamination (see Benn and Evans 2010) most are more likely to have resulted from subglacial processes (see Piotrowski 1992; Hart and Roberts 1994; Roberts and Hart 2005).

Glaciotectonics. Coleman *et al.* (2020) cited that an apparent absence of glaciotectonic deformation structures (micro-scale folding and faulting) both within the pebbly clay units and in underlying sediment supports subaqueous deposition (see Eyles and Eyles 1983). Furthermore, they suggested that observed downward-dipping clasts and poorly oriented fabrics in the pebbly clays indicate deposition as mass flows.

In contrast, we have observed numerous meso- and macro-scale deformation structures at Drigg that affect the pebbly clay units together with underlying sediment, and understand that structures such as these, and poorly developed tectonic fabrics, are a common feature in the wider study area (Nirex 1997e, g, k). We have explained how such deformation features are generally associated with the passage of grounded ice over wet sediment and that they are commonly partitioned into discrete structural zones of deformation (see Phillips *et al.* 2007), as shown in the palaeoenvironmental reconstruction in Figure 19. However, although the presence of these structures is a useful criterion for defining a subglacial traction till (Evans *et al.* 2006), their local absence is not a useful indicator to distinguish subglacial and lacustrine deposition.

Accumulation style. Coleman *et al.* (2020) argued that preferential accumulation within topographic lows indicates gravity-driven sedimentation. However, although some fine-grained units towards the top of the sequence (e.g. Sandy Acre Clay and Silt Member; SACS) undoubtedly occupy basins and exhibit thin, graded, draped, onlapping lamination (Fig. 10b–d) characteristic of lacustrine sedimentation, others do not. We maintain that three of the units are much more likely to represent subglacial traction till. At Drigg Beach, the boundaries of the pebbly clay beds are generally non-gradational (location y, Figs 10f and 17) and thin stringers of silt and sand were not observed within them.

Summary. Our study demonstrates that it is crucial to ensure distinct glaciotectonic evidence (including published information) is not overlooked, where the interpretation of ice-marginal/ice-contact successions is used as the basis of robust 3D geological models, particularly where it can support unconvincing sedimentological evidence. They then used the apparent absence of glaciotectonic deformation to support their glaciolacustrine depositional interpretation without further investigation. In contrast, the comprehensive structural and micropetrological evidence we present strongly indicates the presence of at least three subglacial traction till units interbedded with clastic deposits, which fully supports the generally accepted glacial readvance scenario based on

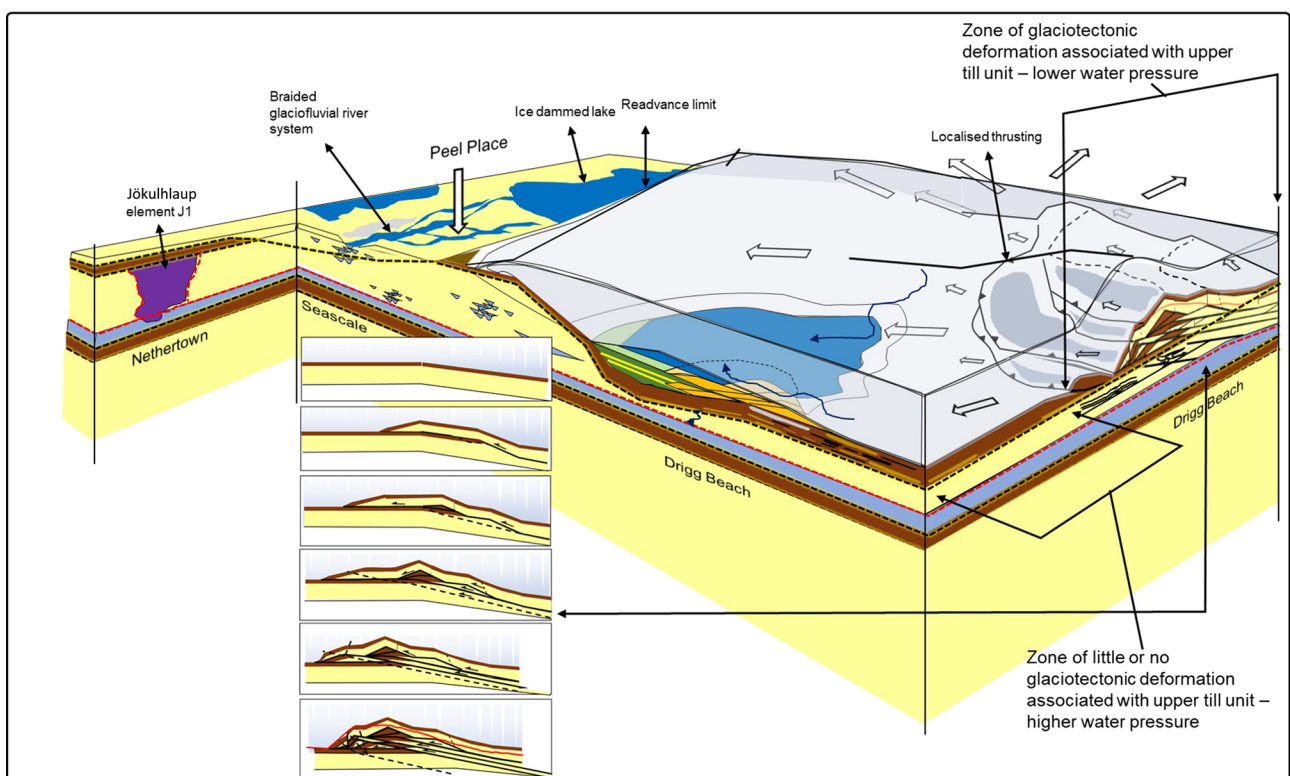


Fig. 19. Conceptual model to illustrate the creation, deformation and relationships of facies associations observed in the study area.

considerable evidence reported by Nirex and summarized by Merritt and Auton (2000).

The controversy regarding the ponding of ice-marginal lakes and associated glacial readvances during latter stages of the last glaciation in west Cumbria is not unique in the UK. For example, analogous large ice-marginal lakes also occupied the Durham lowlands, particularly in valleys of the Tyne and Wear, and Teesside (Smith and Francis 1967; Smith 1994; Stone *et al.* 2010; Davies *et al.* 2012). The largest was Glacial Lake Wear, which stood at several levels up to 132 m OD, governed by the elevations of spillways that became available sequentially and ponded along the coast behind ice streaming southeastwards in the North Sea basin. The lakes were filled with up to 60 m of mainly thinly laminated clay and silt with dropstones, intercalated with pebbly clay diamicton and gravel (Tyne–Wear Glaciolacustrine Formation of McMillan *et al.* 2011). Similar to sediments beneath Lower Wasdale, complex interdigitation of units is common, especially towards the coast, and understanding the composition and 3D distribution of the fine-grained glaciolacustrine deposits is also important, particularly because they pose major geotechnical problems. The relatively high water content of the laminated silts and clays renders them plastic and potentially very weak with low shear strength (Smith 1994).

As in west Cumbria, these glaciolacustrine deposits are widely capped by thin (<2 m), laterally persistent beds of soft, plastic silty clay with well-dispersed pebbles ('Pelaw Clay', 'Prismatic Clay') (Smith 1994). Elsewhere they are capped by more clast-rich diamicton ('Butterby Till'), but with low shear strength, inverted strength profile and local absence of a preferred fabric (Smith and Francis 1967). As with the glaciolacustrine model of Coleman *et al.* (2020), these units were generally believed not to be subglacial tills, but to have formed as cohesive debris flows into water from ice margins, as solifluxion flows from surrounding deglaciated slopes, or by redistribution of unconsolidated lake sediments following periodic lake drainage (Smith and Francis 1967; Hughes *et al.* 1998; Smith 1994). However, more recent research in the region, particularly at the coast, has firmly established that the ice-marginal lakes existed and that they were affected by several surges of the North Sea Ice Stream (Davies *et al.* 2009, 2012).

Discussion 2: heterogeneity and its application to high-resolution subsurface 3D geological modelling

Three levels of heterogeneity have been recognized in the study area (*sensu* Slomka and Eyles 2013). Level 1 heterogeneity is recorded on a vertical scale of centimetres to metres, whereas Level 2 is on a lateral resolution of <10 m to several hundreds of metres and a vertical resolution of <1 m to several metres. The lowest resolution of heterogeneity, Level 3, is recorded on a vertical scale of <1 m to several metres and a horizontal scale of up to several hundred to thousands of metres (i.e. the scale of Figs 1 and 2). Level 3 generally encompasses lithostratigraphic units and is identified at outcrop through integrating the topology, geometric characteristics and genetic relationship of component architectural elements constrained within fifth-, sixth- and seventh-order bounding surfaces. Correlation between borehole logs based on Level 3 heterogeneity and using fifth-order bounding surfaces will consequently result in the lowest resolution of 3D geological model.

Finer grained facies within the sheet-like FA1 and FA4 facies associations form lower permeability confining layers that have in places been eroded out beneath younger channelized units of higher permeability FA2, and FA5. This results in vertical hydraulic connectivity between facies associations of different lithostratigraphic units, and, for example, results in 'perched' aquifers above the main groundwater aquifer at Sellafield (Kuras *et al.* 2016). The geometry of the sixth-order surfaces that bound facies associations

ranges from virtually flat to low-relief, long-wavelength, long-amplitude undulations. Modifications to this geometry result from subglacial or glaciotectonic deformation, which may lead to localized 'shrink-and-swell' relationships, removal or stacking. However, understanding the complex arrangements of coherent lithological units, their extent and their geometries, is the key to ascertaining where potentially contaminated groundwater may flow. Of paramount importance is the location and geometry of fine-grained, impermeable lithologies with respect to coarser material. Guidance such as BS5930:2015, together with corresponding lithology codes (e.g. the c. 120 AGS codes of the Association of Geotechnical and Geoenvironmental Specialists), provides some basis for correlation, but the possibility of up to 10 depositional sequences could result in a modelling stratigraphy of over 1000 units, which would be challenging for even the most enthusiastic 3D correlation-based modeller.

We address this issue here by mapping the permeability ranges, predominant flow mechanisms and ranges in hydraulic conductivity for various lithological sequences onto lithofacies and/or relevant architectural elements and facies associations that are of interest to the hydrogeological modeller (as per Lewis 1989; Lewis *et al.* 2006) (see Fig. 20). This demonstrates that most of the end-members of permeability that are of interest can be correlated and modelled at Level 2 (Slomka and Eyles 2013), apart from units of gravel, sand and silt within architectural elements MD (convoluted), F5 and F6, which ought to be correlated at Level 3 heterogeneity. However, field evidence including graded third-order bounding surfaces between silt and sand lithofacies units within element F5, the complex arrangement of fining-upward, small (metre-scale) sand and gravel units within element F6, and the chaotic array of various, similarly small lithofacies units (resulting from cryoturbation) with a huge range of upper and lower bounding surface geometries within element MD (convoluted), mean it is sensible to base correlation on defining the Level 2 bounding surface geometries. For elements F5 and MD (convoluted), we base the permeability range and hydraulic conductivity on the dominant lithology denoted by the borehole lithology log. Neither gravel nor sand is dominant within element F6, so we have assigned the sand and gravel hydraulic conductivity and permeability ranges of Lewis (1989) and Lewis *et al.* (2006), as in Figure 20.

The parameters of Lewis (1989) and Lewis *et al.* (2006) suggest that for the definition of architectural elements, borehole lithology logs may be rationalized down to bulk lithology, whilst utilizing full log descriptions to inform unit definition and correlation of architectural elements and their tops and bases. In Figure 21, we define 21 generic architectural element geometries including undeformed units and those that have undergone secondary subglacial or proglacial deformation. These have been used along with the architectural element analysis to facilitate the creation of several small-scale (hundreds of metres) 3D geological models of the Quaternary sequence at the Sellafield site using the workflow shown in Figure 22a–l. They are based on the gradual development of a 3D fence model of correlation cross-sections (a)–(e) constrained by a topography upper surface (in this case we have used the most recent Environment Agency aerial LiDAR digital terrain model) and a bedrock (rockhead) surface created in this study from interpolation of borehole and outcrop data. The architectural element analysis within this study illustrates that a typical glacial advance–retreat–readvance cycle comprises a fine-grained till at the base followed by a fining-upward sequence of glaciofluvial material (Fig. 22g) representing high-energy, ice-proximal deposition with upward-decreasing flow. However, this cycle may be repeated, because prograding and retrograding glacial advance and retreat episodes may result in apparently coarsening-upward sequences, such as at Peel Place Quarry. The gradual creation of a 3D fence model of sections within this study illustrates some of these

(A) Facies associations for Sellafield site and vicinity	(B) Relevant architectural elements for Sellafield site and vicinity	(C) Lithofacies within architectural elements	(D) Lithologies with ranges in hydraulic conductivity (after Lewis, 1989; Lewis et al, 2006)	(E) Typical flow mechanisms and permeability codes (Lewis et al, 2006)			
				Predominant flow mechanism	Maximum permeability	Minimum permeability	
ICE CONTACT ARCHITECTURE							
FA1	MD – MDc	DIAMICT (till) (Dmm, Dml, Dms, Dcm(s))	Till	10^{-7} to 5×10^{-1}	Mixed	High to moderate	Low
	DLbr						
	Mp	SAND (Mgt(a))	Sand	10^{-1} to 5×10^2	Intergranular	High	High
	Mnp	SAND (Mgt(a))	Sand	10^{-1} to 5×10^2	Intergranular	High	High
	MD / F5 convoluted	GRAVEL (Gm); SAND (Sm)	Gravel	5×10^1 to 5×10^4	Intergranular	Very high	Very high
		TILL (Dmm, Dml, Dms, Dcm(s))	Till	10^{-7} to 5×10^{-1}	Mixed	High to moderate	Low
FA2	F1	GRAVEL (Gp, Gt)	Gravel	5×10^1 to 5×10^4	Intergranular	Very high	Very high
	F2	GRAVEL (Gm)					
	F3	GRAVEL (Gp)					
	F4	SAND (Sr, Sp) SILT (Fl)	Sand	10^{-1} to 5×10^2	Intergranular	High	High
	F5	SAND (Ss, St, Sp, Sr, Sh) SILT (Fl)	Silt	10^{-3} to 10^{-1}	Intergranular	Moderate	Low
FA3	F6	GRAVEL (Gp, Gt), SAND (Ss, St, Sp), SILT (Slt)	Sand and gravel	5×10^2	Intergranular	Very high	High
	Rh	CLAY & SILT (Fl, Fiv) PEAT	Clay	5×10^{-7} to 10^{-3}	Fracture / mixed /intergranular	Low to very low	Very low
PROGLACIAL ARCHITECTURE							
FA2	F1	GRAVEL (Gp, Gt)	Gravel	5×10^1 to 5×10^4	Intergranular	Very high	Very high
	F2	GRAVEL (Gm, Gp)					
	F3	GRAVEL (Gp)					
	F4	SAND (Sr, Sp) SILT (Slt)	Sand	10^{-1} to 5×10^2	Intergranular	High	High
	F5	SAND (Ss, St, Sp, Sr, Sh) SILT (Slt)	Silt	10^{-3} to 10^{-1}	Intergranular	Moderate	Low
FA4	F1	GRAVEL (Gp, Gt)	Gravel	5×10^1 to 5×10^4	Intergranular	Very high	Very high
	F2	GRAVEL (Gm, Gp)					
	F6	GRAVEL (Gp, Gt), SAND (Ss, St, Sp), SILT (Slt)	Sand and gravel	5×10^2	Intergranular	Very high	High
FA5	HDC	GRAVEL (Gb, Gm, Gp)	Gravel	5×10^1 to 5×10^4	Intergranular	Very high	Very high

Fig. 20. Facies associations, architectural elements and their component lithofacies with corresponding lithologies, hydraulic conductivity ranges, predominant flow mechanisms and inferred permeabilities (after Lewis *et al.* 2006).

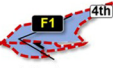
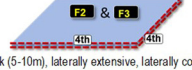
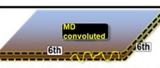
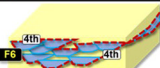
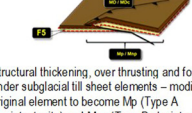
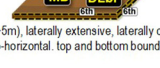
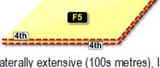
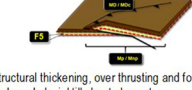
Maximum to Minimum permeability	Relevant lithology & lithofacies	Architectural element	Geometry (undeformed)	Order of geometry defining surfaces	Geometrical subglacial deformation effects	Geometrical proglacial deformation effects	
Very high to very high ■ ■	GRAVEL (Gb, Gt)	F1	 Concave-up, 4th order base surface, horizontal, hummocky 4th order upper surface	4th	Negligible	 Shallow-angle thrusts	
	GRAVEL (Gm, & Gp)	F2 F3	 Thin (<0.5m to thick (5-10m), laterally extensive, laterally continuous sheets, 4th order horizontal to sub-horizontal, top and bottom bounding surfaces.	4th	Negligible	 Compressional thrust ramp antidi-conjugate extensional faults; structural thickening and sequence repetition.	
	GRAVEL (Gb, Gm, Gp)	HDC	 Concave up, sometimes undercutting, 4th order surface at base, flat top, J1 units are thick (>10m)	4th	Negligible	None observed	
	GRAVEL (Gm)*	MD convoluted	 Thin (~0.5m to 2m) sheets of melange material - 6th order upper & lower surfaces typically convoluted as are lower order bounding surfaces of individual lithofacies units	6th	None observed	None observed	
Very high to high ■ ■	GRAVEL (Gp, Gt); SAND (Ss, St, Sp); SILT (Fi)	F6	 Whilst easily definable in the field, bounding surfaces of individual lithofacies units would be difficult to correlate in a 3D model. Generally, easily defined concave-up, 4th order base surface, and horizontal 4th order upper surface, both hummocky in appearance. Whole element laterally unextensive: W=10 to 30m)	4th	None observed	None observed	
	High to high ■ ■	SAND (Sr, Sp); SILT (Si)	F4	 Concave-upwards 4th order surface at base; flat, 4th order, horizontal-sub-horizontal upper surface. H = -0.5 to 5m; W = up to 20m. Arcuate geometry in plan view.	4th	None observed	None observed
		SAND (Ss, St, Sp, Sr, Sh);	F5	 Thin (~0.5m to 10m), laterally extensive (100s metres), laterally continuous sheets of sand and silt typically flat or draped with abrupt or indistinct upper and lower 4th order bounding surfaces	4th	 Structural thickening, over thrusting and folding under subglacial till sheet elements - modifying original element to become Mp (Type A glacioteconite) and Mnp (Type B glacioteconite)	 Compressional thrust ramp antidi-conjugate extensional faults - structural thickening and sequence repetition
SAND (Gm)*	MD convoluted	 Thin (~0.5m to 2m) sheets of melange material - 6th order upper & lower surfaces typically convoluted as are lower order bounding surfaces of individual lithofacies units	6th	None observed	None observed		
High / moderate to low ■ ■	TILL (Dmm, Dmf, Dms, Dmc(s))	MD	 Thin (<0.5m to thick (~5m), laterally extensive, laterally continuous sheets. 6th order horizontal to sub-horizontal, top and bottom bounding surfaces	6th	 Structural thickening, over thrusting and folding, sometimes incorporating underlying glacioteconites. Only observed in TA-TB.	 Compressional thrust ramp antidi-conjugate extensional faults - structural thickening and sequence repetition	
	TILL (Dmm, Dmf, Dms, Dmc(s))*	MD convoluted	 Thin (~0.5m to 2m) sheets of melange material - 6th order upper & lower surfaces typically convoluted as are lower order bounding surfaces of individual lithofacies units	6th	None observed	None observed	
Moderate to low ■ ■	SILT (Fi)	F5	 Thin (~0.5m to 10m), laterally extensive (100s metres), laterally continuous sheets of sand and silt typically flat or draped with abrupt or indistinct upper and lower 4th order bounding surfaces	4th	 Structural thickening, over thrusting and folding under subglacial till sheet elements	 Compressional thrust ramp antidi-conjugate extensional faults - structural thickening and sequence repetition	
Low to very low ■ ■	CLAY & SILT (Fl, Fiv); PEAT	Rh	 Concave-up, 4th order base surface, horizontal, flat 4th order upper surface	4th	None observed	 Shallow-angle thrusts, structural thickening, shortening, repetition	

Fig. 21. Generic bounding surface geometries for undeformed, subglacially deformed and proglacially deformed sequences of differing maximum to minimum permeabilities, for use in 3D correlation between data points.

complexities, which are represented by the development of an appropriate 3D geological modelling stratigraphy encompassing the bounding surfaces of over 400 units (Fig. 22h). Although this may seem to be a large number, it considers both vertical and lateral heterogeneity, and captures features such as braided river systems, glacially dammed and oxbow lakes, and till deposits, all of which may have undergone syn- and post-depositional deformation. In this study, the resulting 3D fence diagram (Fig. 22i) subsequently allowed the creation of a high-resolution 3D surface model (Fig. 22j) that could be explored in various ways, including looking at individual architectural elements such as till units (Fig. 22k) on their own, or in the context of other units such as sands (Fig. 22l).

To increase the effectiveness of high-resolution 3D modelling of geologically complex areas, such as around Sellafeld, Lelliott *et al.* (2009) recommended utilizing a high density of site investigation data points within the dataset, based on the premise that a model is only as geologically valid as the data used to create it and that 'something is usually better than nothing'; missing out data points just increases uncertainty, unless the geology is simple. Kessler *et al.* (2009) and Lelliott *et al.* (2009) noted that each cross-section should be constructed considering data points that may not lie along the correlation section line by projecting nearby boreholes onto the section line. Furthermore, such data points can be used to inform the creation of new sections that bisect them. This technique has been successfully deployed by the British Geological Survey within their

GSi3D (Geological Surveying and Interpretation in 3D) workflows (Kessler *et al.* 2009; Lelliott *et al.* 2009; Smith 2010) and Groundhog software. Quantifying uncertainty is important where the data density is low, but calculations for this type of exercise are

relatively easy to undertake (Lelliott *et al.* 2009). For example, uncertainty estimates calculated for each geological surface generally match the intuitive interpretation of the geologist building the model, who decides where the greatest uncertainty occurs.

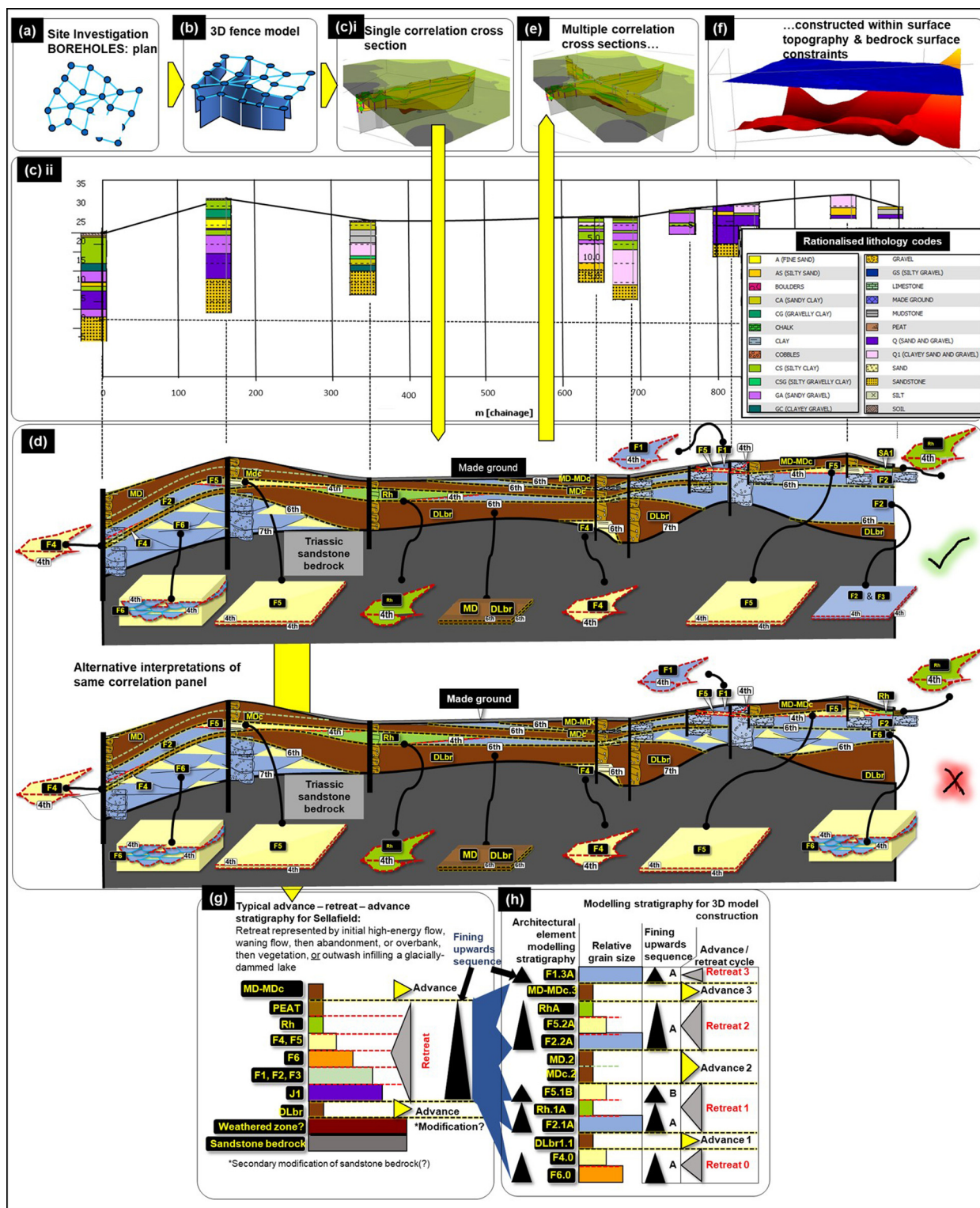


Fig. 22. Workflow depicting the process of using geologically valid correlation between data points at an architectural element level of heterogeneity to create high-resolution 3D geological models using sample boreholes from the Sellafield site. Boreholes (a) are used to create a 3D fence model (b) and correlation cross-section (ci, cii) based on correlation of local and regional architectural elements and relevant generic unit and surface geometries. Alternative sections (d) are then tested in the context of nearby data represented by the most appropriate chosen bisecting sections. Multiple sections (e) are then constrained by topographical and rockhead surfaces (f), together with knowledge and understanding of stratigraphy gathered during architectural element analysis of field exposures (g) and glacial history (h).

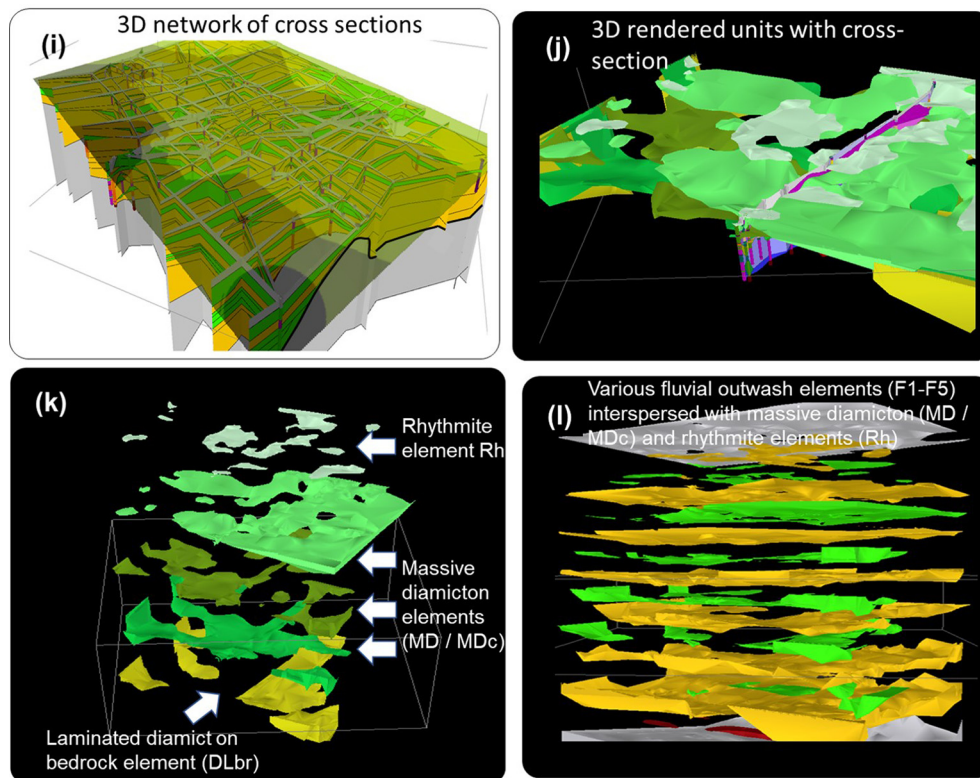


Fig. 22. Continued. (i) Modelling stratigraphy utilized to create high-resolution 3D geological model based on network of cross-sections; (j) 3D rendering of geological units; (k, l) exploded models showing relationships of various elements.

Lelliott *et al.* (2009) noted, however, that the calculated estimates required validation through the drilling of additional boreholes, meaning that an uncertainty estimate exercise can effectively form the basis of a data gap analysis, alongside other statistical approaches such as the Data Quality Objectives (DQO) process (US Environmental Protection Agency 2006).

In this paper we recommend that a reliable, high-resolution 3D geological model can be built following thorough data review and utilizing all available data points, and indeed have constructed several ourselves, one of which is shown in Figure 22 (another is described by Kuras *et al.* 2016). Reducing data decreases uncertainty in lithostratigraphic correlation, but removal of such data takes away possibly the only source of information on the lithology of a unit, its distribution and geometry. The case example published recently by Coleman *et al.* (2020) took a more simplified, less time-consuming approach to 3D geological modelling at the UK's LLWR, incorporating fewer data. These researchers did not include, for example, data such as historical records not completed to current standards such as BS5930:2015, data not supported by geotechnical records such as cone penetration tests (CPT), or data collected by potentially less reliable investigation techniques relative to rotary cored boreholes. We agree that 'understanding and modelling the complex glacial geology in West Cumbria is challenging' (Coleman *et al.* 2020, p. 1), but it is essential to build upon all available knowledge for developing robust hydrogeological models. Coleman *et al.* did not cite, for example, any of the detailed and comprehensive research work undertaken for Nirex in the 1990s (Nirex 1995, 1996, 1997a, b, c, d, e, f, g, h, i, j, k, l, m).

The new wholly glaciolacustrine interpretation proposed by Coleman *et al.* (2020) for the succession of clays and outwash sands and gravels exposed in the cliffs of the study area, and concealed beneath Lower Wasdale, is an interesting supposition that those researchers then extrapolated to the LLWR site, some 500 m distant. They integrated it with lithological and geotechnical information obtained from boreholes drilled within and in the vicinity of the

LLWR site, geophysical data and regional geomorphological information, and then used it in the construction of a 3D geological model of the site. For this they deployed a prioritized borehole review approach resulting in the initial utilization of data of only 64% of 746 boreholes (Coleman *et al.* 2020), coupled with a revision of the site 'event stratigraphy' that aligned with their new interpretation and that therefore precluded the possibility of subglacial traction till being present.

This paper, which describes the application of architectural element analysis of local outcrop analogues to high-resolution 3D geological modelling for the nearby Sellafield nuclear site, has, by necessity, included a critical review of the evidence on which the glaciolacustrine hypothesis rests. We find it inappropriate to dismiss the generally accepted glacial readvance scenario. In contrast, by collecting detailed sedimentary, structural and micropetrological evidence, we demonstrate the unequivocal presence of up to three well-exposed subglacial traction tills, in a succession that includes glaciofluvial and glaciolacustrine sediments. We suggest that this provides a much more reliable basis for the 3D geological modelling of the nuclear sites within the study area.

Conclusions

This paper presents a detailed analysis of the sedimentary and glaciotectonic architectural characteristics of fine-grained glaciogenic and fine- to coarse-grained glaciofluvial deposits exposed at field locations in and around the Sellafield nuclear works, Cumbria, England. In total, 19 lithofacies units have been recognized within 11 sedimentary architectural elements and including two glaciotectonic-mélange elements that result mainly from modification of existing sediment during emplacement of overlying subglacial diamicton.

We show how the high-resolution lithological and geometrical information required for contaminant transport modelling at complex industrial sites such as nuclear plants can be obtained through 3D geological modelling via correlation of erosion

bounding surfaces at an architectural element level of heterogeneity. We present a new workflow showing how the architectural elements recognized in the Sellafeld area have been used to develop a suitable 3D modelling stratigraphy and a high-resolution 3D geological model. The latter includes the definition of 21 generic unit or bounding surface geometries at local outcrops to help inform accurate correlation between data points (mainly boreholes) at the Sellafeld site.

This study confirms the generally accepted evidence presented by Merritt and Auton (2000) for the presence of at least three laterally extensive, subglacial traction tills along the coast between Sellafeld and Ravenglass. These units are closely associated with two glaciotectionic mélange architectural elements, which represent penetrative (Type A) and non-penetrative (Type B) glaciotectionites (*sensu* Benn and Evans 1996; Evans 2018) respectively.

These elements are not laterally continuous, and whereas the first element (Mp) always occurs in tandem with an underlying zone of the second (Mnp), both may be absent whilst locally only Mnp may be present.

This is consistent with published literature, but importantly it shows that whereas the presence of a sub-till glaciotectionite is indicative of subglacial traction, its absence does not negate the unit above being subglacial traction till.

At Drigg Beach, a remarkable NW-verging thrust duplex is preserved, resulting in overthrusting of two members and the creation of a second S₂ crenulation fabric within overthrust Type A glaciotectionite. This indicates a local lowering of subglacial water pressure during emplacement that resulted in coupling of the ice mass to its bed (*sensu* 'sticky spots' of Stokes *et al.* 2007). Elsewhere along the coast, clay-lined hydrofractures have been identified that were formed by pressurized water, which is likely to have played a significant role in controlling subglacial processes. The local uncoupling of ice from its base (*sensu* Lesemann *et al.* 2010) may have provided accommodation for the subglacial deposition of thin, lensoidal units of glaciofluvial and rhythmically laminated sediment that commonly lie in the former 'down-ice' lee of anticlinal structures affecting subglacial till units, creating a shrink-and-swell architecture. At least two episodes of proglacial compressional and extensional deformation have been identified.

The depositional and structural findings presented in this paper support the lithostratigraphy and history of events outlined by Merritt and Auton (2000) and Smith and Merritt (2008), including deposition and deformation associated with several glacial readvances and not the revised, wholly glaciolacustrine model proposed by Coleman *et al.* (2020).

Acknowledgements This paper is published with the permission of the National Nuclear Laboratory, UK and the Executive Director of the British Geological Survey (UKRI). The authors thank Sellafeld Ltd for provision of borehole data, and for permission to reproduce the photograph used in Figure 13. Tendley Quarries Ltd are thanked for permission to access Peel Place Quarry during several field visits over the last 15 years and for use of images of the quarry. The paper benefited from reviews by an anonymous reviewer and J. Lee (British Geological Survey), who are both thanked for their comments and suggestions. N.T.S. was supported by the National Nuclear Laboratory (NNL) Core Science Research and Development (R&D) Programme (Decontamination Science Theme). J.W.M. and E.R.P. publish with permission of the Director of the British Geological Survey. J. Hyde, J. Griffiths, M. Smith, A. Bull, A. Wareing, C. Lennon, S. Kwong, L. Edmiston, J. Graham and D. Connor (all NNL), and J. Taylor-Bray (ONR) are thanked for assistance in the field and for informal manuscript review.

Author contributions NTS: conceptualization (lead), data curation (lead), formal analysis (lead), funding acquisition (lead), investigation (lead), methodology (lead), project administration (lead), resources (lead), software (lead), validation (lead), visualization (lead), writing – original draft (lead), writing – review & editing (lead); JWM: data curation (equal), formal analysis (equal), funding acquisition (equal), investigation (equal), validation (equal), visualization (equal), writing – original draft (supporting), writing – review & editing (equal); ERP: formal analysis (equal), funding acquisition (equal),

investigation (equal), validation (equal), visualization (equal), writing – original draft (supporting), writing – review & editing (supporting)

Funding This research received no specific grant from any funding agency in the public, commercial or not-for-profit sectors.

Competing interests The authors declare that they have no known competing financial interests or personal relationships that could have appeared to influence the work reported in this paper.

Data availability Some borehole logs analysed during the current study are not publicly available owing to nuclear site restrictions but may be made available from the corresponding author on reasonable request. Please note some historical field exposures are now lost owing to erosion, quarrying or construction.

Scientific editing by Jonathan Smith; Christopher Swainston

References

- Akhurst, M.C., Chadwick, R.A. *et al.* 1997. *The Geology of the West Cumbria District. Memoir of the British Geological Survey, Sheets 28, 27 and 47.* British Geological Survey, Keyworth, Nottingham.
- Backert, N., Ford, M. and Malartre, F. 2010. Architecture and sedimentology of the Kerinitis Gilbert-type fan delta, Corinth Rift, Greece. *Sedimentology*, **57**, 543–586. <https://doi.org/10.1111/j.1365-3091.2009.01105.x>
- Ballantyne, C.K., Stone, J.O. and Fifield, L.K. 2009. Glaciation and deglaciation of the SW Lake District, England: implications of cosmogenic ³⁶Cl exposure dating. *Proceedings of the Geologists' Association*, **120**, 139–144. <https://doi.org/10.1016/j.pgeola.2009.08.003>
- Banham, S.G. and Mountney, N.P. 2014. Climatic versus halokinetic control on sedimentation in a dryland fluvial succession. *Sedimentology*, **61**, 570–608. <https://doi.org/10.1111/sed.12064>
- Barnes, R.P., Ambrose, K.A., Holliday, D.W. and Jones, N.S. 1994. Lithostratigraphic subdivision of the Triassic Sherwood Sandstone Group in west Cumbria. *Proceedings of the Yorkshire Geological Society*, **50**, 51–60. <https://doi.org/10.1144/pygs.50.1.51>
- Benn, D.I. and Evans, D.J.A. 1996. The interpretation and classification of subglacially-deformed materials. *Quaternary Science Reviews*, **15**, 23–52. [https://doi.org/10.1016/0277-3791\(95\)00082-8](https://doi.org/10.1016/0277-3791(95)00082-8)
- Benn, D.I. and Evans, D.J.A. 2010. *Glaciers and Glaciations*, 2010 edn. Hodder Arnold, London.
- Bennett, M.R., Huddart, D. and Thomas, G.S.P. 2002. Facies architecture within a regional glaciolacustrine basin: Copper River, Alaska. *Quaternary Science Reviews*, **21**, 2237–2279. [https://doi.org/10.1016/S0277-3791\(02\)00027-6](https://doi.org/10.1016/S0277-3791(02)00027-6)
- Bowden, R.A., Bumpus, C. and Littleboy, A.K. 1998. An overview and update of the site characterisation studies at Sellafeld. *Proceedings of the Yorkshire Geological Society*, **52**, 125–137. <https://doi.org/10.1144/pygs.52.2.125>
- Boyce, J.I. and Eyles, N.I. 2000. Architectural element analysis applied to glacial deposits: internal geometry of a late Pleistocene till sheet, Ontario, Canada. *Geological Society of America Bulletin*, **112**, 98–118. [https://doi.org/10.1130/0016-7606\(2000\)112<98:AEAATG>2.0.CO;2](https://doi.org/10.1130/0016-7606(2000)112<98:AEAATG>2.0.CO;2)
- British Geological Survey 1999. *Gosforth. England and Wales Sheet 37. Solid and Drift Geology 1:50,000.* British Geological Survey, Keyworth, Nottingham.
- British Geological Survey 2006. *Solway East. Scotland Special Sheet. Superficial Deposits and Simplified Bedrock 1:50,000 Geology Series.* British Geological Survey, Keyworth, Nottingham.
- Brodzikowski, K. and Van Loon, A.J. 1987. A systematic classification of glacial and periglacial environments. *Earth-Science Reviews*, **24**, 297–381. [https://doi.org/10.1016/0012-8252\(87\)90061-4](https://doi.org/10.1016/0012-8252(87)90061-4)
- BS5930:2015. *The Code of Practice for Site Investigations.* British Standards Institution, Milton Keynes.
- Busby, J.P. and Merritt, J.A. 1999. Quaternary deformation mapping with ground penetrating radar. *Journal of Applied Geophysics*, **41**, 75–91. [https://doi.org/10.1016/S0926-9851\(98\)00050-0](https://doi.org/10.1016/S0926-9851(98)00050-0)
- Cain, S.A. and Mountney, N.P. 2009. Spatial and temporal evolution of a terminal fluvial fan system: the Permian Organ Rock Formation, South-east Utah, USA. *Sedimentology*, **56**, 1774–1800. <https://doi.org/10.1111/j.1365-3091.2009.01057.x>
- Chang, K.H. 1975. Unconformity-bounded stratigraphic units. *Geological Society of America Bulletin*, **86**, 1544–1552. [https://doi.org/10.1130/0016-7606\(1975\)86<1544:USU>2.0.CO;2](https://doi.org/10.1130/0016-7606(1975)86<1544:USU>2.0.CO;2)
- Chiverrell, R.C., Thrasher, I.M. *et al.* 2013. Bayesian modelling the retreat of the Irish Sea Ice Stream. *Journal of Quaternary Science*, **28**, 200–209. <https://doi.org/10.1002/jqs.2616>
- Chiverrell, R.C., Smedley, R.K. *et al.* 2018. Ice margin oscillations during deglaciation of the northern Irish Sea Basin. *Journal of Quaternary Science*, **36**, 673–680. <https://doi.org/10.1002/jqs.3326>

- Clark, C.D., Hughes, A.L. and Greenwood, S.L. 2012. Pattern and timing of retreat of the last British–Irish Ice Sheet. *Quaternary Science Reviews*, **44**, 112–146, <https://doi.org/10.1016/j.quascirev.2010.07.019>
- Clarke, B.G. 2018. The engineering properties of glacial tills. *Geotechnical Research*, **5**, 262–277, <https://doi.org/10.1680/jgere.18.00020>
- Coleman, C.G., Grimoldi, E., Wollard, H., Holton, D. and Shevelan, J. 2020. Developing 3D geological and hydrogeological models for the Low Level Waste Repository site, west Cumbria, UK. *Quarterly Journal of Engineering Geology and Hydrogeology*, **54**, <https://doi.org/10.1144/qjegh2020-026>
- Cross, M., Attya, A. and Evans, D.J.A. 2018. The susceptibility of glaciogenic deposits to liquefaction under seismic loading conditions: a case study relating to nuclear characterization in West Cumbria. *Proceedings of the Yorkshire Geological Society*, **55**, 116–132, <https://doi.org/10.1144/pygs2018-003>
- Culshaw, M.G., Entwisle, D.C., Giles, D.P., Berry, T., Collings, A., Banks, V.J. and Donnelly, L.J. 2017. Material properties and geohazards. *Geological Society, London, Engineering Geology Special Publications*, **28**, 599–740, <https://doi.org/10.1144/EGSP28.6>
- Davies, B.J., Roberts, D.H., Ó Cofaigh, C., Bridgland, D.R., Riding, J., Philipps, E.R. and Teasdale, D.A. 2009. Interlobate ice-sheet dynamics during the Last Glacial Maximum at Whitburn Bay, County Durham, England. *Boreas*, **38**, 555–578, <https://doi.org/10.1111/j.1502-3885.2008.00083.x>
- Davies, B.J., Roberts, D.H., Bridgland, D.R. and Ó Cofaigh, C. 2012. Dynamic Devensian ice flow in NE England: a sedimentological reconstruction. *Boreas*, **41**, 337–336, <https://doi.org/10.1111/j.1502-3885.2011.00237.x>
- Duller, R.A., Mountney, N.P. and Russell, A.J. 2008. Architectural analysis of a volcanoclastic jökulhlaup deposit, southern Iceland: sedimentary evidence for supercritical flow. *Sedimentology*, **55**, 939–964, <https://doi.org/10.1111/j.1365-3091.2007.00931.x>
- Eastwood, T., Dixon, E.E.L., Hollingworth, S.E. and Smith, B. 1931. *The Geology of the Whitehaven and Workington District. Memoir of the Geological Survey of Great Britain, England and Wales, Sheet 28*. Geological Survey of Great Britain, London.
- Emery, D. and Myers, K. 1996. *Sequence Stratigraphy*. Blackwell, Oxford.
- Emery, D. and Myers, K. 2009. *Sequence Stratigraphy*. Wiley, Chichester.
- Evans, D.J.A. 2017. Conceptual glacial ground models: British and Irish case studies. *Geological Society, London, Engineering Geology Special Publications*, **28**, 369–500, <https://doi.org/10.1144/EGSP28.4>
- Evans, D.J.A. 2018. *Till: A Glacial Process Sedimentology*. Wiley–Blackwell, Chichester.
- Evans, D.J.A. and Benn, D.I. 2021. Facies description and the logging of sedimentary exposures. In: Evans, D.J.A. and Benn, D.I. (eds) *A Practical Guide to the Study of Glacial Sediments*, 2nd edn. Quaternary Research Association and Glacial Landscapes Working Group, London, 17–79.
- Evans, D.J.A., Clark, C.D. and Mitchell, W.A. 2005. The last British ice sheet: a review of the evidence utilised in the compilation of the glacial map of Britain. *Earth-Science Reviews*, **70**, 253–312, <https://doi.org/10.1016/j.earscirev.2005.01.001>
- Evans, D.J.A., Phillips, E.R., Hiemstra, J.F. and Auton, C.A. 2006. Subglacial till formation, sedimentary characteristics and classification. *Earth-Science Reviews*, **78**, 115–176, <https://doi.org/10.1016/j.earscirev.2006.04.001>
- Evans, D.J.A., Rother, H., Hyatt, O.M. and Shulmeister, J. 2013. The glacial sedimentology and geomorphological evolution of an outwash head/moraine-dammed lake, South Island, New Zealand. *Sedimentary Geology*, **284–285**, 45–75, <https://doi.org/10.1016/j.sedgeo.2012.11.005>
- Evans, D.J.A., Roberts, D.H. and Evans, S.C. 2016. Multiple subglacial till deposition: a modern exemplar for Quaternary palaeoglaciology. *Quaternary science reviews*, **145**, 183–203.
- Eyles, N. and Clark, B. 1985. Gravity-induced soft sediment deformation in glacial sequences of the Upper Proterozoic Port Askaig Formation, Scotland. *Sedimentology*, **32**, 789–814, <https://doi.org/10.1111/j.1365-3091.1985.tb00734.x>
- Eyles, C.H. and Eyles, N. 1983. Sedimentation in a large lake: a reinterpretation of the Late Pleistocene stratigraphy at Scarborough Bluffs, Ontario, Canada. *Geology*, **11**, 146–152, [https://doi.org/10.1130/0091-7613\(1983\)11<146:SIALLA>2.0.CO;2](https://doi.org/10.1130/0091-7613(1983)11<146:SIALLA>2.0.CO;2)
- Eyles, N. and McCabe, A.M. 1989. The Late Devensian (<22 000 BP) Irish Sea Basin: the sedimentary record of a collapsed ice-sheet margin. *Quaternary Science Reviews*, **8**, 307–351, [https://doi.org/10.1016/0277-3791\(89\)90034-6](https://doi.org/10.1016/0277-3791(89)90034-6)
- Eyles, C.H., Eyles, N. and Gostin, V.A. 1998. Facies and allostratigraphy of high-latitude, glacially influenced marine strata of the early Permian southern Sydney Basin, Australia. *Sedimentology*, **45**, 121–161, <https://doi.org/10.1046/j.1365-3091.1998.00138.x>
- Feltrin, L., McLellan, J.G. and Oliver, N.H.S. 2009. Modelling the giant, Zn–Pb–Ag Century deposit, Queensland, Australia. *Computers and Geosciences*, **35**, 108–133, <https://doi.org/10.1016/j.cageo.2007.09.002>
- Fielding, C.R. 2006. Upper flow regime sheets, lenses and scour fills: extending the range of architectural elements for fluvial bodies. *Sedimentary Geology*, **190**, 227–240, <https://doi.org/10.1016/j.sedgeo.2006.05.009>
- Fookes, P.G. 1997. Geology for engineers: the geological model, prediction and performance. *Quarterly Journal of Engineering Geology*, **30**, 293–424, <https://doi.org/10.1144/GSL.QJEG.1997.030.P4.02>
- Gehrmann, A., Meschede, M., Hüneke, H. and Pedersen, S.A.S. 2019. Sea cliff at Kieler Ufer (Pleistocene stripes 11–16) – large-scale architecture and kinematics of the Jasmund Glaciotectonic Complex. *Deuqua Special Publications*, **2**, 19–27, <https://doi.org/10.5194/deuquasp-2-19-2019>
- Ghazi, S. and Mountney, N.P. 2009. Facies and architectural element analysis of a meandering fluvial succession: the Permian Warchha Sandstone, Salt Range, Pakistan. *Sedimentary Geology*, **221**, 99–126, <https://doi.org/10.1016/j.sedgeo.2009.08.002>
- Griffiths, J.S. and Martin, C.J. 2017. *Engineering Geology and Geomorphology of Glaciated and Periglaciated Terrains*. Engineering Group Working Party Report. Engineering Geology Special Publications **28**, Geological Society, London.
- Harris, C., Brabham, P., Eaton, G. and McCarroll, D. 1997. Glaciotectonised Quaternary sediments at Dinas Dinlle, Gwynedd, North Wales, and their bearing on the style of deglaciation in the Eastern Irish Sea. *Quaternary Science Reviews*, **16**, 109–127, [https://doi.org/10.1016/S0277-3791\(96\)00050-9](https://doi.org/10.1016/S0277-3791(96)00050-9)
- Hart, J.K. 1999. Identifying fast ice flow from landform assemblages in the geological record: a discussion. *Annals of Glaciology*, **28**, 59–66, <https://doi.org/10.3189/172756499781821887>
- Hart, J.K. and Boulton, G.S. 1991. The interrelation of glaciotectonic and glaciodepositional processes within the glacial environment. *Quaternary Science Reviews*, **10**, 335–350, [https://doi.org/10.1016/0277-3791\(91\)90035-S](https://doi.org/10.1016/0277-3791(91)90035-S)
- Hart, J.K. and Roberts, D.H. 1994. Criteria to distinguish between subglacial glaciotectonic and glaciomarine sedimentation, I. Deformation styles and sedimentology. *Sedimentary Geology*, **91**, 191–213, [https://doi.org/10.1016/0037-0738\(94\)90129-5](https://doi.org/10.1016/0037-0738(94)90129-5)
- Huddart, D. 1971. A relative glacial chronology from the tills of the Cumberland lowland. *Proceedings of the Cumberland Geological Society*, **3**, 21–32.
- Hjellbakk, A. 1997. Facies and fluvial architecture of a high-energy braided river: the Upper Proterozoic Segladden Member, Varanger Peninsula, northern Norway. *Sedimentary Geology*, **114**, 131–161, [https://doi.org/10.1016/S0037-0738\(97\)00075-4](https://doi.org/10.1016/S0037-0738(97)00075-4)
- Huddart, D. 1991. The glacial history and glacial deposits of the north and west Cumbrian lowlands. In: Ehlers, J. and Rose, J. (eds) *Glacial Deposits in Great Britain and Ireland*. Balkema, Rotterdam, 151–183.
- Huddart, D. 1994. The Late Quaternary glaciogenic sequence: landforms and environments in coastal Cumbria. In: Boardman, J. and Walden, J. (eds) *Cumbria Field Guide*. Quaternary Research Association, Oxford, 59–77.
- Huddart, D. and Clark, R. 1994. Conflicting interpretations of glacial sediments and landforms in Cumbria. *Proceedings of the Cumberland Geological Society*, **5**, 419–436.
- Huddart, D. and Glasser, D.F. 2002. *The Quaternary of Northern England*. Joint Nature Conservation Committee, Peterborough.
- Huddart, D. and Tooley, M.J. 1972. *Field Guide to the Cumberland Lowland*. Quaternary Research Association, Cambridge.
- Huddart, D., Tooley, M.J. and Carter, P. 1977. The coasts of North West England. *Geological Journal Special Issue*, **7**, 119–154.
- Hughes, P.D. 2010. Geomorphology and Quaternary stratigraphy: the roles of morpho-, litho-, and allostratigraphy. *Geomorphology*, **123**, 189–199, <https://doi.org/10.1016/j.geomorph.2010.07.025>
- Hughes, D.B., Clarke, B.G. and Money, M.S. 1998. The glacial succession in lowland northern England. *Quarterly Journal of Engineering Geology*, **31**, 211–234, <https://doi.org/10.1144/GSL.QJEG.1998.031.P3.05>
- Jones, N.S. and Ambrose, K. 1994. Triassic sandy braidplain and aeolian sedimentation in the Sherwood Sandstone Group of the Sellafeld area, west Cumbria. *Proceedings of the Yorkshire Geological Society*, **50**, 61–70, <https://doi.org/10.1144/pygs.50.1.61>
- Kessler, H., Mathers, S. and Sobisch, H.-G. 2009. The capture and dissemination of integrated 3D geospatial knowledge at the British Geological Survey using GIS3D software and methodology. *Computers and Geosciences*, **35**, 1311–1321, <https://doi.org/10.1016/j.cageo.2008.04.005>
- Kostic, B. and Aigner, T. 2007. Sedimentary architecture and 3D ground penetrating radar analysis of gravelly meandering river deposits (Neckar Valley, SW Germany). *Sedimentology*, **54**, 789–808, <https://doi.org/10.1111/j.1365-3091.2007.00860.x>
- Kostic, B., Becht, A. and Aigner, T. 2005. 3-D sedimentary architecture of a Quaternary gravel delta (SW-Germany): Implications for hydrostratigraphy. *Sedimentary Geology*, **181**, 147–171, <https://doi.org/10.1016/j.sedgeo.2005.07.004>
- Krige, D.G. 1951. A statistical approach to some basic mine valuation problems on the Witwatersrand. *Journal of Chemical, Metallurgical and Mining Society of South Africa*, **52**, 119–139.
- Kuras, O., Wilkinson, P.B. *et al.* 2016. Geoelectrical monitoring of simulated subsurface leakage to support high-hazard nuclear decommissioning at the Sellafeld site, UK. *Science of the Total Environment*, **566–567**, 350–359, <https://doi.org/10.1016/j.scitotenv.2016.04.212>
- Lee, J. 2018. Glacial lithofacies and stratigraphy. In: Menzies, J. and van der Meer, J.J.M. (eds) *Past Glacial Environments*. Elsevier, Amsterdam, 377–429.
- Lee, J.R., Phillips, E., Rose, J. and Vaughan-Hirsch, D. 2017. The Middle Pleistocene glacial evolution of northern East Anglia, UK: a dynamic tectonostratigraphic–parasequence approach. *Journal of Quaternary Science*, **32**, 231–260, <https://doi.org/10.1002/jqs.2838>
- Lelliott, M.R., Cave, M.R. and Wealthall, G.P. 2009. A structured approach to the measurement of uncertainty in 3D geological models. *Quarterly Journal of Engineering Geology and Hydrogeology*, **42**, 95–105, <https://doi.org/10.1144/1470-9236/07-081>

- Lesemann, J.-E., Alsop, G.I. and Piotrowski, J.A. 2010. Incremental subglacial meltwater sediment deposition and deformation associated with repeated ice-bed decoupling: a case study from the Island of Funan, Denmark. *Quaternary Science Reviews*, **29**, 3212–3229, <https://doi.org/10.1016/j.quascirev.2010.06.010>
- Lewis, M.A. 1989. Water. In: McCall, J. and Marker, B. (eds) *Earth Science Mapping for Planning, Development and Conservation*. Graham and Trotman, London, 53–77.
- Lewis, M.A., Cheney, C.S. and ÓDocharthaigh, É. 2006. *Guide to Permeability Indices*. British Geological Survey, Keyworth, Nottingham.
- Livingstone, S.J., Evans, D.J.A. et al. 2012. Glaciodynamics of the central sector of the last British–Irish ice sheet in northern England. *Earth-Science Reviews*, **111**, 25–55, <https://doi.org/10.1016/j.earscirev.2011.12.006>
- Longhitano, S.G. 2008. Sedimentary facies and sequence stratigraphy of coarse-grained Gilbert-type deltas within the Pliocene thrust-top Potenza Basin (Southern Apennines, Italy). *Sedimentary Geology*, **210**, 87–110, <https://doi.org/10.1016/j.sedgeo.2008.07.004>
- Maizels, J. 1997. Jökulhlaup deposits in proglacial areas. *Quaternary Science Reviews*, **16**, 793–819, [https://doi.org/10.1016/S0277-3791\(97\)00023-1](https://doi.org/10.1016/S0277-3791(97)00023-1)
- Marren, P.M. 2005. Magnitude and frequency in proglacial rivers: a geomorphological and sedimentological perspective. *Earth-Science Reviews*, **70**, 203–251, <https://doi.org/10.1016/j.earscirev.2004.12.002>
- Martin, C. J., Morley, A. L. and Griffiths, J. S. 2017. Introduction to engineering geology and geomorphology of glaciated and periglacial terrains. In: Griffiths, J. S. and Martin, C. J. (eds) *Engineering Geology and Geomorphology of Glaciated and Periglacial Terrains*, Engineering Group Working Party Report, Engineering Geology Special Publications **28**, Geological Society, London, 1–30. <https://doi.org/10.1144/EGSP28.1>
- McCarroll, D. 2001. Deglaciation of the Irish Sea Basin: a critique of the glaciomarine hypothesis. *Journal of Quaternary Science*, **16**, 393–404, <https://doi.org/10.1002/jqs.626>
- McCarroll, D. and Rijdsdijk, K. 2003. Deformation styles as a key for interpreting glacial depositional environments. *Journal of Quaternary Science*, **18**, 473–489, <https://doi.org/10.1002/jqs.780>
- McClay, K.R. 1992. Glossary of thrust tectonics terms. In: McClay, K.R. (ed.) *Thrust Tectonics*. Chapman and Hall, London, 419–433.
- McMillan, A.A. and Merritt, J.W. 2012. A new Quaternary and Neogene lithostratigraphical framework for Great Britain and the Isle of Man. *Proceedings of the Geologists' Association*, **123**, 679–691, <https://doi.org/10.1016/j.pgeola.2012.05.007>
- McMillan, A.A., Hamblin, R.J.O. and Merritt, J.W. 2011. *A Lithostratigraphical Framework for Onshore Quaternary and Neogene (Tertiary) Superficial Deposits of Great Britain and the Isle of Man*. British Geological Survey, Keyworth, Nottingham.
- Medici, G., Boulesteix, K., Mountney, N.P., West, L.J. and Odling, N.E. 2015. Palaeoenvironment of braided fluvial systems in different tectonic realms of the Triassic Sherwood Sandstone Group, UK. *Sedimentary Geology*, **329**, 188–210, <https://doi.org/10.1016/j.sedgeo.2015.09.012>
- Medici, G., West, L.J. and Mountney, N.P. 2018. Characterization of a fluvial aquifer type at a range of depths and scales: the Triassic St Bees Sandstone Formation, Cumbria, UK. *Hydrogeology Journal*, **26**, 565–591, <https://doi.org/10.1007/s10040-017-1676-z>
- Merritt, J.A. and Auton, C.A. 2000. An outline of the lithostratigraphy and depositional history of Quaternary deposits in the Sellafeld district, west Cumbria. *Proceedings of the Yorkshire Geological Society*, **53**, 129–154, <https://doi.org/10.1144/pygs.53.2.129>
- Merritt, J.W., Roberson, S. and Cooper, M.R. 2018. A critical review and re-investigation of the Pleistocene deposits between Cranfield Point and Killeel, Northern Ireland: implications for regional sea-level models and glacial reconstructions of the northern Irish Sea basin. *Proceedings of the Geologists' Association*, **129**, 583–609, <https://doi.org/10.1016/j.pgeola.2018.04.001>
- Miall, A.D. 1977. A review of the braided-river depositional model environment. *Earth-Science Reviews*, **13**, 1–62, [https://doi.org/10.1016/0012-8252\(77\)90055-1](https://doi.org/10.1016/0012-8252(77)90055-1)
- Miall, A.D. 1985. Architectural-element analysis: a new method of facies analysis applied to fluvial deposits. *Earth-Science Reviews*, **22**, 261–308, [https://doi.org/10.1016/0012-8252\(85\)90001-7](https://doi.org/10.1016/0012-8252(85)90001-7)
- Miall, A.D. 1988. Architectural elements and bounding surfaces in fluvial deposits: anatomy of the Kayenta Formation (lower Jurassic), Southwest Colorado. *Sedimentary Geology*, **55**, 233–262, [https://doi.org/10.1016/0037-0738\(88\)90133-9](https://doi.org/10.1016/0037-0738(88)90133-9)
- Miall, A.D. 1996. *The Geology of Fluvial Deposits: Sedimentary Facies, Basin Analysis and Petroleum Geology*. Springer, Berlin.
- Miall, A.D. 1997. *The Geology of Stratigraphic Sequences*. Springer, Berlin.
- Miall, A.D. 2006a. Reconstructing the architecture and sequence stratigraphy of the preserved fluvial record as a tool for reservoir development: a reality check. *AAPG Bulletin*, **90**, 989–1002, <https://doi.org/10.1306/02220605065>
- Miall, A.D. 2006b. *The Geology of Fluvial Deposits, Sedimentary Facies, Basin Analysis and Petroleum Geology*. Springer, Berlin.
- Michie, U. and Bowden, R.A. 1994. UK Nirex geological investigations at Sellafeld. *Proceedings of the Yorkshire Geological Society*, **50**, 5–9, <https://doi.org/10.1144/pygs.50.1.5>
- Mountney, N.P. and Thompson, D.B. 2002. Stratigraphic evolution and preservation of aeolian dune and damp/wet interdune strata: an example from the Triassic Helsby Sandstone Formation, Cheshire Basin, UK. *Sedimentology*, **49**, 805–833, <https://doi.org/10.1046/j.1365-3091.2002.00472.x>
- Murton, J.B. and French, H.M. 1993. Thermokarst involutions, Summer Island, Pleistocene Mackenzie Delta, Western Canadian Arctic. *Permafrost and Periglacial Processes*, **4**, 217–229, <https://doi.org/10.1002/ppp.3430040304>
- NACSN 1983. North American stratigraphic code. *AAPG Bulletin*, **67**, 841–875.
- NACSN 2005. North American stratigraphy code. *AAPG Bulletin*, **89**, 1547–1591, <https://doi.org/10.1306/07050504129>
- Nirex 1995. *Characterisation of the Onshore Quaternary Deposits Around Sellafeld, Cumbria: Phase II*. UK Nirex Ltd, Harwell.
- Nirex 1996. *The 3D Geological Structure of the PRZ: March 1996 Update*. UK Nirex Ltd, Harwell.
- Nirex 1997a. *Sellafeld Geological and Hydrogeological Investigations. The Quaternary of the Sellafeld Area*. UK Nirex Ltd, Harwell.
- Nirex 1997b. *Synthesis of the Hydrogeological Characteristics of Quaternary Sequences in the Sellafeld Area*. UK Nirex Ltd, Harwell.
- Nirex 1997c. *A Structural Analysis of Drift Deposits in the Sellafeld District*. UK Nirex Ltd, Harwell.
- Nirex 1997d. *A Summary of the Correlation and Nature of Onshore and Offshore Quaternary Sediments of the Sellafeld Area*. UK Nirex Ltd, Harwell.
- Nirex 1997e. *A Synthesis of the Nature and Origin of Deformation Features Within the Quaternary Sequences*. UK Nirex Ltd, Harwell.
- Nirex 1997f. *The Quaternary of the Sellafeld Area*. UK Nirex Ltd, Harwell.
- Nirex 1997g. *Field Investigation, Provenance, Mineralogy, Geochemistry and Micropalaeontology of Quaternary Sediments in the Sellafeld District*. UK Nirex Ltd, Harwell.
- Nirex 1997h. *Quaternary Characterisation, Logging and Interpretation of the Holmrook Boreholes*. UK Nirex Ltd, Harwell.
- Nirex 1997i. *The Lithology and Thickness of Drift Deposits in the Upper Calder Catchment, West Cumbria*. UK Nirex Ltd, Harwell.
- Nirex 1997j. *Logging and Interpretation of Nirex Quaternary Boreholes (QBH) Drilled in the Sellafeld Area During 1996*. UK Nirex Ltd, Harwell.
- Nirex 1997k. *Analytical Studies of the Provenance, Micropalaeontology and Chronology of Quaternary Sediments from the Sellafeld Area, 1996*. UK Nirex Ltd, Harwell.
- Nirex 1997l. *Quaternary Lithostratigraphy of the Sellafeld District*. UK Nirex Ltd, Harwell.
- Nirex 1997m. *Assessment of Geological and Hydrogeological Data from the 1995 Quaternary Drilling Programme*. UK Nirex Ltd, Harwell.
- Olariu, C. and Bhattacharya, J.P. 2006. Terminal distributary channels and delta front architecture of river-dominated delta systems. *Journal of Sedimentary Research*, **76**, 212–233, <https://doi.org/10.2110/jsr.2006.026>
- Opluštil, S., Martinek, K. and Tasárová, Z. 2005. Facies and architectural analysis of fluvial deposits of the Nýrany Member and the Týnec Formation (Westphalian D - Barruelian) in the Kladno-Rakovnik and Pilsen basins. *Bulletin of Geosciences*, **80**, 45–66.
- Pedersen, S.A.S. 2014. Architecture of glaciotectionic complexes. *Geosciences*, **4**, 269–296, <https://doi.org/10.3390/geosciences4040269>
- Pedersen, S.A.S. and Boldreel, L.O. 2015. Thrust–fault architecture of glaciotectionic complexes in Denmark. *Geological Survey of Denmark and Greenland Bulletin*, **33**, 17–20, <https://doi.org/10.34194/geusb.v33.4479>
- Pedersen, S.A.S. and Gravesen, P. 2009. Structural development of Maglevandsfald: a key to understanding the glaciotectionic architecture of Møns Klint, SE Denmark. *Geological Survey of Denmark and Greenland Bulletin*, **17**, 29–32, <https://doi.org/10.34194/geusb.v17.5007>
- Phillips, E.R. and Merritt, J.W. 2008. Evidence for multiphase water-escape during rafting of shelly marine sediments at Clava, Inverness-shire, NE Scotland. *Quaternary Science Reviews*, **27**, 988–1011, <https://doi.org/10.1016/j.quascirev.2008.01.012>
- Phillips, E.R., Evans, D.J.A. and Auton, C.A. 2002. Polyphase deformation at an oscillating ice margin following the Loch Lomond Readvance, central Scotland, UK. *Sedimentary Geology*, **149**, 157–182, [https://doi.org/10.1016/S0037-0738\(01\)00250-0](https://doi.org/10.1016/S0037-0738(01)00250-0)
- Phillips, E.R., Merritt, J.W., Auton, C. and Gollege, N. 2007. Microstructures in subglacial and proglacial sediments: underr. *Quaternary Science Reviews*, **26**, 1499–1528, <https://doi.org/10.1016/j.quascirev.2007.03.007>
- Phillips, E., Lee, J. and Burke, H. 2008. Progressive proglacial to subglacial deformation and syntectonic sedimentation at the margins of the Mid-Pleistocene British Ice Sheet: evidence from north Norfolk, UK. *Quaternary Science Reviews*, **27**, 1848–1871, <https://doi.org/10.1016/j.quascirev.2008.06.011>
- Phillips, E., Everest, J. and Reeves, H. 2013a. Micromorphological evidence for subglacial multiphase sedimentation and deformation during overpressurized fluid flow associated with hydrofracturing. *Boreas*, **42**, 395–427, <https://doi.org/10.1111/j.1502-3885.2012.00261.x>
- Phillips, E., Lipka, E. and van der Meer, J.J.M. 2013b. Micromorphological evidence of liquefaction, injection and sediment deposition during basal sliding of glaciers. *Quaternary Science Reviews*, **81**, 114–137, <https://doi.org/10.1016/j.quascirev.2013.10.005>
- Piotrowski, J.A. 1992. Was ist ein Till? *Geowissenschaften*, **10**, 100–108.
- Powell, R.D. 1984. Glaciomarine processes and inductive lithofacies modelling of ice shelf and tidewater glacier sediments based on Quaternary examples. *Marine Geology*, **57**, 1–52.
- Rawson, P.F., Allen, P.M. et al. 2002. *Stratigraphical Procedure: Geological Society Professional Handbook*. Geological Society, London.
- Reesink, A.J.H. and Bridge, J.S. 2009. Influence of bedform superimposition and flow unsteadiness on the formation of cross strata in dunes and unit bars.

- Sedimentary Geology*, **222**, 274–300, <https://doi.org/10.1016/j.sedgeo.2009.09.014>
- Roberts, D.H. and Hart, J.K. 2005. The deforming bed characteristics of a stratified till assemblage in north East Anglia, UK: investigating controls on sediment rheology and strain signatures. *Quaternary Science Reviews*, **24**, 123–140, <https://doi.org/10.1016/j.quascirev.2004.03.004>
- Roberts, D.H., Dackombe, R.V. and Thomas, G.S.P. 2007. Palaeo-ice streaming in the central sector of the British–Irish Ice Sheet during the Last Glacial Maximum: evidence from the northern Irish Sea Basin. *Boreas*, **36**, 115–129, <https://doi.org/10.1111/j.1502-3885.2007.tb01186.x>
- Rose, J. and Menzies, J. 1996. Glacial stratigraphy. In: Menzies, J. (ed.) *Past Glacial Environments - Sediments, Forms and Techniques*. Butterworth–Heinemann, Oxford, 253–284.
- Russell, A.J., Tweed, F.S. and Knudsen, Ó. 2000. Flash flood at Sólheimajökull heralds the reawakening of an Icelandic subglacial volcano. *Geology Today*, **16**, 102–106, <https://doi.org/10.1046/j.1365-2451.2000.00005.x>
- Russell, A.J., Tweed, F.S., Roberts, M.J., Harris, T.D., Gudmundsson, M.T., Knudsen, Ó. and Marren, P.M. 2010. An unusual jökulhlaup resulting from subglacial volcanism, Sólheimajökull, Iceland. *Quaternary Science Reviews*, **29**, 1363–1381, <https://doi.org/10.1016/j.quascirev.2010.02.023>
- Salvador, A. 1994. *International Stratigraphic Guide*, 2nd edn. International Union of Geosciences and Geological Society of America, Boulder, CO.
- Scourse, J.D., Chiverrell, R.C. *et al.* 2021. Maximum extent and readvance dynamics of the Irish Sea Ice Stream and Irish Sea Glacier since the Last Glacial Maximum. *Journal of Quaternary Science*, **36**, 780–804, <https://doi.org/10.1002/jqs.3313>
- Slomka, J.M. and Eyles, C.H. 2013. Characterizing heterogeneity in a glaciofluvial deposit using architectural elements, Limehouse, Ontario, Canada. *Canadian Journal of Earth Sciences*, **50**, 911–929, <https://doi.org/10.1139/cjes-2013-0020>
- Slomka, J.M. and Eyles, C.H. 2015. Architectural–landsystem analysis of a modern glacial landscape, Solheimajokull, southern Iceland. *Geomorphology*, **230**, 75–97, <https://doi.org/10.1016/j.geomorph.2014.11.006>
- Smith, S.A. 1990. The sedimentology and accretionary styles of an ancient gravel-bed stream: the budleigh salterton pebble beds (Lower Triassic), southwest England. *Sediment. Geology*, **67**, 199–219
- Smith, D.B. 1994. *Geology of the Country Around Sunderland. Memoir of the British Geological Survey, sheet 21 (England and Wales)*. British Geological Survey, Keyworth, Nottingham.
- Smith, D.B. and Francis, E.A. 1967. *Geology of the Country Between Durham and West Hartlepool. Memoir of the Geological Survey of Great Britain, sheet 27 (England and Wales)*. British Geological Survey, Keyworth, Nottingham.
- Smith, N.T. 2010. *To What Extent can GIS be Used to Address the Needs of 2D, 3D and 4D Environmental Conceptual Modelling at UK Nuclear Sites*. MSc thesis, Manchester Metropolitan University, Manchester.
- Smith, N.T. and Merritt, J.W. 2008. Further insights into the superficial geology of west Cumbria using 3D geological modelling: implications for Devensian palaeogeographic evolution. 33rd International Geoscience Convention, Oslo, Norway.
- Smith, N.T., Shreeve, J. and Kuras, O. 2020. Multi-sensor core logging (MSCL) and X-ray computed tomography imaging of borehole core to aid 3D geological modelling of poorly exposed unconsolidated superficial sediments underlying complex industrial sites: an example from Sellafeld nuclear site, UK. *Journal of Applied Geophysics*, **178**, 1–14, <https://doi.org/10.1016/j.jappgeo.2020.104084>
- Smith, S.A. and Edwards, R.A., 1991. Regional sedimentological variations in Lower Triassic fluvial conglomerates (Budleigh Salterton Pebble Beds), southwest England: some implications for palaeogeography and basin evolution. *Geological Journal*, **26**, 65–83.
- Stokes, C.R., Clark, C.D., Lian, O.B. and Tulaczyk, S. 2007. Ice stream sticky spots: a review of their identification and influence beneath contemporary and palaeo-ice streams. *Earth-Science Reviews*, **81**, 217–249, <https://doi.org/10.1016/j.earscirev.2007.01.002>
- Stone, P., Millward, D., Young, B., Merritt, J.W., Clarke, S.M., McCormac, M. and Lawrence, D.J.D. 2010. *British Regional Geology: Northern England*, 5th edn. British Geological Survey, Keyworth, Nottingham.
- Thomas, G.S.P. and Chiverrell, R.C. 2007. Structural and depositional evidence for repeated ice-marginal oscillation along the eastern margin of the Late Devensian Irish Sea Ice Stream. *Quaternary Science Reviews*, **26**, 2375–2405, <https://doi.org/10.1016/j.quascirev.2007.06.025>
- Thomas, G.S.P., Chiverrell, R.C. and Huddart, D. 2004. Ice-marginal depositional responses to readvance episodes in Late Devensian deglaciation of the Isle of Man. *Quaternary Science Reviews*, **23**, 85–106, <https://doi.org/10.1016/j.quascirev.2003.10.012>
- Trotter, F.M. and Hollingworth, S.E. 1932. The glacial sequence in the North of England. *Geological Magazine*, **69**, 374–380, <https://doi.org/10.1017/S0016756800097995>
- Trotter, F.M., Hollingworth, S.E., Eastwood, T. and Rose, W.C. 1937. *Gosforth District. Memoir of the Geological Survey of Great Britain, England and Wales. Sheet 37*. Geological Survey of Great Britain, London.
- US Environmental Protection Agency 2006. *Guidance on Systematic Planning Using the Data Quality Objectives Process*. US Environmental Protection Agency, Office of Environmental Information, Washington, DC.
- Wang, G., Pang, Z., Boisvert, J.B., Hao, Y., Cao, Y. and Qu, J. 2013. Quantitative assessment of mineral resources by combining geostatistics and fractal methods in the Tongshan porphyry Cu deposit (China). *Journal of Geochemical Exploration*, **134**, 85–98, <https://doi.org/10.1016/j.gexplo.2013.08.004>
- Williams, G.D., Brabham, P.J., Eaton, G.P. and Harris, C. 2001. Late Devensian glaciotectionic deformation at St Bees, Cumbria. *Journal of the Geological Society, London*, **158**, 125–135, <https://doi.org/10.1144/jgs.158.1.125>
- Williams, P.F. and Rust, B.R. 1969. The sedimentology of a braided river. *Journal of Sedimentary Petrology*, **39**, 649–679.
- Wycisk, P., Hubert, T., Gossel, W. and Neumann, C. 2009. High-resolution 3D spatial modelling of complex geological structures for an environmental risk assessment of abundant mining and industrial megasites. *Computers and Geosciences*, **35**, 165–182, <https://doi.org/10.1016/j.cageo.2007.09.001>
- Yong Technology Inc. 2014. GeoRose. Edmonton, AB, <http://www.yongtechnology.com/download/georose>